Deanship of Graduate Studies

Al-Quds University

Gas Detection Using Photoacoustic Effect in Conjunction with Michelson Interferometer

Ahmad Saifaldin Ameen Jabr

M.Sc. Thesis

Jerusalem- Palestine

1430 / 2009

Gas Detection Using Photoacoustic Effect in Conjunction with Michelson Interferometer

Prepared by:

Ahmad Saifaldin Ameen Jabr

B.Sc.: An-ajah National University Palestine

Supervisor: Prof. Dr. Mohammed I. Abu-Taha

A thesis Submitted in Partial fulfillment of requirements for the degree of Master of physics from Physics Dept. / program of physics/ Fuculty of Graduate studies/ Al-Quds University

1430 / 2009

Al-Quds University
Deanship of Graduate Studies
Physics Department

Thesis Approval

Gas Detection Using Photoacoustic Effect in Conjunction with Michelson Interferometer

Prepared by: Ahmad Saifaldin Ameen Jabr
Registration No: 20411587

Supervisor: Prof. Dr. Mohammed I. Abu-Taha

Master thesis submitted and accepted, Date: 30 / 06 / 2009
The names and signatures of the examining committee members are as follows:

1- Head of committee: Prof. Dr. Mohammed Abu-Taha signature:
2- Internal Examiner: Dr. Musa Abu Teir signature:
3- External Examiner: Dr. Khaleel Moh'd Dabayeneh signature:

Jerusalem- Palestine

1430 / 2009

Dedication

To my family, with love

Ahmad Saifaldin Ameen Jabr

Declaration:

I certify that this thesis submitted for the degree of Master, is the result of my own research, except where otherwise acknowledged, and that this study (or any part of the same) has not been submitted for a higher degree to any other university or institution.

Signed

Ahmad Saifaldin Ameen Jabr

Date: 30 / 06 / 2009

Acknowledgments

Acknowledgements are first of all presented to my supervisor Prof. Dr. Mohammed Abu-Taha for being supportive and understanding, then to my lab mate Miss Fida' Buss for the help she proposed while constructing and building up the investigation system. Acknowledgements are also presented to the academic stuff in the Department of Physics in Al-Quds University especially to Prof. Imad Barghouthi and Dr. Rushdi Kitaneh for their care and to my friends Mr. Faris Zhour for the valuable ideas he gave while constructing the system and Miss Ayah Shehadeh for her opinions while discussing the data.

Best acknowledgements are presented to my wife Shaima' Hatem Jabr for her patience in raising up my kids and taking care of all of us through the years of my study and research. Thanks are also due to my father and mother for their care and prayers and to my oldest brother Khalid and his family for their care and support, in addition to the rest of my family; brothers and sisters. Best acknowledgements are also presented to my family in law for their care especially for my father and mother in law for their prayers.

Acknowledgements are also presented to all of my friends whom are not explicitly mentioned here and to all peoples who cared about me.

Acknowledgements are presented to Al-Quds University for offering the unique chance for students to fulfill their Master degree in different specializations and for providing the equipment needed for this research. Acknowledgements are also presented to the Faculty of Science and Technology especially to the Department of physics and its academic stuff for their care and help.

Abstract

In this study, and for the first time in the history of spectroscopy, photoacoustic signals were detected inside Michelson interferometer cavity. The system of investigation was built up by the researcher, and the first run of the system was launched in September, 2008. Data were collected in November, 2008 through the end of January, 2009.

The main item of this thesis deals with trace gas detection using the photoacoustic (PA) effect in conjunction with Michelson interferometer in a trial to figure out a relation between the photoacoustic and the Michelson fringe signals. The photoacoustic signal was successfully detected – for the first time – inside Michelson interferometer cavity. For this purpose, a set of samples were investigated for trace gas emission among which chlorophorm was used to test the reliability and stability of the constructed system, while other samples, like essential oils and plant tissues were used to figure out a relation between both signals.

The main goals of this thesis involve the ability of detecting the PA signals inside Michelson interferometer cavity and to try figuring out a relation between PA and Michelson fringe signals by comparing both signals with each other. The sensitivity of both detection techniques subject to IR absorption was investigated. This thesis also aimed to building up a new detection technique based on the combined Michelson-PA chamber in which, laser irradiation was replaced by a wideband-pulsed IR source in a trial to improve system's portability and to judge the sensitivity of both detection techniques subject to IR absorption.

In the presented study, common experimental procedure has been followed. The constructed system was investigated many times and at different dates using the same amount of chlorophorm and the same results were observed. The constructed system was tested and investigated under different experimental conditions and optimizing parameters

using different samples of chlorophorm. The reliability of the system was investigated using different samples of essential oils along with the part of the plant from where these essential oils are usually extracted. Both investigation techniques, Michelson interferometry and PA spectroscopy, have shown good correlations between the signals of the plant tissue and it's corresponding oil. The new introduced system was also used to compare the trace gas of tap water with that of Zamzam water in a trial to investigate the detectability of the system to minute changes in the sample.

PA signals have been studied for the first time inside the cavity of Michelson interferometer and were successfully detected. PA and Michelson fringe signals have shown good correlations compared with each other. The combined Michelson-PA chamber technique has shown an edge over conventional PAS, and has demonstrated a higher sensitivity of Michelson interferometry compared with PA spectroscopy subject to IR absorption.

Results were encouraging and so, opens the door widely to use this new introduced investigation technique in different manners and criteria regarding trace gas emission.

Table of contents

List of figures

Chapter one

Historical background

1.1 Introduction

The main goal of this thesis is to introduce a new spectroscopic detection technique based on the combined Michelson-Photoacoustic (PA) signal detection, and to investigate the usefulness of using Michelson's interferometer in monitoring trace gases, hence, this chapter will be focused on the historical background of both detection schemes throughout literature. A brief review of all topics relative to this detection technique in addition to the investigated samples will be introduced.

Spectroscopy – born to life as a result of Newton's researches – is the daughter of mother optics in which spectrum analysis is involved (Hecht and Zajac, 1974). Photoacoustic spectroscopy is a version of photothermal spectroscopy in which the absorbed energy is deactivated into heat thus resulting in a localized pressure wave i.e. sound wave (Rosencwaig and Pines, 1977; Kirkbright and Miller, 1982; Jenkins, 1985; Meyer and Sigrist, 1990; Bicanic et al, 1990; Schmidt and Beckmann, 1998; George et al, 2000; J. Szurkowski, 2001; Yang and Zhang, 2003; Philip K et al, 2007). Photoacoustic spectroscopy is a spectroscopic investigation technique that is based on the Bell's discovery of the PA effect in 1880 (Soldner and Stephan, 1999; Autrey et al, 2001; Haisch and Niessner, 2002). Gas analysis was the first report of the application of PAS for analytical purposes (Haisch and Niessner, 2002). Since the advent of lasers in 1960s, photoacoustic spectroscopy has

become widely applicable as a vigorous investigation technique in all matter phases (Meyer and Sigrist, 1990). Among the pioneers in using lasers in photoacoustic spectroscopy were Kerr and Atwood (Bernegger and Sigrist, 1990).

After Bell's discovery of the PA effect in 1880, the field laid dormant until 1976 when Rosencwaig and Gersho postulated their R-G theory which settled down the theoretical basis of the effect in solids (Haisch and Niessner, 2002). Upon settling down the theoretical basis of the PA effect, the technique was used to investigate the hydration and chemical alteration effects of the new porn rat stratum corneum (Rosencwaig and Pines, 1977). Patel and Tam in the beginnings of 1980s, have demonstrated an enhanced sensitivity for PAS over conventional and modulated techniques in measuring small absorption coefficients. Their experiments were carried by using a pulsed laser and a piezoelectric transducer being in contact with a liquid (Autrey et al, 2001). In the early 1980s, Miranda has laid down the theoretical basis of the PA effect in semiconductors (Crippa and Viappiani, 1990; Villegas-Lelovsky et al, 2003). Since the publication of the R-G theory, PAS has found large interest in different fields like chemistry, biology and medicine (Schmidt and Beckmann, 1998). In the field of environmental pollution, PAS showed high capabilities of monitoring the concentration of some gaseous pollutants in the atmosphere in the sub-ppbv level (Bicanic et al, 1990). The PA technique was successfully introduced at elevated temperature to record the absorption of low-volatility hydrocarbons in addition to those of hot band excitations in carbon dioxide molecules (Kastle and Sigrist, 1996). In biomass monitoring, PAS was found to be useful in determining the number of the cells being contained in fermentation (Schmidt and Beckmann, 1998). With the aid of powerful CO_2 lasers, the PA effect was successfully applied to study different essential oils within the plant tissues without the necessity for the former to be steam-distilled (El-Kahlout et al, 1998). In the field of semiconductors, and in addition to thermal parameters, PAS provides sufficient information about both; carrier-transport properties and electron-phonon energy relaxations (Lelovsky et al, 2003). PAS has showed high capabilities of being an alternative method for simultaneously measuring different photosynthetic parameters

like light absorption, oxygen evolution and energy storage over a wide temperature range (Herbert et al, 2006). The technique was successfully applied to study the thermal characterization of ceramic tapes (Philip K et al, 2007). It was also used to study the molecular relaxation effects in hydrogen chloride (Besson et al, 2008).

Michelson interferometer is a versatile investigation tool that is based on the double beam interference (Hecht and Zajac, 1974; Halliday and Resnick, 1988; Fowles, 1989). The interferometer was invented by A. A. Michelson in 1880 in his trial to measure the effect of the motion of the earth through the ether (Gamow, 1961; French, 1968; Hecht and Zajac, 1974; Hazelett and Turner, 1979; Tolman, 1987; Halliday and Resnick, 1988; Basu, 2001; Carmichael, 2008). The main frame of work of Michelson's interferometer involves detecting the differences in path length between the two arms of the interferometer where light waves propagates at right angles (Gamow, 1961; Steel, 1983; Fowles, 1989; Bartusiak, 2000; Hariharan, 2006). This path length difference results in a slight change in the phase of one beam relative to the other leading the two beams to interfere, thus, forming the interferogram (Cano and Mattioli, 1966; Hallam, 1968; Bartlett et al, 1976; Jongbloets et al, 1979; Steel, 1986; Kobayashi and Misawa, 1997; Bartusiak, 2000). After being the first precisely used instrument to insure the inexistence of the proposed ether, Michelson interferometer was devoted to measure dimensions, refractive indices, wavelengths and surface roughness (Halliday and Resnick, 1988; Kobayashi and Misawa, 1997). It was also been used to determine the wavelength of spectral lines very accurately. These precise determinations of the wavelength of spectral lines lead the scientific community – in full agreement – to define the meter to be 1,650,763.73 times the wavelength of the orange-red spectral line of Krypton-86 (Halliday and Resnick, 1988; Hariharan, 2003; http://physics.usask.ca/~angie/ep421/ lab3/theory.html). In Fourier transform infrared spectroscopy, Michelson's interferometer is the most commonly used type of interferometers

over the whole IR range (http://www.prenhall.com/settle/ chapters/ch15.pdf). Michelson interferometer founds many applications in different fields regarding Fourier transform spectroscopy (Gebbie and Stone, 1964; Genzel and Kuhl, 1977; Valentin, 1996; Simeoni, 1997; Montgomery et al, 2004). It was used to study the absorption spectra of gases at high pressures in the range of 10 – 110 cm^{-1} (Gebbie and Stone, 1964). It has also been used in IASI – Infrared Atmospheric Sounding Interferometer – which was meant to be launched on the European meteorological platform to observe the spectra of the earth's atmosphere from the outer space (Simeoni, 1997). Michelson's interferometer was evaluated to be an alternative precise detection procedure for the evaluation of corrosion in electrochemical systems (Cruz et al, 2006).

The part of the electromagnetic spectrum that extends from the red end of the visible region to that of the microwave is known as the infrared (IR) radiation. It covers the 100 – 1 μm wavelength range in the EM spectrum (Hallam, 1968; Banwell, 1972). The story of IR radiation goes back to the beginning of the nineteenth century when Herschel noticed a higher change in the reading of a thermometer after passing the red end of the sun's visible spectrum. Fraunhofer's discovery of the dark lines in the spectrum of the sun in 1914 and the efforts of Kirchoff and Wood laid the basis for the modern IR spectroscopy (Kumar, 1993). IR spectroscopy involves the measurement of the different absorbed IR frequencies by a sample being irradiated by IR radiation (http://prenhall.com/settle/ chapters/ch15.pdf). The classic researches of Coblentz in 1903 had lunched the application of IR spectroscopy in the field of chemistry. It was until 1930s, when the value of chemical IR spectroscopy became realized. With the technological improvement in spectrometers and sensors, IR spectroscopy has become one of the most valuable investigation techniques in the field of trace analysis. Thomas, Hilger and Watts in 1965 were pioneers in applying IR spectroscopy in the field of trace analysis for atmospheric pollution studies (Hallam, 1968). Most of the pollutants and molecules –excluding homonuclear diatomics – having

absorption lines in the IR region due to the allowed vibrational and or vibrational-ratational transitions, give rise to the uniqueness of the IR spectroscopy (Miklos and Feher, 1996; Bernath, 2000). In non-aqueous solvents, IR spectroscopy is regarded as a useful tool for the study of acid-base equilibrium (Dawa and Gowland, 1978). Interference spectroscopy (interferometry), which involves using interferometers, was the result of H. A. Gebbie and his group's work on NIR spectroscopy in the National Physical Laboratory in 1964 (Hallam, 1968). Once a sample is irradiated with IR source, molecules within the sample are subject to IR absorption if and only if the radiant energy matches with one molecular vibtational energy (http://orgchem.colorado.edu/hndbksupport/IRtutor/tutorial.html). The amount of IR radiation a molecule is capable to absorb is sensitive to the type of vibrational motion a specific bond achieves whether stretching or bending which in turn depends of the strength of the covalent bond between the atoms (http://www.oilanalysis. com/article_detail.asp? articleid =1109). Essential oils usually absorb energy in the range of IR region. They are volatile concentrated liquid extracts containing aromatic compounds. They are basically driven from different plant tissues like leaves, flowers, seeds, barks, resins, wood and peels (Cristina, 2004; http://en.wikipedia.org/ wiki/Essential_oil). They are usually extracted from plant tissues by steam distillation (Reverchon and Porta, 1995; Aqel and Shaheen, 1996; Burits and Bucar, 2000; Cristina, 2004; Qin et al, 2007). Essential oils are used for their therapeutic properties in the first place. According to their chemical composition, essential oils were found to have antiseptic, antimicrobial, antifungal, antioxidant, inhibitor and carminative effects (Aqel and Shaheen, 1996; Burits and Bucar, 2000; Cristina, 2004; Ramadan, 2007; Matan and Matan, 2008; Ebru et al, 2008). Aromatic plants were used over history for different purposes like skin care, perfumes and healing salves. Sandalwood and cinnamon, as mentioned in Vedas – Hidus most ancient and sacred literature –, were used 4000 years ago (Cristina, 2004). Essential oils were used by the Egyptians for embalming, cosmetics, perfumes and love potions about 5000 years ago (Robins, 1999).

In this study, chlorophorm was used to investigate the ability, steadiness and reliability of the new combined trace gas technique.

1.2 Statement of the problem

This thesis is concerned with trace gas detection using photoacoustic spectroscopy (PAS) in conjunction with Michelson interferometer. It is obvious through literature that PAS – mostly carried out with powerful lasers as irradiation sources especially in the IR range – has showed high capabilities in the field of trace gas detection. Also, a quick review of the available literature shows that Michelson's interferometry was successfully applied to precise determinations of refractive indices. The used laser in this technique has nothing to do with the PA signal. laser is used to illuminate the interferometer and to sense the optical changes within the cell which arise through the generation of the PA signal.

This combination between both PAS and Michelson interferometer was aimed to achieve the following goals:

* To measure the PA signal inside Michelson cavity.
* To figure out a relation between the PA and Michelson fringe signals.
* To compare the sensitivity of both signals subject to IR absorption.
* To build up a new detection method based on the combined Michelson-PA cell.
* To replace laser irradiation with a wideband-pulsed IR source to improve system's portability.

1.3 Thesis plan

In this thesis, chapter one represents an introduction to all topics involved in the title of the presented thesis, meanwhile, chapter two presents the theoretical background which deals with the theoretical aspects of Michelson interferometry, PA effect and IR spectroscopy in addition to a brief review of the investigated samples. In chapter three, a description of the experimental approach which deals with the instruments and equipment being used to build up the system and with the experimental procedure of investigation is given. The collected data and experimental results will be presented in chapter four accompanied with their relative figures. Chapter five gives a discussion for the data presented in chapter four, while conclusion and further work are given in chapter six followed by a list of references.

Chapter two

Theoretical background

2.1 Introduction

The theoretical background of the main topics needed in the discussion of this thesis subject is presented thoroughly. Different spectroscopic methods are discussed in brief as a preface to this chapter. An introduction to Photoacoustic spectroscopy and microphone implementation in gas trace detection in view of the use of Helmholtz cell and its resonance frequency is introduced. Michelson interferometer as the new approach technique in monitoring gas trace detection will be introduced. Theories of PA spectroscopy and Michelson interferometery are both thoroughly reviewed. Relevant information about the investigated samples are discussed.

2.2 Spectroscopic Methods

Spectroscopy – the interaction of light with matter – is the most valuable analytical tool that mostly serves both chemists and physicists. It has many sub-branches regarding the used part of the electromagnetic spectrum and the physical quantity being involved (Banwell, 1972). Molecular spectroscopy may be defined as the study of the interaction of electromagnetic waves and matter (Banwell, 1972). Since the advent of lasers and technological revolution in the past few decades, different spectroscopic techniques are of increasingly growing interest. This development and tuneability of lasers facilitates sample

detection at very low concentrations (Meyer and Sigrist, 1990). Since the study of these aspects depends on the amount of energy that molecules and atoms absorb, emit, or scatter, then spectroscopic signals are functions of wave length (wave number) or any other related physical quantities. As a result, three main types of spectroscopic methods arise; Absorption spectroscopy, Emission spectroscopy, and Scattering spectroscopy, for each of which belongs many different branches. Mixture analysis; qualitative or quantitative, bond lengths and angles of some certain molecule and electron distribution in organic substances are different fields of spectroscopy (Banwell 1972). Emission spectroscopy involves radiative decays and so, the range of the electromagnetic spectra at which the material (substance) gives off energy through emission; it is illustrated as the de-excitation of some excited state – "where excitation is the result of absorption" – via radiative decay. Emission spectroscopy is attractive for the reason that it has an improved signal to noise ratio compared to absorption spectroscopy. All experiments that are carried in the field of IR emission require that, the source and detector are at different temperatures. If both, the source and detector are at same temperature, then, a zero net flux falling on the detector is the consequence (Bernath, 2000). Scattering spectroscopy involves the measurement of the amount of light being scattered from the sample at certain wavelength and or certain angles. Scattered light being detected at the opposite side of the sample is treated according to the theory of transmission spectroscopy, whereas, that being detected at the same side of the sample is treated according remission spectroscopy (http://en.wikipedia.org/wiki/ Absorption_spectroscopy). In Raman Scattering spectro- scopy, the inelastic interaction between photons and irradiated molecules results in the shift of the incident radiation frequency. This shift is due to the characteristic vibrational-rotational frequencies of the molecule under study (Meyer and Sigrist, 1990). In electron scattering spectroscopy, the bombardment of target species with free electrons results in the induced transitions

between molecular energy states. This method is based on collecting these scattered electrons and measuring their intensities as a function of the incident electron energy, final energy and scattering angles. Absorption spectroscopy involves the comparison of the intensity of a beam of light before and after illuminating the sample under study. The difference in the available energy levels of different sample's constituents determines the wavelength at which the incident photon was absorbed (http://en.wikipedia.org/wiki/ Absorption spectroscopy). Absorption spectroscopy differs from fluorescence spectroscopy in that, the absorbed energy is not reemitted via radiative decay; rather, it is dissipated within the sample as induced photothermal effects via nonradiative decay. Infrared, near infrared, microwave, and photoacoustic spectroscopic techniques are all examples of absorption spectroscopy. UV-visible spectroscopy involves the measurement of how much light a sample absorbs from a particular wavelength. Since DNA absorbs light in the UV range, then measuring the absorbance of UV light in the sample determines the amount of DNA. The fact that DNA absorbs light in the UV range is what makes sunlight partly dangerous (http://en.wikipedia.org/wiki/Absorption _spectroscopy). Photomultiplier tubes – light sensitive surfaces that gives off electrons when irradiated with light – are the most sensitive detection devices in the uv-visible region (Banwell 1972).

Photo thermal spectroscopic methods involve measuring the induced effects in the sample as a result of absorbing modulated electromagnetic radiation (Bicanic et al, 1990). Refractive index gradient, surface deformation, acoustic emission, and phase change are different examples of photothermal induced effects. Measurements based on thermal induced effects were found to be useful in locating and characterizing different phases in liquid crystal compounds (George et al, 2000). Elemental analysis and electronic structures in materials are usually carried out via x-ray spectroscopy. Both, X-ray absorption and emission involves the interaction between the applied external field and electrons. Once a

material absorbs light in the X-ray range, one of its atomic inner shell electrons is excited to an unoccupied bound state or became ionized leaving the shell partially vacant. For this vacancy to be filled, one of the outer shell electrons makes a transition by emitting a photon in the X-ray domain (Mukoyama, 2004). In molecular spectroscopy, the range at which a particular source gives off radiation and the bandwidth which results in the excitation of a particular molecule is what determines the method to be used. The interaction between the electric and or magnetic fields that associate the radiation and the sample under investigation must result in some change in the nuclear, atomic and or molecular level, for example; NMR and ESR spectroscopy involve changes in spin orientation, microwave spectroscopy involve changes in molecule's orientation (rotation), infrared spectroscopy involve changes in molecule's configuration (vibration), visible, UV, and X-ray spectroscopic methods involve changes in electron distribution (excitation and de-excitation), while γ-ray spectroscopy involve changes in nuclear configuration (Banwell 1972). This is the first time a microphone is fitted in the Michelson cavity to detect photoacoustic induced signals.

2.3 Photoacoustic spectroscopy (PAS)

Photoacoustic spectroscopy is a spectroscopic technique that is based on the PA effect firstly discovered by Bell in 1880 (Autrey et al, 2001). The discovery of the effect was based on Alexander's Graham Bell work regarding the transmission of sound without a cable connection (Haisch and Niessner, 2002). While experiencing his photophone, he observed that an audible signal of nonelectrical fashion was possible to be directly obtained. The idea involves the transformation of the absorbed energy into kinetic energy

within the sample via energy exchange processes which results in locally heating the sample and thus creating a pressure wave or sound. The absorbed energy by the sample is released in radiation-less decay as heat, thus, enhancing the PA effect particularly useful in this study (Crippa and Viappiani, 1989). PA effect involves the deactivation of the absorbed photon energy into sound based on collisional relaxations which are followed by the generation of a pressure wave which is detected by a sensitive microphone (Bicanic et al, 1990). The technique is totally based on periodically heating a sample being illuminated by the absorption of modulated optical radiation (George et al, 2000). Sample heating which generates periodic pressure fluctuations and thus PA signal is directly correlated to the absorbed electromagnetic energy. The uniqueness of PAS originates from the fact that neither scattered nor does reflected light contribute to the signal. This uniqueness is attractive for absorption measurements in gaseous, liquid and solid materials (Haisch and Niessner, 2002). Since photoacoustic signals are directly proportional to the absorbance of the sample, then, the method is regarded as a zero back-ground one. This implies that, if no light is absorbed within the sample, no periodic heating will be generated, thus, no PA signal could be detected (Schmidt and Beckmann, 1998). Absorbing modulated light will result in the excitation of a fraction of the ground state molecules into higher energy levels. Excited molecules might relax through either radiative or nonradiative decay (Meyer and Sigrist, 1990). PA spectroscopy involves molecular nonradiative relaxations for which, the dissipated energy results in localized temperature rise in the volume of the sample (Schmidt and Beckmann, 1998). If the temperature rises faster than volume expansion, a local pressure increase is the consequence (Haisch and Niessner, 2002). The produced modulated pressure rise may be detected by a sensitive microphone (Dewey Jr et al, 1973). Photoacoustic spectroscopy involves measuring the fraction of the optical energy that is reemitted as heat after the absorption of modulated or pulsed light (Schmidt and

Beckmann, 1998). Fig 2.1 shows a schematic diagram of the principle of any photoacoustic experiment. Different spectroscopic techniques, including photoacoustic, are carried out today with laser light sources, but PAS is much older than the development of the first laser in 1960 (Haisch and Niessner, 2002). Photoacoustic effect, discovered by bell in 1880, has been applied to analyze gases, to measure lifetimes of excited molecular states and to study photochemical reactions etc., long before the advent of lasers (Bernegger and Sigrist, 1990). However, the applications of PAS were limited due to the low spectral brightness of radiation sources being available.

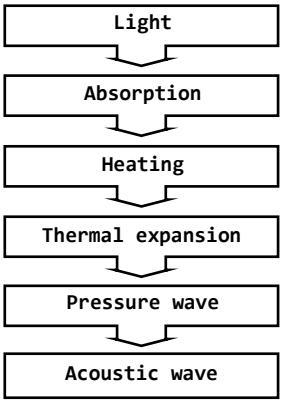

Fig 2.1 Principle of photoacoustic experiments, (After: Haisch and Niessner, 2002).

The first to use lasers in photoacoustic spectroscopy was Kerr and Atwood. With a cw CO_2 laser they achieved a minimum detectable absorption coefficient $\alpha_{min} = 10^{-7}$ cm^{-1} for carbon dioxide buffered in nitrogen. A detection limit of 10 ppbv of methane in nitrogen with the aid of a HeNe laser operating at 3.39 μm was reached by Kreuzer (Bernegger and Sigrist, 1990). Gas analysis was the oldest application of PA spectroscopy for analytical purposes (Haisch and Niessner, 2002). PA signals are usually detected via two main configurations; the firs involve using a sensitive microphone while the other involves using a piezoelectric transducer. In the gas-microphone configuration, a tight sealed cell encloses the sample. Thermal waves at the surface of sample periodically heats up a thin layer of

gas which will act as an acoustic piston resulting in the generation of periodic pressure fluctuations inside the cavity. A sensitive microphone coupled to the cavity is used to detect this pressure fluctuation (George et al, 2000). The resultant periodic pressure fluctuates in the cell at the same frequency as that of modulation of the incident radiation (Kirkbright and Miller, 1982; George et al, 2000). As the amplitude of pressure fluctuations depends on the absorbance of the sample, a variable-wavelength source will result in an absorption spectrum (Kirkbright and Miller, 1982). Fig 2.2 shows a schematic diagram of the gas-microphone photoacoustic cell.

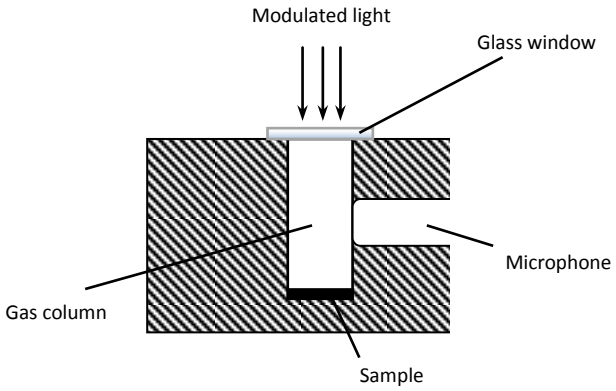

Fig 2.2 A Scheme of the gas-microphone photoacoustic cell, (After: Jenkins, 1985).

Since the PA signal has exactly the same frequency as the excitation source, then the frequency of modulation is taken as a reference for the PA signal, (Haisch and Niessner, 2002). The determination of the PA signal of the sample as a function of the wavelength of the incident light results in the photoacoustic spectrum (http://www.movar.pate.hu/~mathphys/pas.html). In PA configurations where piezoelectric transducers are used, pressure fluctuations in a solid or a liquid can be probed (Haisch and Niessner, 2002). The strong damping of thermal waves propagating through a solid sample, make detecting them directly a difficult task. In PAS, the generated elastic or acoustic waves can travel much greater distances than thermal waves. Since elastic waves do not interact with sample's

microscopic features, then, they simply carry the information being generated by the much shorter wavelength thermal waves (Jenkins, 1985). Pressure fluctuations inside the cavity which contains the sample to be investigated, can be observed using optical methods rather than photoacoustics (Haisch and Niessner, 2002).

PA imaging, depth profiling, PA microscopy, and the determination of thermal and optical properties of materials are different interesting applications of PAS based on measuring the PA signal in the frequency domain (Benedetto et al, 1987). Depth profiling is one of the well known and attractive capabilities of photoacoustic spectroscopy (Donini and Michaelian, 1984). In depth profiling, depths which thermal waves can probe were found to be sensitive to the used frequency of modulation (Jenkins, 1985). Using the gas-microphone photoacoustic configuration, depths of ~50 μm can be probed; meanwhile piezoelectric photoacoustic configurations allows depths of ~1μm to be probed (Jenkins, 1985). In piezoelectric PA configurations, piezoelectric transducers are either submerged within liquid samples or coupled with solid samples via good thermal contact. In solids, the periodic absorption of the incident radiation results in the periodic heating of the sample which develops thermal stresses and strains at the surface of the sample. Fig 2.3 shows a schematic diagram of a piezoelectric transducer being in contact with a solid sample and the sources of surface strain.

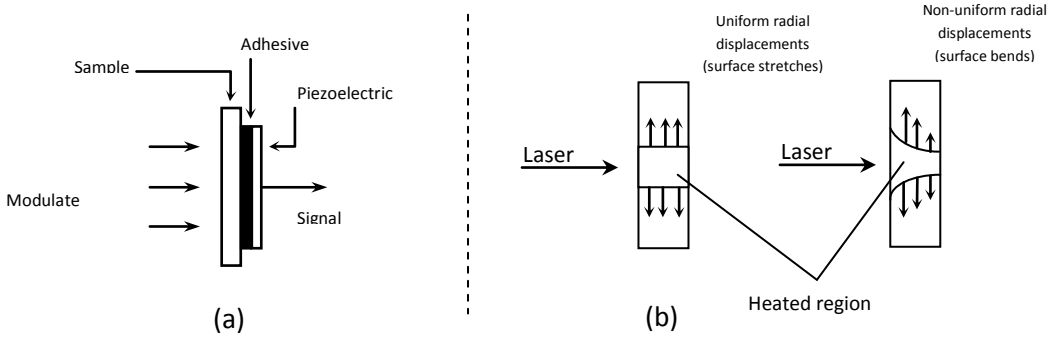

Fig 2.3 (a) Schematic diagram of the piezoelectric PA cell
(b) Sources of surface strain, (After: Jenkins, 1985)

Photoacoustic spectroscopy (PAS) is regarded as recognized technique in various applications that involve trace gas detection (Besson et al, 2008). For the study of atmospheric pollutants, Kreuzer has introduced a new method, based on optoacoustics for the measurement of trace gaseous constituents which combines both; optical simplicity and strong signals of absorption techniques. Kreuzer's method was found to be highly comparable with fluorescence measurements (Dewey Jr. et al, 1973). The photoacoustic technique has been found to be useful and efficient in investigating the chemical and physical properties of many samples. It is also found to be applicable over any type of solids whether being crystalline, powder, or gel (Yang and Zhang, 2003). Tam and Patel in the beginning of 1980s have used pulsed laser and piezo transducers to measure small absorption coefficients of liquids. Their results demonstrate the enhanced sensitivity of PAS being compared with conventional and modulated techniques (Autrey et al, 2001). In the field of condensed matter, Tam and Patel have demonstrated the waveguide effect for photoacoustic waves in quartz as a substrate material (Lai et al, 1982). During the 1990s, the great need of nondestructive characterization of thermal, optical, and structural properties of materials, led to several developments in detection methods. Due to its simple, flexible and neat experimental setup, laser photoacoustic spectroscopy has gained high popularity in measuring the required thermo-physical parameters very accurately (Philip K et al, 2007). In CO_2 laser PAS; the contribution of a particular gaseous component to the total absorption within the wavelength range versus the minimum detectable absorption of the system determines the detectability of that gaseous component (Meyer and sigrist, 1990). Photoacoustic studies of the vapors of different essential oils have been carried out using a line-tunable waveguide CO_2 laser in conjunction with a heat-pipe type over the temperature range of 20 - 180°C (El-Kahlout et al, 1998). Different studies have confirmed that PAS has an edge over conventional methods in the study of

highly reflecting samples such as powders (Sathiyamoorthy and Vijayan, 2007). In addition, numerous interesting results in characterizing liquid crystals have been produced using the PA technique (George et al, 2000). Photoacoustic spectroscopy is widely applied in the study of solids, particularly of semiconductors. The original work of Miranda in 1982 has laid down the theoretical description of photoacoustic effect in semiconductors taking into account the diffusion and recombination of non-equilibrium carriers (Lelovsky et al, 2003). PAS was found to have good capabilities in directly monitoring energy gaps and non-radiative relaxation processes in semiconductors (Hu et al, 2007). In addition to providing us with thermal parameter about semiconductors, PAS was found to provide additional information regarding carrier-transport properties and electron-phonon energy relaxations (Lelovsky et al, 2003). McClelland and Knisely have employed the gas-microphone photoacoustic configuration to characterize germanium surfaces being subject to irradiation by high intensity c.w. laser sources (Jenkins, 1985). Mcfarlane *et al* have used PA technique in investigating damage effects in semiconductors. In an attempt to determine optical absorption coefficients below the optical gap, the PA technique was been applied to amorphous semiconductors. Different studies based on PAS were carried out to determine the density of dislocations in semiconductors. The group of Mikoshiba *et al* has demonstrated the sensitivity of PA spectra to the existence of dislocations in GaAs, meanwhile, dislocations in Si and InP has been studied by Suezawa and Auzel respectively using photoacoustic spectroscopy (Jenkins, 1985). Recently, the excitonic transitions of semiconductors nanocrystals were observed to be well resolved in PA spectra compared with the corresponding optical absorption spectra (Toyoda et al, 2002). Thermal and thermoelastic effects in solids with residual stress have been studied using the PA technique (Muratikov and Glazov, 2003).

After the publication of the R-G theory, photoacoustic and photothermal techniques have found wide interests in different fields like chemistry, biology and medicine (Schmidt and Beckmann, 1998). The PA technique has been successfully used by Braslavsky and Heibel to investigate different aspects of photophysics and photochemistry of dyes. In studying electron-transfer between a triplet magnesium porphyrin and different quinines in polar and nonpolar solvents, Mauzerall et al have employed time-resolved pulsed PA techniques (Sathiyamoorthy and Vijayan, 2007). Photoacoustic spectroscopy has been evaluated as useful in the field of biology to determine the number of cells in fermentation (Schmidt and Beckmann, 1998). Photoacoustic systems modified for precise temperature control were used to study the photoacoustic and photosynthetic properties of plant leaves. In leaf samples, the aqueous cytoplasm of the cell has been found to be the medium through which PT signals propagate from leaf pigments to the surface of the leaf cells by thermal diffusion (Herbert et al, 2006). In photosynthetic studies, part of the laser beam was found to be absorbed by leaf pigments. Photochemical products of photosynthesis were found to store a variable fraction of the absorbed light pulse. The reminder of the absorbed light is deactivated into heat through the sample thus, producing an acoustic wave which is detected by the microphone (Pinchasov et al, 2006). The non-invasive methodology and light scattering independency makes PAS a valuable tool in forest-decline research for detecting the environmental stress. Inclusive measurements of photoacoustic signals in green plant leaves were found to provide new information regarding signatures of photosynthesis process in leaves and their structure (Szurkowski, 2001). The short time response and ease of sampling makes CO_2 laser photoacoustic spectroscopy in combination with resonant cells very suitable for real-time analysis. Monitoring several gaseous atmospheric pollutants with low concentrations has been already performed under realistic conditions at the sub-ppbv level using PA techniques. A combination of PAS and

powerful carbon dioxide laser functioning in the 10 μm range has been applied to study the time evolution of ethylene metabolism in stressed Cymbidium flowers (Bicanic et al, 1990).

The intrinsically zero back-ground nature, high sensitivity, less time consuming and achromaticity of the photoacoustic technique, which result in a very simple setup arrangement applicable over a broad spectral region ranging from the ultraviolet to the mid infrared, are the main advantages of this spectroscopic technique (Besson et al, 2008; George et al, 2000). In addition to producing direct optical absorption spectra, PA technique is used to perform depth profiling analysis, thermal characterization besides to the investigation of nonradiative relaxation processes (George et al, 2000). Photoacoustic spectroscopy is capable to show and observe some features that are not shown up in optical spectroscopy (Sathiyamoorthy and Vijayan, 2007). In stratosphere – with a balloon-borne system – or in the troposphere with a system installed in a mobile trailer, *in situ* measurements were carried out depending on the simple arrangement of PAS devices (Meyer and sigrist, 1990). Both, amplitude and phase of response of a sample are the most important characteristic information PAS can provide. PA amplitude signal was found to be dependent on both, optical absorption properties and thermal properties of the sample (Hu et al, 2007). PA signal phase information was found to be a convolution of depth and thermal difusivity information (Kirkbright and Miller, 1982). The photoacoustic phase is the time delay that occurs during PA signal generation process: from the light being absorbed by the sample to the acoustic signal being detected by the microphone. Geometry of the photoacoustic cell, response of the detecting system, optical absorption coefficient, non-radiative de-excitation paths, etc are different sources contributing to the data being extracted from signal's phase (Hu et al, 2007). Inspite of the above-mentioned advantages, PAS is an indirect method since the detection of the absorbed optical energy by sample's

molecules is carried out through an acoustic wave being generated in the gas due to thermal expansion resulting from the vibration-to-translation (V-T) relaxation of the excited molecules. The conversion of optical energy to thermal energy depends on the physico-thermal properties of the gas, and so, the detecting sensor requires calibration. In most cases, molecular relaxation of the excited rovibrational state is measured instantaneously; whereas, some particular gas mixtures result in a much slower detection process for which, PA signals needs to be precisely analyzed (Besson et al, 2008).

2.4 Photoacoustic Theory

In most photoacoustic experimental setups, the sample being enclosed in the well sealed cavity is exposed to a modulated beam of light which results in the periodic heating of the sample. The periodic heating, which consequently results in the periodic fluctuations of the pressure inside the cavity and thus, generating the PA signal, was found to be strongly dependent on three factors; namely, optical absorption coefficient, light-into-heat conversion efficiency and heat diffusion through the sample. Light-into-heat conversion efficiency has been found to be strongly dependent on the nonradiative de-excitation process taking place within the sample (George et al, 2000). The PA signal was found to be sensitive only to the nonradiative relaxation process, according to Adams *et al*. the PA signal (*P*) can be written as,

$$P = KA_{abs}\gamma \tag{2.1}$$

where A_{abs} is the absorbency of the sample, γ is the probability of noradiative transitions after excitation, and *K* is a coefficient determined by the thermal properties of the sample and by the spectrometer (coating Yang and Zhang, 2003). In general, the generation of the

PA signal involves two main aspects; heat production and the generation of acoustic waves. Heat production concerns with the absorption process bumped into a particular gas sample and the consequent energy transfer from vibrational to translational degrees of freedom (*V-T* relaxation). This energy transfer results in what is called heat production rate *H*. The second aspect of PA theory concerns the acoustic wave generation which is related to the heat production rate (Meyer and Sigrist, 1990).

2.4.1 Heat production rate

Exposing a gas with molecular density *N* to modulated light will result in the excitation of some vibrational states. This gas can be described by a two-level system consisting of vibrational ground state with density $N - N'$ and excited state with density N'. To calculate the density N', the following rate equation can be used (Meyer and Sigrist, 1990):

$$\frac{dN'}{dt} = (N - N')R - N'\left(R + \frac{1}{\tau}\right). \tag{2.2}$$

where τ is the total life time of the excited state and *R* is the rate of excitation caused by the incident radiation for which, the energy corresponds to the wave number k and photon flux Φ such that:

$$R = \Phi\sigma. \tag{2.3}$$

where σ is the molecular absorption cross section.

$$(\tau)^{-1} = (\tau_n)^{-1} + (\tau_r)^{-1} \tag{2.4}$$

where τ_n , τ_r denotes the nonradiative and radiative relaxation time constants respectively. Since $\tau_r \gg \tau_n$, then τ is of the order of τ_n.

The rate constant R is usually sufficiently small, therefore, N' is considerably smaller than N. Under these approximations eqn. (2.2) can be reduced to (Meyer and Sigrist, 1990):

$$\frac{dN'}{dt} = NR - N'\frac{1}{\tau} \tag{2.5}$$

The complex harmonic modulation of the incident radiation is given by eqn. (2.6). in which, the time-dependent term with the angular frequency ω is what contributes to the PA signal.

$$\Phi = \Phi_{.}\left(1 + e^{i\omega t}\right) \tag{2.6}$$

$\Phi_{.}$ is the incident photon flux.

Substituting eqns. (2.3) and (2.6) in eqn. (2.5) yields:

$$\frac{dN'}{dt} = N\sigma\Phi_{.}\left(1 + e^{i\omega t}\right) - N'\frac{1}{\tau} \tag{2.7}$$

According to Meyer and Sigrist, 1990, eqn. (2.7) has the following solution:

$$N' = \frac{N\Phi_{.}\sigma\tau}{[1+(\omega\tau)^2]^{1/2}} e^{i(\omega t-\varphi)} \tag{2.8}$$

$$\varphi = \arctan(\omega\tau) \tag{2.9}$$

with φ representing the phase lag between N' and photon flux Φ .

The heat production rate H is related to N' through the following relation

$$H = N'(hc\Delta k/\tau_n) \tag{2.10}$$

where $(hc\Delta k)$ is the average thermal energy released due to the nonradiative relaxation of the excited state. h denotes Planck's constant and c the speed of light. If the de-excitation process results in the conversion of the excited state to the ground state, then $\Delta k = k$, and since $\tau_n = \tau$, eqn. (2.10) can be written as (Meyer and Sigrist, 1990):

$$H = N^{'}(hck/\tau) \tag{2.11}$$

Substituting eqns. (2.8) and (2.9) in eqn. (2.11) yields

$$H = \frac{N\Phi_{.}\sigma\tau}{[1+(\omega\tau)^2]^{1}/_{2}}\, e^{i(\omega t-\varphi)}\left(\frac{hck}{\tau}\right) \tag{2.12}$$

Since the amplitude $I_{.}$ of the light intensity can be represented by

$$I_{.} = \Phi_{.}hck \tag{2.13}$$

then, the heat production rate H is related to $I_{.}$ as follows

$$H = \frac{N\sigma I_{.}}{[1+(\omega\tau)^2]^{1}/_{2}}\, e^{i(\omega t-\varphi)} \tag{2.14}$$

Define

$$H_{.} = \frac{N\sigma I_{.}}{[1+(\omega\tau)^2]^{1}/_{2}} \tag{2.15}$$

Hence,

$$H = H_{.}\, e^{i(\omega t-\varphi)} \tag{2.16}$$

For low modulation frequencies $\omega \ll 10^6\ S^{-1}$, i.e., for $\omega\tau \ll 1$, eqn. (2.15) can be simplified to (Meyer and Sigrist, 1990):

$$H_{.} = N\sigma I_{.} \tag{2.17}$$

and the phase shift vanishes. These results in

$$H = N\sigma I_{.}\, e^{i(\omega t)} \tag{2.18}$$

Since the conditions of low modulation frequency i.e., $\omega \ll \tau^{-1}$, and absence of optical saturation i.e., $R \ll \tau^{-1}$, are usually fulfilled, then eqn. (2.18) contains the essence of most PA studies (Meyer and Sigrist, 1990).

2.4.2 Generation of acoustic waves

The second aspect of PA theory involves the generation of the acoustic wave which is related to the heat production (Meyer and Sigrist, 1990). In PAS experiments, light absorption results in an electronically or vibrationally excited state. The nonradiative decay of the excited state generates an acoustic pressure wave as a result of volume expansion which is created by the local increase in temperature as shown in the following scheme in which A denotes the molecule in its lowest energy (ground state) while A^* denotes the excited molecule (Autrey et al, 2001).

$$A + h\upsilon \rightarrow A^*$$

$$A^* \rightarrow A + heat$$

Pressure waves generated by the released heat due to the nonradiative decay of the sample can be detected by means of a microphone or a piezoelectric transducer.

As shown in eqn. (2.6). The alternating component of the heating function can be written as (Khan and Diebold, 1996):

$$H = \alpha I_{\circ} e^{-i\omega t} \tag{2.19}$$

where α is the optical absorption coefficient, $I_{\circ}$ is the incident beam intensity, and ω is the frequency of modulation. If the pressure of the gas is low enough such that, there is no pressure broadening (Lachish et al, 1987), the optical absorbance coefficient α will be related to the gas density N throughout the molecular absorption cross section σ, where

$\alpha = \sigma N$. Rosencwaig and Gersho in 1976 have developed the theory of the PA effect. They have shown that PA theory involves a one-dimensional heat flow model applicable in most cases (George et al, 2000). Morse and Ingard in 1961 have shown that the PA signal can be expressed as a solution of the following partial differential equation:

$$\nabla^2 P(r,t) - \frac{1}{c_o^2}\frac{\partial^2}{\partial t^2} P(r,t) = -\frac{(\gamma-1)}{c_o^2}\frac{\partial}{\partial t} H(r,t) \qquad 2.20$$

Kreuzer had intensively studied the generation of acoustical waves in resonant cells. According to these studies, the pressure inside a cylindrical resonant cell operating at its first radial mode is given by:

$$P_1(r,t) = A_1(\omega)\tilde{P}_1(r)exp\big(i(\omega t - \phi)\big) \qquad 2.21$$

with

$$A_1(\omega) = \frac{\omega}{\left[(\omega^2-\omega_1^2)^2+(\omega\omega_1/Q_1)^2\right]^{1/2}} \frac{\gamma-1}{V} \times \int_V \tilde{P}_1^*(r)\tilde{H}(r,\omega)dV \qquad 2.22$$

and

$$\phi = arctan\left(\frac{\omega^2-\omega_1^2}{\omega\omega_1/Q}\right) \qquad 2.23$$

(Meyer and Sigrist, 1990).

The normalized pressure amplitude $\tilde{P}_1(r)$ of the first radial normal mode is related to the 0^{th} order Bessel function J_o, and $\tilde{P}_1^*(r)$ is its complex conjugate. The eigenfrequency ω_1 corresponding to such situation is given by:

$$\omega_1 = c_o\left(\frac{\pi\alpha_{01}}{r_o}\right) \qquad 2.24$$

c_o is the speed of sound within the sample.

r_o is the radius of the cell.

Q is the quality factor regarding the first radial mode damping as a result of heat conduction and viscosity losses of the acoustical energy.

$\pi\alpha_{01}$ is the first solution of the 0th order Bessel function usually calculated by applying the boundary conditions at $r = r_o$ such that

$$\frac{dJ_o(x)}{dx} = 0 \qquad 2.25$$

$\pi\alpha_{01} = 3.832$

γ is the specific heat ratio defined as:

$$\gamma = \frac{C_p}{C_v} \qquad 2.26$$

C_p, C_v are the specific heat capacity at constant pressure and volume respectively.

For PA resonant cells, the coupling integral of eqn. 2.21 can be expressed as (Meyer and Sigrist, 1990):

$$\int_V \hat{P}_1^*(r)\tilde{H}(r,\omega)dV = Gl\tilde{H}_o e^{-i\hat{\theta}} \qquad 2.27$$

where *G* is the geometrical factor, *l* is the length of the cell, $\tilde{H}_o, \hat{\theta}$ denotes the amplitude and phase shift of the heat rate with respect to laser-beam modulation. Substitution of eqns. 2.22, 2.23 and 2.27 into eqn. 2.20, will result in the pressure taking the following form (Meyer and Sigrist, 1990):

$$P_1(r,t) = (\gamma - 1)G(l/V)(Q/\omega_1)\tilde{H}_o\hat{P}_1(r)e^{i(\omega_1 t - \hat{\theta})} \qquad 2.28$$

2.5 Helmholtz resonator

Helmholtz resonance is simplified as the phenomenon of air resonance inside a cavity. The device was created in the 1850s by Hermann Von Helmholtz, and bearing his name, to show the height of various tones (http://en.wikipedia.org/wiki/Helmholtz_resonator). Helmholtz resonator or oscillator is a gas container with an open port**.** The volume of air in the open hole vibrates because of the oscillatory motion of air particles inside. A good example of Helmholtz resonator is an empty bottle with one blowing across its top (McLennan, 2003). Conventional Helmholtz resonators consist of a cavity connected to a neck having length and cross-sectional diameter much smaller than the dimension of the cavity. Once the air inside the cavity is forced, its pressure will increase. When the external force eliminates, the higher-pressure air inside will flow out. Due to the inertia of the air in the neck, this rush of air flowing out the resonator will tend to over-compensate, thus, the pressure inside the cavity will be left at a slightly lower value than outside. This negative pressure will result in air being drawn back into the cavity (http://en.wikipedia. org/wiki/Helmholtz_resonator). Thus, the air in the neck can vibrate like a mass on a spring (McLennan, 2003). Fig 2.4 shows a schematic diagram of the operation principle of a Helmholtz resonator. The air in the neck represents the mass (http://en.wikipedia.org/wiki/Helmholtz_resonator), meanwhile, the trapped air pressure inside the cavity represents the spring, and so, periodic changes in the pressure inside the chamber causes the air in the neck to move in and out the neck.

The well-known Helmholtz resonator has found applications in a wide variety of technological significant problems. Tang and Sirignano has provided an excellent discussion of the use of this resonator in reducing the organized oscillations inside jet engines(coating, Selamet and Dickey, 1995). The concept of Helmholtz resonance and its classical theory have been applied to design and analyze different systems, including tuned intake manifolds of vehicles, tuned pulse combustors, discharge systems of compressors

and small engines, as well as noise reduction elements (Selamet and Dickey, 1995). Helmholtz resonance was also applied to internal combustion engines, subwoofers and acoustics (http://en.wikipedia. org/wiki/Helmholtz_resonator).

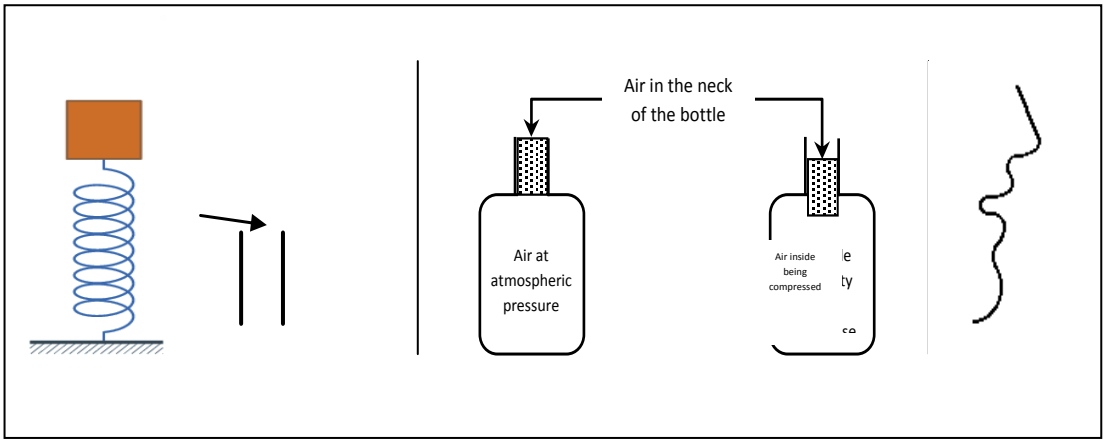

Fig 2.4 A scheme simulating the operation of Helmholtz resonator, (After: Mclennan, 2003).

It has been very useful in dealing with the low-frequency noise propagating inside air conditioners in which flow velocities are usually less than 20 m/s. Since the conventional dissipative type silencers are usually not effective for low-frequency noise attenuation and produce significant static air pressure loss, then, the design of the resonator is of great importance in building noise control. The development of active control has provided another means to undertake the low-frequency channel noise problem. The stable and vigorous performance of Helmholtz resonators makes them one of the best choices in the noise control industry (Tang, 2005). In the past few decades, extensive efforts on how to improve the transmission loss produced by such resonator have been made, whereas, different geometries and arrangements have been considered. For example, the effects of different orifice shapes has been studied by Chanaud, Dicky and Selamet have investigated the cavity aspect ratio effects, Selamet and Lee proposed extending the neck into the resonator cavity and Griffin et al suggested coupling two resonators. The acoustic

impedance and the sound absorption coefficient of a Helmholtz resonator with a tapered neck are investigated experimentally by Tang, 2005. The geometry of the resonator was found to affect the resonance frequency of the resonator (Chanaud, 1997). In photoacoustic experiments, a sensitive microphone is attached to the neck of the resonator in order to record the springiness of the air inside, where the springiness of air in the neck is caused by the periodic change of the air pressure in the cavity produced as a result of periodic heat deposition from the investigated sample into the surrounding media, usually air.

2.5.1 Quantitative explanation

The design of the previous low frequency resonators to predict the resonance frequency and transmission loss characteristics were commonly studied using the classical theory of Helmholtz resonator. This theory applies Newton's second law to a slab mass in the resonator's neck acting between an adiabatically compressed volume at one end and the incident pressure on the resonator at the other (Selamet and Dickey, 1995).

A pressure change ΔP being applied on a column of air with cross sectional area A will result in a force of the form:

$$F = A\ \Delta P \qquad 2.5.1$$

multiplying both sides by $\frac{\Delta V}{\Delta V}$ yields:

$$F = A\ \Delta P = A\frac{\Delta P}{\Delta V}\ \Delta V \qquad 2.5.2$$

where ΔV is the change in volume of a slice of air with cross sectional area A and thickness L, being displaced by x meters, then eqn. 2.5.2 becomes (http://scienceworld .wolfram.com/physics/helmholtzresonator.html).:

$$F = A\ \Delta P = A\frac{\Delta P}{\Delta V}\ Ax \qquad 2.5.3$$

multiplying both sides by $\frac{V}{V}$ yields:

$$F = A\ \Delta P = AV\frac{\Delta P}{\Delta V}\frac{Ax}{V} \qquad 2.5.4$$

were *V* is the volume of the air inside the cell.

The property that determines the extent to which an element of the medium changes its volume as the pressure applied to it increases or decreases, is the *bulk modulus B,* defined as (Halliday and Resnick, 1988):

$$B = -\frac{\Delta P}{\Delta V/V} = -V\frac{\Delta P}{\Delta V} \qquad 2.5.5$$

Plugging eqn. 2.5.5 into 2.5.4 yields:

$$F = A\ \Delta P = A\left(V\frac{\Delta P}{\Delta V}\right)\frac{Ax}{V} = -AB\frac{Ax}{V} = -A^2B\frac{x}{V} \qquad 2.5.6$$

For an adiabatic process,

$$\left(\frac{\partial P}{\partial V}\right)_s = \frac{C_P}{C_V}\left(\frac{\partial P}{\partial V}\right)_T \qquad 2.5.7$$

For an ideal gas

$$\left(\frac{\partial P}{\partial V}\right)_T = -\frac{P}{V} \qquad 2.5.8$$

(Sears and Salinger, 1975), and so, eqn. 2.5.7 becomes:

$$\left(\frac{\partial P}{\partial V}\right)_s = -\frac{C_P}{C_V}\frac{P}{V} \quad \Rightarrow \quad -V\left(\frac{\partial P}{\partial V}\right)_s = \gamma P \qquad 2.5.9$$

where $\gamma = \frac{C_P}{C_V}$ is the specific heat ratio. Therefore, eqn.2.5.5 can be written as:

$$B = \gamma P \qquad 2.5.10$$

where *P* is the undisturbed pressure. Hence, eqn. 2.5.6 now becomes:

$$F = -\frac{A^2\gamma P}{V}\ x \qquad 2.5.11$$

According to Newton's 2nd law being applied to the slice of air:

$$F = ma = \rho AL\ \frac{d^2x}{dt^2} \qquad 2.5.12$$

with $m = \rho AL$, and $a = \frac{d^2x}{dt^2}$.

Equating eqns. 2.5.11 and 2.5.12 yields (http://scienceworld.wolfram.com/physics /Helmholtzresonator.html,2009):

$$\rho AL \frac{d^2x}{dt^2} = -\frac{A^2\gamma P}{V} x \qquad 2.5.13$$

Rearranging gives:

$$\frac{d^2x}{dt^2} + \left(\frac{A\gamma P}{\rho LV}\right) x = 0 \qquad 2.5.14$$

Eqn. 2.5.14 represents the simple harmonic motion of a slice of air within the neck of the resonator for which, the angular frequency ω is given by:

$$\omega = \sqrt{\frac{A\gamma P}{\rho LV}} = \sqrt{\frac{AB}{\rho LV}} = \sqrt{\frac{B}{\rho}}\sqrt{\frac{A}{LV}} = v\sqrt{\frac{A}{LV}} \qquad 2.5.15$$

The quantity $\sqrt{\frac{B}{\rho}} = v$, where v is the speed of sound (Halliday and Resnick, 1988). The resonance frequency of the resonator is given by $f = \frac{\omega}{2\pi}$, and thus equals to:

$$f = \frac{v}{2\pi}\sqrt{\frac{A}{LV}} \qquad 2.5.16$$

2.4 Microphone

Microphones are types of transducers; devices used to convert energy from one form to another (http://www.mediacollege.com/audio/microphones/condenser.html). A micro-phone converts sound into an electrical signal and thus, is an acoustic-to-electric transducer or sensor. Telephones, tape recorders, hearing aids, live and recorded audio engineering, radio and television broadcasting and in computers for recording voice, VoIP, and for non-

acoustic purposes such as ultrasonic checking are different fields and applications in which microphones are used (http://en.wikipedia.org/wiki/ microphone). All microphones share one thing in common: the Diaphragm, a thin piece of material which vibrates when it is struck by sound waves. In contrast, Different microphone types have different ways of converting energy (http://www.mediacollege. com/audio/microphones/condenser.html). The conversion technology used in microphones and the application they were designed for, represent the main reasons according to which one type of microphones differ from another. Crystal microphones use the phenomenon of piezoelectricity – the ability of some material to produce voltage once being subject to pressure – to convert vibrations into an electrical signal. Piezoelectric transducers are usually used as contact microphones (http://en.wikipedia. org/wiki/microphone). In condenser microphones, energy is stored in an electrostatic field. Condenser microphones usually use an external low bias voltage in the range of 9 volts in addition to a parallel plate capacitor to convert acoustical energy into electrical energy. The front plate of the capacitor is made of a very light material which acts as a diaphragm. When a pressure wave strikes the diaphragm, the distance between the diaphragm and the metal plate decreases, hence, increasing the capacitance between these two surfaces due to the inverse proportionality between capacitance and distance. When the plates become closer, capacitance increases and a charge current occurs. During wave rarefaction, the plates become farther apart resulting in capacity leakage, and so, a discharge current occurs (http://www.mediacollege.com/audio/ microphones/condenser.html). In this study, the used microphone is a condenser microphone. It is a product of *Knowles Electronics* with item number *wz398*. It was used as a sensor of the photoacoustic signals being generated inside the cavity. In this study, the microphone was coupled to the cavity of the Helmholtz resonator in order to detect the springiness of air in the neck of the resonator as a result of the induced periodic pressure

fluctuations in the chamber as a result of periodic heat deposition from the sample into the surrounding air.

2.7 Michelson interferometer

Interferometry is an investigation technique based on the creation of interference patterns once studying optical phenomena (http://www.physics.uiowa.edu/~rvogel/int_lab _2007_1/docs/B1_Michelson_V4.doc). The quick response of IR, visible and UV radiation detectors in the frequency domain (>600 GHz) is sometimes insufficient, alternatively, interferometry is used to record the spectrum in the length domain (Hollas, 1996). In spite of their different shapes and sizes, all interferometers share the same concept of operation characterized by splitting an incoming beam into two equal beams directing through different paths and then recombining them in order to interfere (http://www.physics. uiowa.edu/~rvogel/int_lab_2007_1/docs/B1_Michelson_V4.doc).

Basically, interferometers are optical measurement tools capable of detecting infinitesimal changes in the optical path length of a beam of light (http://skiper.physics. sunysb.edu/~ralf/phy300/lab6.pdf). They are used to precisely measure wavelengths, distances, refraction indices, and temporal coherence of optical beams (http://www.colorado.edu/physics). Interferometers are also widely applied in measuring the variations of the phase front of light among several optical methodologies. In the field of metrology, interferometry has been applied successfully to dimensional and surface roughness measurements with a minimum detection limit below nanometers. One of the

basic configurations of interferometry is the amplitude-division interferometer (ADI) in which, a light beam is divided into two beams, one of which directs through a sample and recombines with the other to result in a fringe pattern. Another configuration is the time-division interferometer (TDI) – in which the probe and reference beams are temporally displaced but travels collinearly in one single arm – used to measure the transient refractive index change (Kobayashi and Misawa, 1997). Among all optical instruments, Michelson interferometer – designed by A. Michelson in 1891 – is one of the most useful ever (http://physics.usask.ca/~angie/ep421/ lab3/theory.html). After his triumph in measuring the speed of light so accurately, and with Morley's help, Michelson set himself to a new challenge represented by detecting the ether – a hypothetical medium through which light waves were proposed to propagate – just as sound waves in the air. The null result of Michelson-Morley experiment in detecting the proposed ether led Einstein to postulate his special theory of relativity regarding the speed of light to be constant in all frames of reference (Http://galileoandeinstein.physics.virginia.edu/lectures/michelson.html, 1996). In Michelson's day, and by international agreement, the meter was defined to be the distance between two fine scratches on a metal bar preserved at Sevres near Paris (Halliday and Resnick, 1988). After that Michelson's interferometer was used to determine the wavelength of spectral lines accurately. According to these measurements, the meter was defined to be 1,650,763.73 times the wavelength of the orange-red spectral line of Krypton-86 (http://physics.usask.ca/~angie/ep421/lab3/theory.html). An extensive revision of the Fourier spectroscopy based on the usage of Michelson's interferometer – with thin beam splitter – in the far-infrared (FIR) limit was given by Chantry (Jongbloets et al, 1980). Spectral analyses in the FIR limit are based on the phase shift of one beam of Michelson's interferometer resulting from the time-dependent refractive index of gaseous plasma (Bartlett et al, 1977). The beam splitter used in Michelson interferometer can either

be a partially silvered mirror or a thin layer – of different refractive index – being sandwiched between two prisms (http://skiper.physics.sunysb. edu/~ralf/phy300/ lab6.pdf). Fig 2.5 shows a scheme of Michelson's interferometer and its basic components. The main concept of operation of Michelson's interferometer, as illustrated in Fig 2.5, is simply the recombination of the two split beams after being reflected from both mirrors to form the fringe pattern (Bartlett et al, 1977).

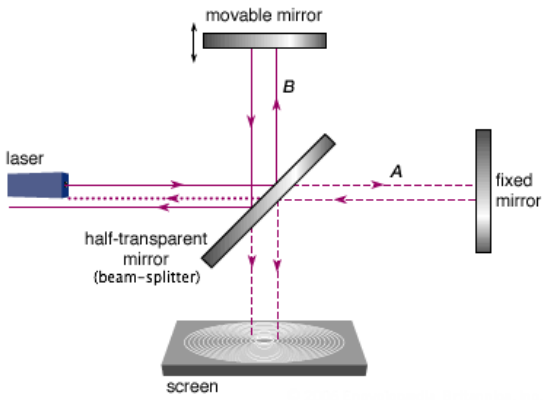

Fig 2.5 A scheme of Michelson Interferometer showing its basic components, (After: http://www.physics.uiowa.edu/~rvogel/int_lab_2007_1/docs/B1_Michelson _V4.doc)

The idea is that, the incoming beam splits into two equal beams once it is encountered by a 50% beam splitter oriented at 45°; one of the two beams transmit through toward the fixed mirror whereas, the second is deflected at 90° toward the movable mirror. The transmitted beam is back reflected toward the beam splitter where 50% of which is deflected at 90° to hit the screen (detector) and the other half transmits through toward the source and so, with no concern. The deflected beam is back reflected from the movable mirror towards the beam splitter where 50% of which transmits through toward the screen (detector) and the other half is deflected at 90° towards the source which is again of no concern. Only two halves of the two main halves that are directed toward the screen interfere to produce the fringes (http://www.colorado.edu/physics). This is a disadvantage of Michelson interferometer assigned as the beam splitter efficiency i.e., for totally constructive interference, only ~ 50% of the incident energy reaches the detector, whereas, the other is sent towards the source (Cano and Mattioli, 1967). The produced interference pattern is a series of sine waves and is called an interferogram usually subjected to a Fourier transformation where a measurement spectrum of the sample is created (Workman and Springsteen, 1998). The transmitted and reflected waves are mutually coherent since they were both derived from the same source (http://www.colorado.edu/physics). A difference in the path length between the beams propagating through the perpendicular arms of the interferometer will result in a stationary fringe pattern (Jongbloets et al, 1980). The optical path length difference between the two arms may be accomplished by either physically translating the movable mirror in a direction normal to its surface, or by introducing a light transparent medium in one arm of the interferometer (http://www.physics. uiowa.edu/~rvogel/int_lab_2007_1/docs/B1_Michelson_V4.doc). In either way, as the path length changes, fringes will in turn be shifted. Bright and dark fringes are the result of the change in path length. If the difference is an integral number of wavelengths, the

central fringe will be bright (constructive interference), meanwhile, if the difference was half-integral number of wavelengths, then the central fringe will be dark (destructive interference) (http://www.colorado.edu/physics). In this study, the difference in the path length will be subject to the change in the refractive index inside the chamber being introduced at one arm of the interferometer.

2.7.1 Quantitative understanding

The amplitude *A* and the intensity *I* of a plane wave are related to each other as follows:

$$I \propto \langle A \rangle^2 \qquad 2.7.1$$

were *A* is the amplitude such that (http://www.physics.uiowa.edu/~rvogel/int_lab_2007_1/docs/B1_Michelson_V4.doc,2007):

$$A(x,t) = a\,sin(\omega t - kx) \qquad 2.7.2$$

with ω being the angular frequency, k the wave number and x the distance travelled from the beam splitter to the detector through the mirrors as shown in Fig 2.6 below.

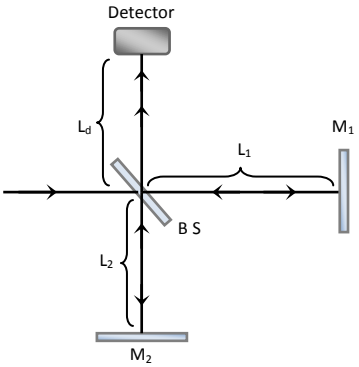

Fig 2.6 Path lengths in Michelson's interferometer.

Once the wave struck the beam splitter it splits into two, the first travels a distance L_1 to mirror M_1 and the other, a distance L_2 to mirror M_2, and then they both travel a distance L_d

from the beam splitter to the detector. By substitution, the two waves reaching the detector are thus:

$$A_1(x,t) = a\ sin\big(\omega t - k(2L_1 + L_d)\big) \qquad 2.7.3$$

$$A_2(x,t) = a\ sin\big(\omega t - k(2L_2 + L_d)\big) \qquad 2.7.4$$

and since they are mutually coherent, they will interfere. The detected signal A_{out} is simply, the superposition of these two waves represented by:

$$A_{out}(x,t) = A_1(x,t) + A_2(x,t) \qquad 2.7.5$$

$$A_{out}(x,t) = 2a\ cos\big(k(L_1 - L_2)\big)\ sin\big(k(L_1 + L_2)\big) \qquad 2.7.6$$

But according to eqn. 2.7.1 and through some algebra it is obvious that the intensity that reaches the detector is given by:

$$I_d = I_0 cos^2\big(k(L_1 - L_2)\big) \qquad 2.7.7$$

Where the time average of sin^2 is $\frac{1}{2}$ and so, the term $sin^2\big(k(L_1 - L_2)\big)$ didn't appear in the intensity relation and its average was included in the I_0 constant. Substituting the value of $k = \frac{2\pi}{\lambda}$, and $\Delta L = |L_1 - L_2|$ in eqn. 2.7.7 yields (http://www.physics.uiowa. edu/~rvogel/ int_lab_2007_1/docs/B1_Michelson_V4.doc, 2007):

$$I_d = I_0 cos^2\left(\frac{2\pi}{\lambda}\Delta L\right) \qquad 2.7.8$$

Eqn. 2.7.8 shows that, a train of maxima and minima of the detected intensity will be the result of the following two cases:

- For the intensity to be maxima, $\frac{2\pi}{\lambda}\Delta L = \pi$ and so, $\Delta L = \frac{m\lambda}{2}$, $\quad m = 0, 1, 2, \ldots$
- For the intensity to be minimal, $\frac{2\pi}{\lambda}\Delta L = \frac{\pi}{2}$ and so, $\Delta L = \frac{\left(m + \frac{1}{2}\right)\lambda}{2}$, $\quad m = 0, 1, 2, \ldots$

As ΔL changes, the phase of the two waves relative to each other will also change where the interference pattern is the consequence. If ΔL equals an integral number of half wavelengths, the two waves will be in-phase and a maxima results, and if it equals a multiple of have integrals of the half of the wavelength, the two waves will be out of phase and a minima results (Halliday and Resnick, 1988; http://www.physics.uiowa.edu; http://physics.usask.ca). When the movable mirror is translated a distance *d*, a train of *N* fringes is the consequence such that, the wavelength or any integral multiple of it equals twice the translated distance, hence (http://www.physics.uiowa.edu/~rvogel/ int_lab_2007_1/docs/B1_Michelson_V4.doc, 2007),

$$2d = N\lambda \qquad 2.7.9$$

or simply:

$$N = \frac{2d}{\lambda} \qquad 2.7.10$$

As mentioned elsewhere, this study deals with the path length changes due to refractive index gradient. The optical path length of a cell that contains a gas of some refractive index *n* is given by (http://www.physics.uiowa.edu/~rvogel/ int_lab_2007_1/docs/B1_ Michelson_V4.doc, 2007):

$$L = nt \qquad 2.7.11$$

where *t* is the optical path length of an evacuated cell. Since the beam traverses the cell twice, the difference in optical path length ΔL is given by:

$$\Delta L = 2(n-1)t \qquad 2.7.12$$

and since $\Delta L = 2d$, and using eqn. 2.7.9 then,

$$N\lambda = 2(n-1)t \qquad 2.7.13$$

solving for *n* yields

$$n = \left(\frac{N\lambda}{2t}\right) + 1 \qquad 2.7.14$$

where n is the refractive index and N is the number of fringes.

The above equation gives the relation between the refractive index and the number of fringes being detected for some given wavelength and length of the cell (http://www.physics. uiowa.edu/~rvogel/int_lab_2007_1/docs/B1_Michelson_V4.doc). According to eqn. 2.7.14, a gradient change in the refractive index of the sealed gas due to heat deposition in the medium i.e., IR absorption, will result in the shift of the fringes by an amount comparable to the absorbed energy. If the gradient in refractive index was sufficiently small such that, it doesn't result in the shift of integral number of fringes, then fringe widening is the consequence and so, a relation between the fringe radius and the refractive index would be sufficient. When two spherical waves of different radii (R_1 and R_2) interfere, circular fringes are the consequence. Fig 2.7 shows the geometrical formation of circular fringes. Reflection of the incident light from the beam splitter will result in the formation of a virtual image of the source S i.e., S'. Replacing the point source S by its image S' will lead to the formation of extra two images; S_1' from mirror M_1' – a virtual image of mirror M_1 – and S2' from mirror M_2. The optical path difference at some point P lying on a circular fringe is given by:

$$\delta = 2\Delta d \cos\theta \qquad 2.7.15$$

Recall that, once $\delta = m\lambda$, point P lays on a bright fringe (http://www.colorado.edu/ physics/phys5430/Michelsoninterferometer.pdf, 2001).

Suppose that Δd is set such that, the center of the fringe pattern is a spot of maximum brightness labeled as P = 0, then the polar angle of the m[th] fringe – where the point P lies – is given by:

$$\theta_p \simeq \frac{R_P}{R_o}, \quad cos\theta_p \approx 1 - \frac{\theta_p^2}{2} = 1 - \frac{R_p^2}{2R_o^2} \qquad 2.7.16$$

Substitution in eqn. 2.7.15 yields:

$$m_p\lambda = 2\Delta d\left(1 - \frac{R_p^2}{2R_o^2}\right) \qquad 2.7.17$$

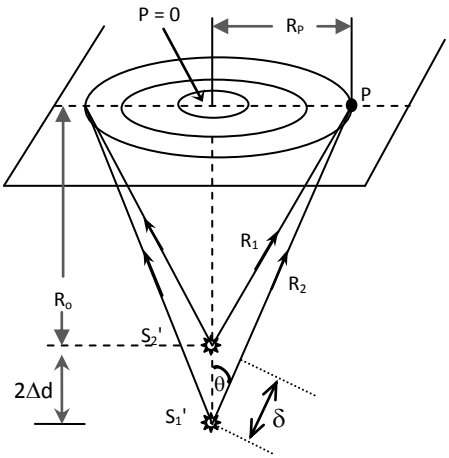

Fig 2.7 Formation of circular fringes, (After: http://www.colorado.edu/physics/ phys5430/ Michelsoninterferometer.pdf, 2001).

For the central spot, $R_p = 0$, and so,

$$1 - \frac{m_o\lambda}{2\Delta d} = 0 \qquad (a)$$

For the m[th] fringe, where P lies;

$$1 - \frac{m_p\lambda}{2\Delta d} = \frac{R_p^2}{2R_o^2} \qquad (b)$$

Subtracting (a) from (b) yields:

$$R_p = R_o\sqrt{\frac{P\lambda}{\Delta d}} \qquad 2.7.18$$

For any slight change in the refractive index, the optical path difference δ – according to eqn. 2.7.12 – is given by:

$$\delta = 2(n-1)t \qquad 2.7.19$$

Rearranging the terms and substituting eqns. 2.7.15 and 2.7.19 in eqn. 2.7.18 and doing some algebra yields:

$$R_p = R_o\left(\frac{1}{\sqrt{\left(\frac{(n-1)t}{P\lambda}\right)+\frac{1}{2}}}\right) \qquad 2.7.20$$

Eqn. 2.7.20 represents the relation between the radius of some fringe with order P and the refractive index n of the gas located at one arm of the interferometer.

2.8 Infra-red spectroscopy

The part of the electromagnetic spectrum extending from the red end of the visible spectrum to the microwave region is the infrared spectrum (Hallam, 1968). This region is defined arbitrarily as 10 – 13000 cm^{-1} (1000 – 1 µm), it includes the far, mid and near-infrared regions (Hollas, 1996). Near-IR region is represented as 13000 – 4000 cm^{-1} (0.78 – 3 µm) with relative energy in the range of 10 – 37 Kcal/mole. Mid-IR region is represented as 4000 – 400 cm^{-1} (3 – 30 µm) with relative energy in the order of 1 – 10 Kcal/mole. Far-IR region is represented as 400 – 10 cm^{-1} (30 – 1000 µm) with relative energy in the range of 0.1 – 1 Kcal/mole (http://orgchem.colorado.edu/hndbksupport /IRtutor/tutorial.html). Infrared spectroscopy is the measurement of the absorbed IR radiation by a sample being encountered by IR beam. It is mostly used in the field of organic and inorganic chemistry (http://prenhall.com/settle/chapters/ ch15.pdf). For

identification analysis and control, areas of infrared transmission, reflection and transmission spectroscopy dominates the commonly used spectroscopic methods (Barr, 1969). Traditionally, IR spectroscopy has been carried out in absorption. In analytical chemistry, the huge concentration was on the basic principles and applications of infrared emission spectroscopy (Bernath, 2000). Historically, infrared spectroscopy in the field of chemistry has began with the research of Goblentz in 1903, whereas, its great potential in that field has became realized about thirty years later (Hallam, 1968). Commercial spectrometers and single-beam prism instruments were produced for the first time in 1949, which were developed into double-beam instruments by the mid of 1950s. By 1960, all research laboratories were claimed to have IR instrumentation (Hallam, 1968). The most important instrument for far-, mid-, and near-infrared spectroscopy nowadays, is a Michelson interferometer based on double-beam interferometry (Hollas, 1996). Once a sample – located at the path of one beam of the interferometer – absorbs IR radiation, a sinusoidal modulation of the interference pattern is the consequence (Hallam, 1968). The uniqueness of IR region arises from the fact that, all molecules, except the homonuclear diatomics, have at least one allowed vibrational-rotational transition. Despite of the existence of infrared electronic transitions and far-infrared rotational transitions accompanied with few light molecules, IR spectroscopy corresponds mostly to vibrational spectroscopy (Bernath, 2000). Once a molecule is exposed to IR radiation, absorption occurs if the radiant energy matches a specific molecular vibrational energy (http://orgchem. colorado.edu/hndbk support/IRtutor/tutorial.html). For the IR radiation to be absorbed by a molecule, a net change in the dipole moment of the absorbing molecule caused by rotations or vibrations must be involved, this change – which is the result of interactions between the electric field of the radiation and the molecular dipole moment – causes the change in the amplitude of molecular vibration (http://teaching.shy.

ac.uk/hwb/chemistry/ tutorials/molspec/irspec1.html). In general, molecules have specific frequencies of rotation and vibration corresponding to discrete energy levels, vibrational modes. IR-active vibrational modes must be associated with permanent dipole moments (http://en.wikipedia.org/wiki/Infrared_spectroscopy). Recall that; for a molecule to be IR-active doesn't ever mean that all possible vibrations within the molecule will result in an absorbing band in the IR region. The condition of dipole moment change implies that homonuclear diatomic molecules like H_2, N_2, etc. cannot be IR-active since they have zero dipole moment and since bond stretching will not produce a one. The IR-activity of heteronuclear diatomic molecules arises from bond stretching which leads to changes in the permanent dipole moment of the molecule in view of the fact that the dipole moment is proportional to the distance between the atoms (http://www.le.ac.uk/ chemistry /pdf/ teachers workshops.pdf). In view of the fact that each atom has 3 degrees of freedom, a molecule of N atoms has $3N$ degrees of freedom. In a non-linear molecule, 3 degrees of freedom are assigned to translational motion and another 3 assigned to rotational motion leaving the molecule with $3N - 6$ internal vibrations (fundamental vibrations). The fundamental vibrations of a linear molecule are $3N - 5$ since there is no rotation about bond axis thus, leaving the molecule with only two rotational degrees of freedom. This means that, for a diatomic heteronuclear molecule like CO, only one fundamental vibration exists but, for a triatomic non-linear molecule like H_2O, there is three allowed vibrational modes (Banwell, 1972). In IR spectroscopy, the number of absorption bands that is experimentally observed differs from the total number of fundamental vibrations; it might be reduced or exceed the total number of fundamental vibrations. The existence of some IR-inactive modes leads the number of fundamental vibrations to be reduced, whereas, appearance of overtones – energy absorptions that arose when the vibrational quantum number is changed by 2 rather than 1 (http://www.umsl.edu/~orglab/ documents

/IR/IR2.html) –, coupling interactions of two fundamental absorption frequencies, combinations of fundamental frequencies and differences of fundamental frequencies leads to the generation of additional bands. The absorbed IR energy is converted to different types of molecular motion were the majority of the converted energy is vibrational. It is usually categorized in two main types; stretching and bending. In spite of the fact that absorption involves discrete, quantized energy levels, molecular vibrations are commonly accompanied by rotational motion. This companion leads the spectrum to contain energy bands, usually observed in the mid-IR region, instead of discrete lines (http://prenhall.com/settle/ chapters/ch15.pdf). While analyzing the IR spectrum of a given compound no matter how simple it is, most of the molecular vibrations are assigned to certain peaks in the spectrum. In the complex pattern of the spectrum below 1500 cm^{-1}, IR absorption is the result of skeletal vibrations, thus, molecular vibrations are hardly assigned to the peaks in this area. Such complexity gives rise to an important advantage, that is, this region in the IR spectrum can serve as a fingerprint of a given compound (Banwell, 1972; http://www.le.ac.uk/chemistry/pdf/teachersworkshops.pdf).

Infrared spectroscopy is usually expressed in the form of a spectrum for which, wave-number and absorption intensity or percent transmittance are the coordinates. Transmittance (T) – the ratio of transmitted power (I) through the sample to that being incident to it (I_o) – is related to the absorbance (A) through the following relation (http://prenhall.com/settle/chapters/ch15.pdf):

$$A = \log_{10}\left(\frac{1}{T}\right) = -\log_{10}T = -\log_{10}\left(\frac{I}{I_o}\right) \qquad 2.8.1$$

According to Beer-Lambert law, the ratio of transmitted to incident powers is related to traversed length of the sample, absorption coefficient and the concentration of the sample such that:

$$\frac{I}{I_o} = e^{(-\varepsilon c l)} \qquad 2.8.2$$

where ε is the absorption coefficient, c is the concentration and l is sample's length. It is of great importance to notice that doubling either of ε, c, l does not result in doubling the absorption (Banwell, 1972). Gases of industrial and environmental importance usually exhibit their fundamental optical absorption in the IR region (Dakin et al, 1995). Since different pollutants have their spectral absorption lines in the IR regions, IR spectroscopy is widely applied in the field of trace gases and short-lived molecules (Miklos and Feher, 1996). The most significant use of IR spectroscopy is in the field of trace analysis (Hallam, 1968). It is usually used when we seek information about the structure of some compound or as an analytical tool in assessing compounds purity (http://orgchem.colorado.edu /hndbksupport/IRtutor/tutorial.html). Fields of study usually govern the range of IR radiation to be used. An example of this is that; far-infrared region is useful for molecules of heavy atoms such as inorganic and organometallic compounds (http://www.le.ac.uk/ chemistry/pdf/teachersworkshops .pdf). Mid-infrared region is widely used when dealing with organic compound (http://orgchem.colorado.edu/hndbk support/IRtutor/tutorial.html), while near-infrared region have gained interest in process control applications (http://prenhall .com/settle/chapters/ch15.pdf).

2.9 Experimental Samples

2.9.1 Chlorophorm ($CHCl_3$):

Trichloromethane, methyl trichloride or simply Chlorophorm – discovered by the American Samuel Guthrie in 1831 – is a member of the trihalomethane group. It is a chemical compound with molecular formula of $CHCl_3$. It is composed of two – ultimately – carbon, one hydrogen and three chlorine atoms, but, since chemists usually denote the carbon and hydrogen atoms as one formyle atom, then $CHCl_3$ is composed of three chlorine and one formyle atoms. This obviously simplifies the reason of having the name "chlorophorm" or chloroform which was driven from chloroformyle (Simpson, 2008). It is usually produced by evaporating a mixture of chlorine and chloromethane which involves the chlorination of chloromethane to produce trichloromethane, simply Chlorophorm (http://en. wikipedia.org/wiki/Chloroform). Fig 2.8 below shows the molecular shape of chlorophorm (left) and its 3D representation (right).

Fig 2.8 chlorophorm, (After: http://en.wikipedia.org/wiki/Chloroform)

Chlorophorm is colorless like water; it is a volatile material with noticeable pleasant, nonirritating odor and a slightly sweet taste. It's a nonflammable material that slightly dissolves in water. According to US EPA, Environmental Protection Agency, chlorophorm is characterized as hazard to human beings. Chlorophorm is usually used in coolant industry and as cleaning agent, dry spot remover. In nature, chlorophorm is a result of the breakdown of chlorine-containing compounds and so, it might be found in chlorinated

drinking water. As a volatile substance, chlorophorm evaporates easily and quickly into the air. It can't be noticed by smelling until it reaches a level of about 300 ppm or higher. Exposure to chlorophorm can be achieved through breathing, drinking, swimming and skin contact with contaminated environment (http://dhs.wisconsin.gov/eh/chemFS/pdf/ chloro.pdf). Inhaling about 900 ppm of chlorophorm will result in dizziness, fatigue and headache. It was reported that, being exposed to high concentrations of chlorophorm for prolonged time periods will result in the damage of liver and kidney. In animals, rats and mice were reported to suffer miscarriage after breathing air containing 30 – 300 ppm of chlorophorm (http://www.atsdr.cdc. gov/tfacts6.pdf).

2.9.2 Essential Oils:

Essential oils, volatile, or ethereal oils is a group of concentrated hydrophobic liquids which – beyond conveying characteristic fragrances – are not constrained to have common chemical properties (http://en.wikipedia.org/wiki/Essential_oil). Glands, canals, scales and hairs of aromatic plants are the main cites of essential oils to be found (Cristina, 2004). Essential oils are usually derived from different parts of the plant like leaves, flowers, seeds, peels, roots, wood, etc. (http://en.wikipedia.org/wiki/Essential_oil). Because of their molecular high reactivity, essential oils have strong pharmacological properties and actions which – by the aid of organic chemistry – can be revealed. More than 380 essential oils are currently used in the field of aromatherapy. Aromatherapy – the application of a plant-based essential oil in achieving the desired healthcare – was not coined, as a word referring to the usage of essential oils, until the publication of Gattefosse's book, *L'Aromatherapie*, in 1937. Historically, the use of essential oils as perfumes, skin care, healing salves, … is

ancient. According to Hindus literature, aromatic plants like sandalwood and cinnamon were mentioned to be used for about 4000 years ago (Cristina, 2004). Through different extraction methods, steam distillation was the main one being used to extract essential oils from plant tissues, other methods were used for the convenience of the plant part essential oils were to be extracted from. Hydrodistillation and crude distillation methods are used when extracting oils from seeds, cold-pressing or mechanical extraction were used in oil extraction from peels before the discovery of distillation (Alvi et al, 2001; Buyukozturk et al, 2005; Wajs et al, 2008). In the case of extraction from flowers, where too little volatile oil exists, and to avoid denaturing of delicate chemical components of the oil, solvents like hexane or supercritical carbon dioxide are used in solvent extraction. Concrete – the product of solvent extraction which is usually composed of a mixture of essential oil, wax, resin, and other lipophilic materials – undergoes another solvent extraction to separate the fragrant oil from the absolute where ethyl alcohol is used as the solvent in which only fragrant low-molecular weight compounds are soluble (http://en.wikipedia.org/wiki /Essential_oil). Steam distillation – the most applicable method in obtaining essential oils – involves the passage of steam through plant tissues allowing aromatic compounds to be accompanied with it. The accompanied steam passes through a coil in which it is condensed back to a liquid composed of both; essential oil and the hydrosol. Both, oil and hydrosol undergoes centrifugal separation process in which the oil is brought apart from the undesired hydrosol (Cristina, 2004). Through over history, essential oils were used in medications and aromatherapy. Usually, one single compound dominates the chemical composition of each specific essential oil (El-Kahlout et al, 1998). In the following, brief introduction, medicinal applications and chemical composition of the investigated samples are given.

2.9.2.1 Mint oil and leaves:

Mentha arvensis is an upright, hairy, odorous Mediterranean native herb, for simplicity referred to as mint, garden mint and or sage of Bethlehem. It belongs to the family of *Lamiaciae* (*Labiatae*). Over history, they are known as hospitality plants due to their therapeutic effects (Alvi et al, 2001; http://www.answers.com/topic/spearmint). The name of the plant (Mentha) was derived from the legendary myth in which Minthe – god's Pluto love – was transformed into a garden plant (http://www.answers.com/topic/ spearmint). The plant ranges from 10 – 60 cm in tall with roughly toothed leaves arranged in opposite pairs and pale purple flowers joined to the stem (http://en.wikipedia.org/wiki /Mentha_arvensis). The essential oil of mint – like most other essential oils – is extracted via steam distillation process. The major constituent of mint oil is Menthol with 40 – 85% of the extracted oil. Menthol is usually separated via crystallization leaving behind the dementholized oil (Alvi et al, 2001). Studies have revealed that, the dementholized oil is composed of ~ 24% menthone and almost a same percent of menthyl acetate and ~ 6% of hydrocarbons among which alpha-pinene, a-1-limonene, carophyllene and cademene are present (http://www.aurumindia.com/ ereports/menthaoil.pdf). In the field of medicine and pharmacy, menthol crystals are known to have antiseptic, stimulant and inhibitor effects. Elsewhere, it is used in cosmetics, food and commercial stuff as flavoring agents (Alvi et al, 2001). In aromatherapy, mint oil and leaves were used to relief the symptoms of asthma, cough, liver and spleen diseases in addition to their carminative effects (http://www. aurumindia.com/ereports /menthaoil.pdf).

2.9.2.2 Jasmine oil and flowers:

Jasmine, derived from Arabic Yasmin, is a shrub plant of compound yellow or white flowers native to all warm temperature and tropical regions of the world. There are more than 200 different species of jasmine belonging to the family of olive, Oleaceae. Jasmine is either evergreen or deciduous. In either case, the plant is usually grown climbing over other adjacent plants or over any assembly like the chicken wire (http://www. answers.com/topic/jasmine). It is usually classified as evergreen plant which grows to about 1 – 3 meters tall and native to Asia (http://en.wikipedia.org/wiki /Jasminum_sambac). Jasmine flowers are usually picked up 2 – 3 hours after sunset where the aroma of the flowers is intense and at its highest rate. The oil is obtained from flowers through the solvent extraction method as a concrete which in turn passes through a separation process by adding alcohol to produce the absolute. The absolute is then steam distilled to produce the essential oil. Jasmine oil is usually priced according to the amount of flowers needed to produce it. It is found that, 1000 lbs of jasmine flowers is needed to produce one pound of jasmine concrete of which only about 0.2% is essential oil (http://www.essentialoils.co.za/essential-oils/jasmine. html). The extracted concrete is found to contain, in addition to fragrance compounds, fatty acids, diterpenes and a high percentage of wax. Linalool, benzyl acetate, benzyl benzoate and phytol are some of the fragrance compounds contained in the concrete of jasmine (Reverchon and Porta, 1995). Jasmine has been used historically in the fields of cosmetics, medicine, perfume and incense by different cultures. It is usually used in skin care through path shampoos and message oils. In addition to its calming and sedative effect on the nervous system, jasmine oil is said to be suitable in preventing post natal depression and help prevent infertility (http://www.wildcrafted.com.au/Jasmine.html).

2.9.2.3 Nigella Sative (black cumin):

Nigella sativa is an annual herb of black seeds belonging to the family of Ranuncu-laceae. It is usually grown and cultivated in Mediterranean countries, middle Europe and western Asia (Wajs et al, 2008). Historically, Nigella sativa seeds are the most ever used and well-regarded medicinal seeds. Its popularity came from the belief that, it has a healing effect for different diseases (Ramadan, 2007). In Arabic literature, Habba Sauda, Habbet el Baraka, Kamun-aswad are different names of Nigella sativa black angular seeds (Burits and Bucar, 2000; Ramadan, 2007). In Middle East countries, black seeds are traditionally used as natural remedies for asthma and other diseases (Buyukozturk et al, 2005). In spite of being mentioned in both holy Bible and Sunnah, it is only 40 years ago that careful studies and researches had been conducted to study Nigella Sativa (Ramadan,2007). N. sativa oil is usually extracted from crushed or powdered seeds via steam distillation mechanisms in which powdered seeds are added to distilled water and the distillate is re-extracted with Chlorophorm. After that an anhydrous material like sodium sulfate is added to the product to get rid of moisture, then, the extract undergoes a 40° water path leading the volatile oil to evaporate (Aqel and Shaheen, 1996). N. sativa seeds are claimed to have about one hundred different components including sources of all known essential fatty acids. Despite the fact that, in medications, N. sativa's oil is the most frequently used, the seeds are widely used in foodstuff. The phytochemical profile of N. sativa seeds shows that they are composed of ~ 1.6% volatile oil, 41% fixed oil, 22% proteins , and 35% distributed over the rest of the other constituents like amino acids, alkaloids, organic acids, tannins, resins, bitter principles, Arabic acid, crude fibers, minerals, vitamins and many others. For N. sativa oil, the crystalline nigellone is the only constituent of the carbonyl fraction. Thymoquinone, dithymoquinone, thymohydroquinone and thymol are the main constituents of the N. sativa volatile oil that are pharmacologically active (Ramadan,

2007). In the treatment of asthma, hypertension, diabetes, inflammation, cough, bronchitis, headache, eczema, fever, dizziness and gastrointestinal diseases, the use of N. sativa seeds was a tradition over centuries. Among all of its attractive potentials, some constituents of N. sativa oil are used in toxicity reduction according to its antioxidant activities (Ebru et al, 2008).

2.9.2.4 Anise (sweet cumin):

Pimpinella anisum, sweet cumin, or simply anise, is an herbaceous annual flowering plant native to eastern Mediterranean countries and south Asia. It is usually grown up to about 3 feet (http://en.wikipedia.org/wiki/Anise). It belongs to the family of Apiaceae. It is usually grown up in Iran, India, Turkey and other worm countries all over the world (Ciftci et al, 2005). It is usually cultivated for its aniseeds, flavor licorice, and to be used in confectionary industries. In backing industry, it is used to flavor cakes, cookies and biscuits (Qin et al, 2007). Anise oil is usually extracted from the seeds via steam distillation, the main used method, but other methods of extraction like solvent extraction and supercritical fluid extraction might be used in order to increase the yield and or to avoid thermal degradation of the product. Traditionally, usage of anise fruit (seeds) and its essential oil was in the treatment of some diseases like seizures, epilepsy and constipation. Furthermore, it has anticonvulsant and muscle relaxant effects. In the medicinal field, anise oil is known for its stimulating effects in digestion, also for its antiparasitic, antibacterial, antifungal, antimicrobial and antipyretic effects. It is also reported that, anise oil increases the digestion of proteins, cellulose, and fat. Besides that, it is reported to enhance and increase the effects of pancreatic lipase and amylase (Ciftci et al, 2005). Anise oil was also reported to inhibit molds and fungi in foodstuff. It has a good potential in the inhibitory

field for *Penicillium chrysogenum* growth (Matan and Matan, 2008). The oil extracted from Star anise– native to China and Vietnam – is mainly composed of trans-anethole which has different pharmacological properties as estrogenic and depressive actions (Kouznetsov et al, 2007). Anise oil is highly composed of anothole ~ 85% as an active material in addition to eugenol, methylchavicol, anisaldehyde and estragol (Ciftci et al, 2005).

2.9.3 Zamzam water:

The main and only source of Zamzam water is the Zamzam well located 20 meters to the east of the holiest place ever on this earth AL-KA'BA. According to Islamic literature, Zamzam water is of a holy value which originates from being the spring water that God, in his mercy, ordered angel Gebriel to scrap the earth with his wing causing the spring to appear, thus providing Hajar – prophet Abraham's wife – and her son prophet Ismail, whom were left alone in the desert, with water after reaching the highest limit of thirst (http://iadr.confex.com/iadr/saudi06/preliminaryprogram/abstract_87084, 2009). The presence of the well goes 4000 years back relative to days of Prophet Abraham. The well is claimed to be about 40 meters in deep. The area surrounding the well is a group of hills basically covered with igneous rocks (El-Zaiat, 2007). Zamzam water has special physical properties leading it to be the advantageous drinking water. Contamination of minerals at higher levels in Zamzam water compared to other water generates the main difference between them. Unlike other spring water or well water, Zamzam water has a universal appeal (http://iadr.confex.com/iadr/saudi06/preliminaryprogram/abstract_87084, 2009). Being compared to tap water, chemical analysis of zamzam water shows that it contains high levels of inorganic elements like Na, Ca, Mg, K, HCO_3, Cl, F, NO_3 and SO_4. Among

these inorganic elements, high levels – to some extent – of calcium and magnesium in zamzam water compared to tap water results in zamzam water to be advantageous over tap water. This is simply because calcium – the most abundant mineral in our bodies – is of high important value in increasing the resistance of our bodies against viruses, parasites, cancer and mouth bacteria that causes tooth decay. The importance of magnesium follows the fact that, magnesium and vitamin D increases calcium absorbance in the body. Higher levels of fluoride are another advantage of zamzam water since exposure to fluoride in drinking water is of great benefit for both oral and general health (http://iadr.confex .com/iadr/saudi06/preliminaryprogram/abstract_87084, 2009). Zamzam water was found to achieve different optical parameters like refractive index, reflectance etc. compared to both distilled and bottled water. Being measured at six wavelengths in the visible region at 24° C, the refractive of zamzam water was the lowest relative to both distilled and bottled water (El-Zaiat, 2007).

Chapter three

Experimental Setup

3.1 Introduction

In this chapter, a thorough description of the experimental system used in this study is provided. The main experimental set up involves the simultaneous detection of photoacoustic and Michelson fringe signals. Photoacoustic spectroscopy involves sealing the sample in a tightly closed rigid cavity and illuminating it with a modulated light beam, then detecting the PA signal by means of a sensitive microphone coupled to the cavity in use. For Michelson's fringe signal, the sample will be sealed by the same cylindrical tube with glassed windows attached to the two ends of it allowing the laser beam to penetrate the cell and so the sample's trace gas. The combined Michelson-PA chamber shown in Fig 3.8 was presented and constructed for the first time in this study to serve such simultaneous detection purpose.

3.2 Combined Michelson-PA Chamber Design

The constructed cell is a hollow aluminum cylinder of open ends. The cell dimensions are: 3.97 cm hight and 3.6 cm in diameter and thus having a volume of 40.409 cm^3. The open ends were intensively polished and closed by two glass windows with a thin circular shell of rubber attached between the cell and the window in order to achieve adhesive sealing of the sample. Glass windows were coupled to the aluminum cylinder by two screwed jaw clamps made up of solid metal rods, while tightening clamps screws, the circular rubber bands became squeezed between the glass windows and the cylinder to obtain maximum sealing of the cell. A hole of 2 mm in diameter was made in the upper side of the cell through which liquid samples are injected inside the cell by means of a micro pipit. After sample injection, the hole was covered using thin aluminum foil stickers to allow the pressure build up in the cell. The IR source was coupled to the cell cavity through a side hole of 1 cm in diameter by means of a rotating screw mechanism, so that it can be easily separated while cleaning the cell or while adding solid samples like plant seeds and or plant tissues into the cell. The rotating screw mechanism is provided by another rubber band in order to achieve the socked sealing of the cell. In the opposite side of that where the source is coupled to the cell, the Helmholtz cell is attached through a small hole.

The Helmholtz cell was used as an adaptor to enhance the microphone signal and is made of two components; neck and cylindrical cup joined as one unit. The neck is 1.9 cm long of inner and outer diameters 0.1 and 0.2 cm respectively. The cylindrical cup - forming the main volume of Helmholtz cell - is of 0.45 cm high, with inner and outer diameters 0.6, and 0.7 cm respectively. The sensitive microphone used to detect the PA signal is a product of Knowles Electronics of item number (wz398) mounted directly over the cylindrical cup constituting the main Helmholtz cavity of volume equal to 0.127 cm^3. Glass windows are of 3 mm thick and 4.2 X 4.2 cm dimensions, glass windows are of

normal type with no given data or characteristic sheet. Fig 3.1 through 3.3 below shows the constructed cell and its constituent's dimensions.

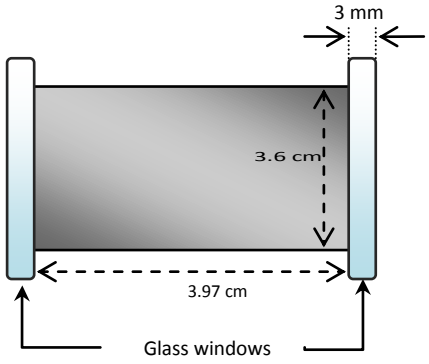

Fig 3.1 Cell dimensions coupled with the two glass windows.

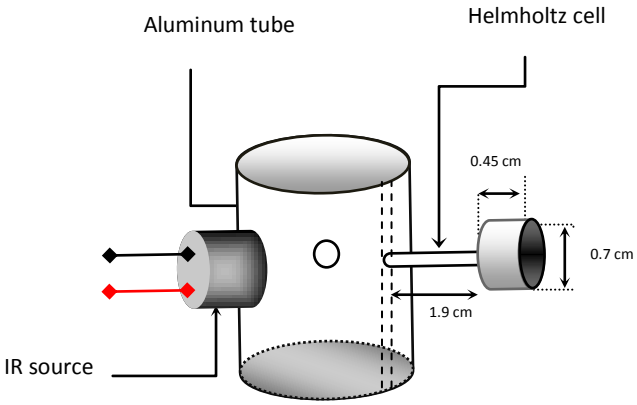

Fig 3.2 The constructed cell to which the source and Helmholtz cell are attached.

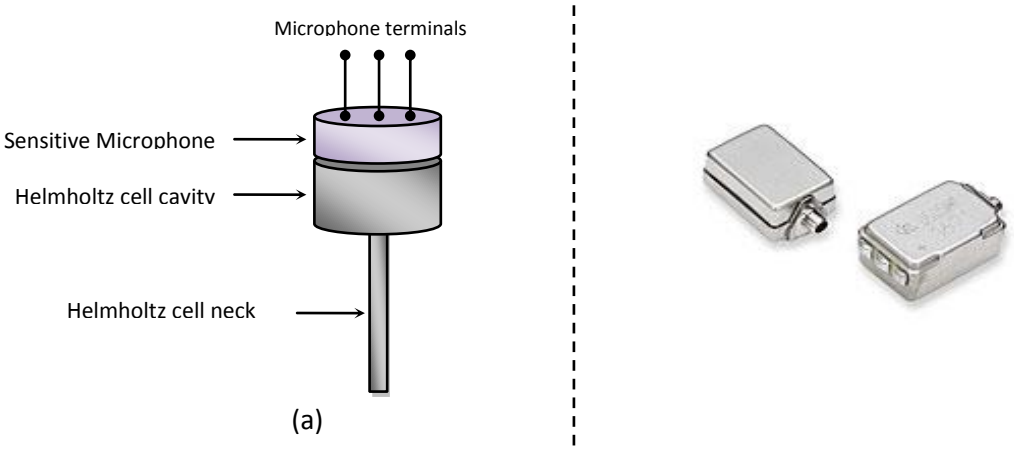

Fig 3.3 (a) Schematic diagram showing the Helmholtz cell coupled with the microphone.

(b) A photo of the microphone been used in the present study, (After: Knowles Electronics 2009).

Fig 3.4 below shows the assemblage of the rubber bands between the aluminum cylinder and the glass windows being squeezed tightly together by means of the clamps.

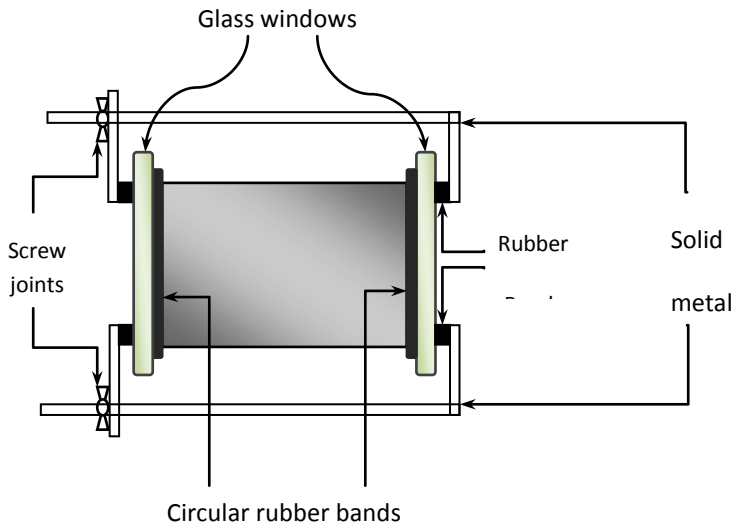

Fig 3.4 Rubber bands assemblage between the glass windows and the cylinder by means of solid rod clamps.

3.3 Pulsed wide band IR thermal source.

A pulsed wideband mid-IR thermal source based on electrical heating of a thin metal alloy foil up to red heat (~ 900°C) and cooled by its own radiation has been used. The emitting area of the source filament of two sided emission is of 12 mm effective diameter based on a bi-spiral suspended metal foil geometry which offers thermal isolation from the supporting structure. The supporting structure is a 15 mm long and 5 mm in diameter

ceramic post with four equispaced 1 mm diameter holes threading its length. Fig 3.5 below shows the used source and its supporting structure. The source filament is 25 µm thick made of Fecralloy foil composed of different elements as follows: Fe 72.6 %, Cr 22%, Al

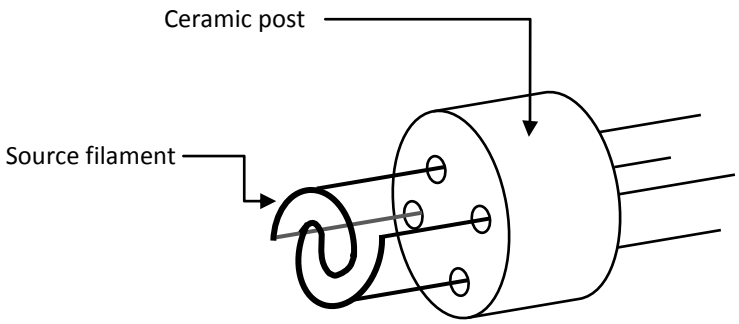

Fig 3.5 A sketch of the miniature pulsed bispiral infrared source showing its filament and supporting ceramic structure, (After: Laine et al, 1997).

4.8 %, Si 0.3 %, and Y 0.3 %. The used foil is of 440 $JK^{-1}Kg^{-1}$ heat capacity and 7.22 X 10^3 Kgm^{-3} density.The source is a wideband IR one emitting in the range of 2 ~ 9.5 µm, it became dull red at 0.6 amperes, and red at 0.8 amperes. For constant driving current, the power increases according to the I^2R relation derived from Joules law due to the slight increase in the filament resistance as the temperature increases. For constant driving voltage, the power decreases according to V^2/R relation also derived from Joules law as a result of the previous mentioned reason. In this study the source was driven by 0.7 amperes at 8.6 DC volts and so, a 6.02 watts driving power.

3.4 Equipment

In this section, the used equipment are presented in details. These equipment include six main parts; detection units, electronic signal processing units, IR source, He-Ne laser unit, Michelson interferometer, and computer aided software. Detection units are either the light

intensity detector representing Michelson's signal, and or the sensitive microphone detector representing the PA signal. Both signal detectors are coupled to the electronic signal processing unit represented by the SciTech Lock-in amplifier and SCASI interface unit. Electronic signal processing unit includes the pre-amplifier circuit, phase sensitive detector represented by the SciTech Lock-in amplifier, SCASI interface unit, DC power supply, 9 volt battery, computer software represented by the data studio program, function generator, and electronic current driving unit, in addition to connecting wires. The PA signal is picked up directly from the microphone to the Lock-in amplifier through the pre-amplifier circuit, then to the SCASI interface unit, then to the computer. Michelson's signal is picked up by allowing the interference fringe pattern to fall on light intensity detector connected to the SCASI interface unit, then to the computer. Both signals are detected simultaneously and processed at same time. The light intensity signal was measured as two signals; the intensity of light and its relative voltage. The signal presented in this study in chapter four is the relative voltage of the laser beam intensity.

The IR radiation is obtained from the miniature pulsed wideband IR source discussed in the previous section. IR radiation is needed to produce PA signal usually excited as a result of light absorption by gas molecules in the optoacoustic cell. The laser used in this study is a He-Ne gas laser with wavelength equal to 628 nm and power in the range of 0.1 mw. The laser beam is used to enhance the functioning of the Michelson interferometer, and to illuminate the sample enclosed within the combined Michelson-PA chamber. The laser intensity is detected by the light intensity detector then processed by the electronic processing unit. A voltage stabilizer is used to drive the He-Ne laser in order to maintain constant illumination intensity, so that, the detected changes in intensity are certainly due to index change occurred within the cell.

Michelson's interferometer used in this study is a PASCO precision interferometer unit shown in Fig 3.6 assembled to work in the Michelson mode. The combined Michelson-PA chamber is coupled to the interferometer so that it lies between the beam splitter and the adjustable mirror as shown in Fig 3.7 below. The laser beam originates through the chamber before the interference occurred and fringe pattern arises. Changes in the fringe pattern like fringe shifts are due to optical changes within the chamber i.e. refractive index gradient and laser beam deviation as a result of IR absorption and or sample evaporation. For computer aiding, an SCASI card (a product of PASCO scientific company) was installed in the computer, accompanied with the well known Data Studio science work shop software. Michelson's interferometer is a very delicate measuring device; it is capable of detecting the very small mechanical collisions and vibrations of the floor and side walls of the room where the experiment is being carried out due to mechanical activities occurred in the neighborhood area like students movement in the corridor or due to sudden doors closer. To avoid such disturbance, a soft spongy base was applied beneath the base of the interferometer.

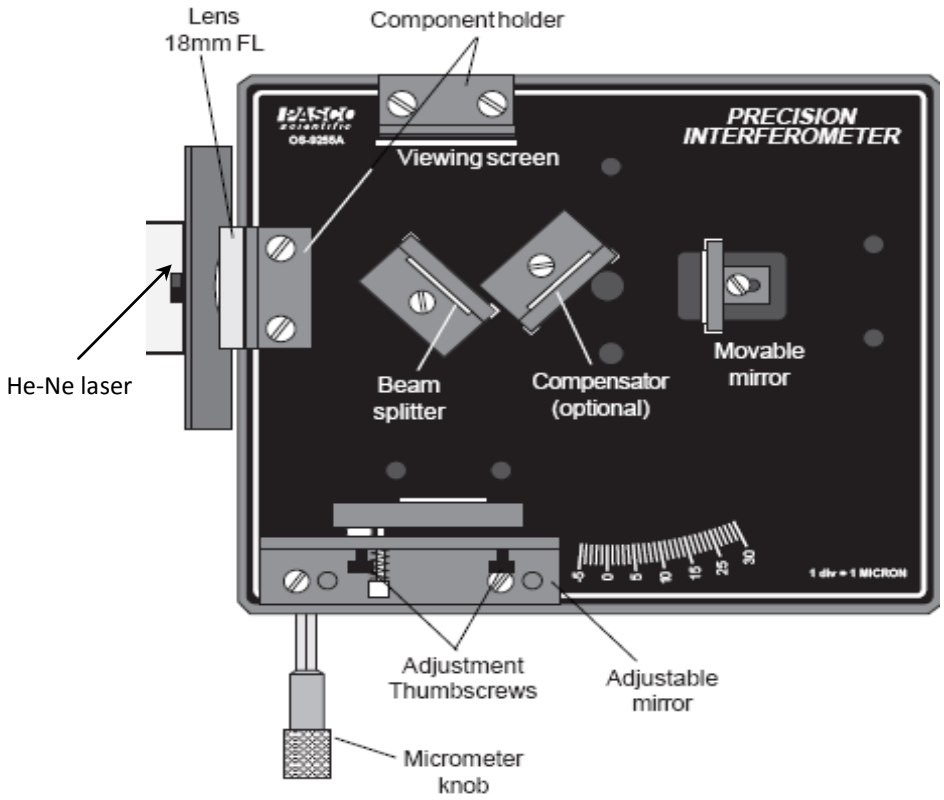

Fig 3.6 PASCO prescision interferometer showing Michelson's interferometer mode.

(After: PASCO scientific manual 1990)

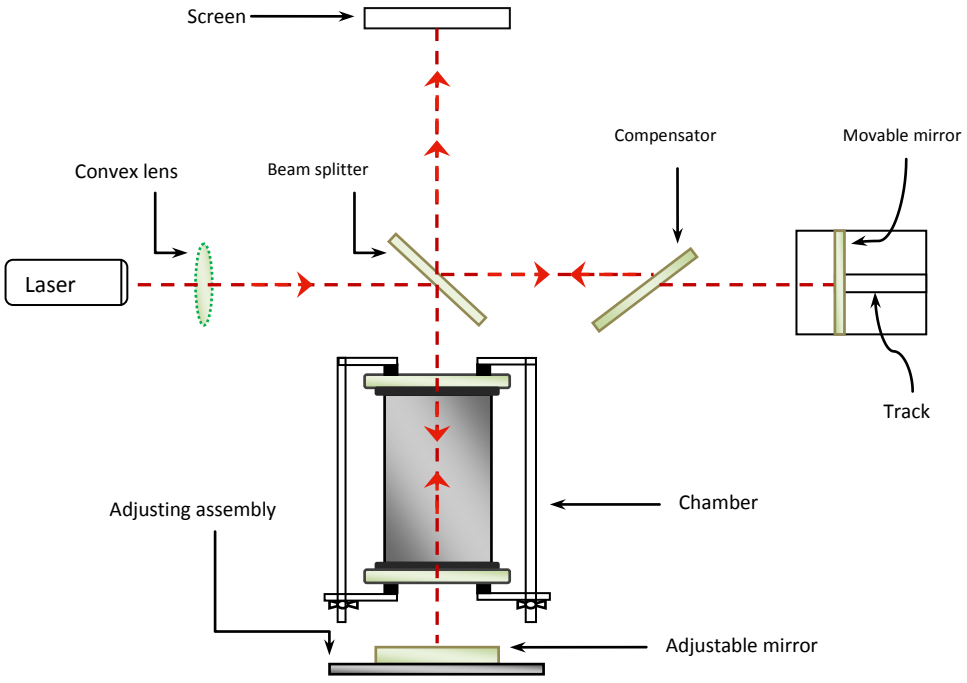

Fig 3.7 A Schematic diagram showing the Michelson-PA coupled system.

3.5 Experimental Setup for the simultaneous Michelson-PA signal detection

The IR radiation of the pulsed wideband IR source is set to fall on the gas molecules being evaporated inside the cell. The source radiates at right angles to the chamber axis, hence illuminating sample's vapor enclosed by the chamber. The absorbed IR radiation by the vapor generates heat waves which results in pressure fluctuations and optical changes within the chamber. Pressure fluctuations are amplified in the Helmholtz cell and detected by the sensitive microphone. The optical changes in the cell, i.e. index change, result in a fringe shift detected by the light detector as change in light intensity.

The arrangement of the used equipment was held the same for all investigated samples. Fig. 3.8 shows the complete experimental set up used to carry out the presented study. A photo of the complete setup taken during the run showing the arrangement of the different used equipment is shown in Fig 3.9.

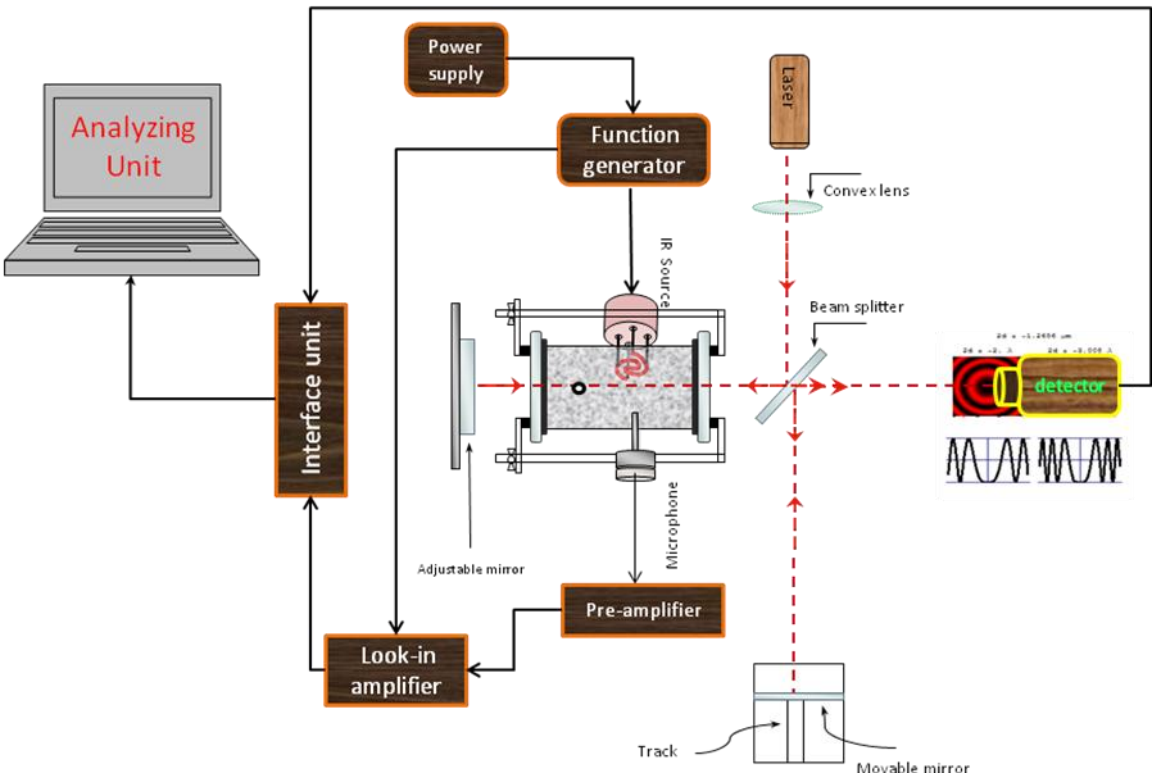

Fig 3.8 The complete combined Michelson-PA signal detection system.

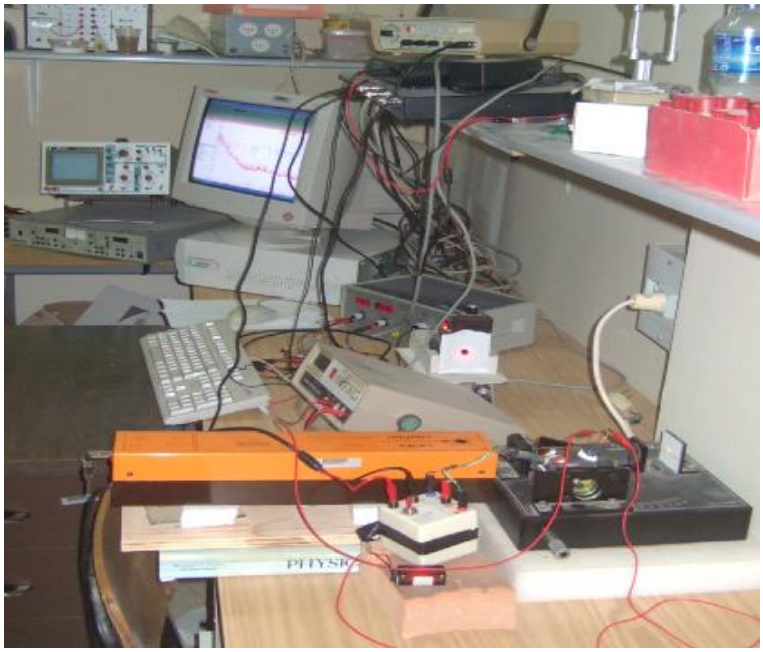

Fig 3.9 A photo of the combined Michelson-PA signal detection system.

3.6 Chamber cleaning

Since the main proposed approach of detection involves IR absorption by samples vapors, then it is important to clean up the chamber from any previous residuals like sample molecules or samples thin films condensate over the glass windows. In order to achieve sufficient results, three ways of chamber cleaning were applied; (a) leaving the cell opened for about five minutes after the removal of each sample. (b) Wiping the glass windows with a piece of cotton soaked with cleaning agent and then rinsing them with water. (c) Applying a hot air flow within the chamber so that any residual molecules within the Helmholtz cell neck is surely driven out.

Chapter four

Experimental Results

4.1 Introduction

Results of the combined Photo acoustic-Michelson interferometer trace gas detection of natural oils vapors, plant seeds, green leaves, citric acid solution, NaCl solution, Zamzam water and some others were utilized. The system stability was checked using the trace of Chlorophorm samples tested many times and at different times. For the combined Michelson-PA chamber, the cell focusing was on IR absorption (the generator of both signals) in the mid range, i.e. 400 – 8000 cm^{-1}. Parameters that optimize both signals

amplitude will be kept constant all over the experiment, i.e. 12 Hz modulation frequency and 0.7 Amp's driving source current, unless changed on purpose.

Michelson fringe and PA signals were both compared with each other in order to authenticate the use of Michelson interferometer as a monitor of gas traces. The optimizing parameters i.e. changing modulating frequency, driving current, samples volume were investigated for chlorophorm. The source was turned ON after about 15 seconds from adding the sample and starting the Run for all samples. Both signals were measured versus time by means of computer using SCASI card installed in the computer aided with interface device and two voltage and light sensors using DATA STUDIO program.

4.2 Liquid vapor detection using CMIPACT

The abbreviation CMIPACT stands for "Combined Michelson Interferometer Photo Acoustic Chamber Technique".

In this section, the investigated liquid samples and their relevant figures is introduced briefly. For the combined Michelson-PA cell CMIPACT, Chlorophorm ($CHCl_3$) samples were used to investigate system's reliability and stability since it is a well-known material. Mint, Jasmine, Anise and Nigella Sativa (Black Cumin) oils were tested and investigated too, they were bought from a local shop with unknown concentrations or properties data sheet, so dealt with as pure undiluted oils.

4.3 Traces of essential oils in different plant tissues

Seeds of Anise and Nigella Sativa, also bought from the same local shop and claimed to be from this year crop, were investigated for trace gas detection via the new introduced

technique. Fresh plant tissues, from where some of the above-mentioned essential oils are usually extracted, were taken directly from the garden at the same day of investigation. The main idea is to test our system's ability to detect traces of different samples in addition to compare Michelson fringe and photoacoustic signals with each other in order to judge the detectability of photoacoustic signals inside Michelson cavity and the use of Michelson Interferometer as a monitor of trace gas detection.

4.4 Results of Chlorophorm

In this part of the experiment, Chlorophorm ($CHCl_3$), as a volatile material, was investigated to deduce or judge the new approach of trace gas detection in addition to check up its reliability compared with the PA technique.

Chlorophorm ($CHCl_3$) is a volatile chemical compound that gives a trace gas, which can be easily detected by means of the PA technique. In this study, a new technique is introduced to detect trace gases by means of Michelson interferometer and PA effect simultaneously, using the empirical system shown in Fig. 3.8, at different experimental conditions.

Fig. 4.1 below shows the combined Michelson-PA signal versus evaporation time for 2µl of chlorophorm investigated at 12 Hz modulation frequency of the IR source driven by a current of 0.7 Amps.

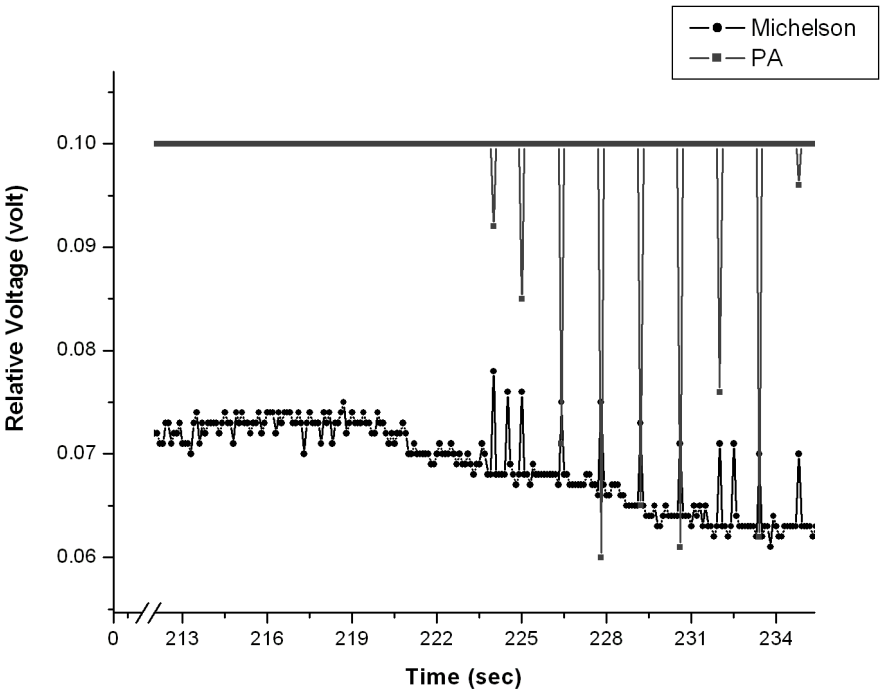

Fig 4.1 The combined Michelson-PA signal versus evaporation time for 2 microliters of chlorophorm

4.4.1 Effect of the volume of the sample

The effect of the sample's volume on the combined Michelson-PA signal using the CMIPACT was investigated using Chlorophorm samples of different volumes tested under constant optimizing conditions of 12 Hz modulating frequency and 0.7 Amperes driving source current. The volume of the tested samples was 1 µl, 2 µl, 3 µl, 4 µl, and 5 µl. The results were as shown in Fig 4.2 below.

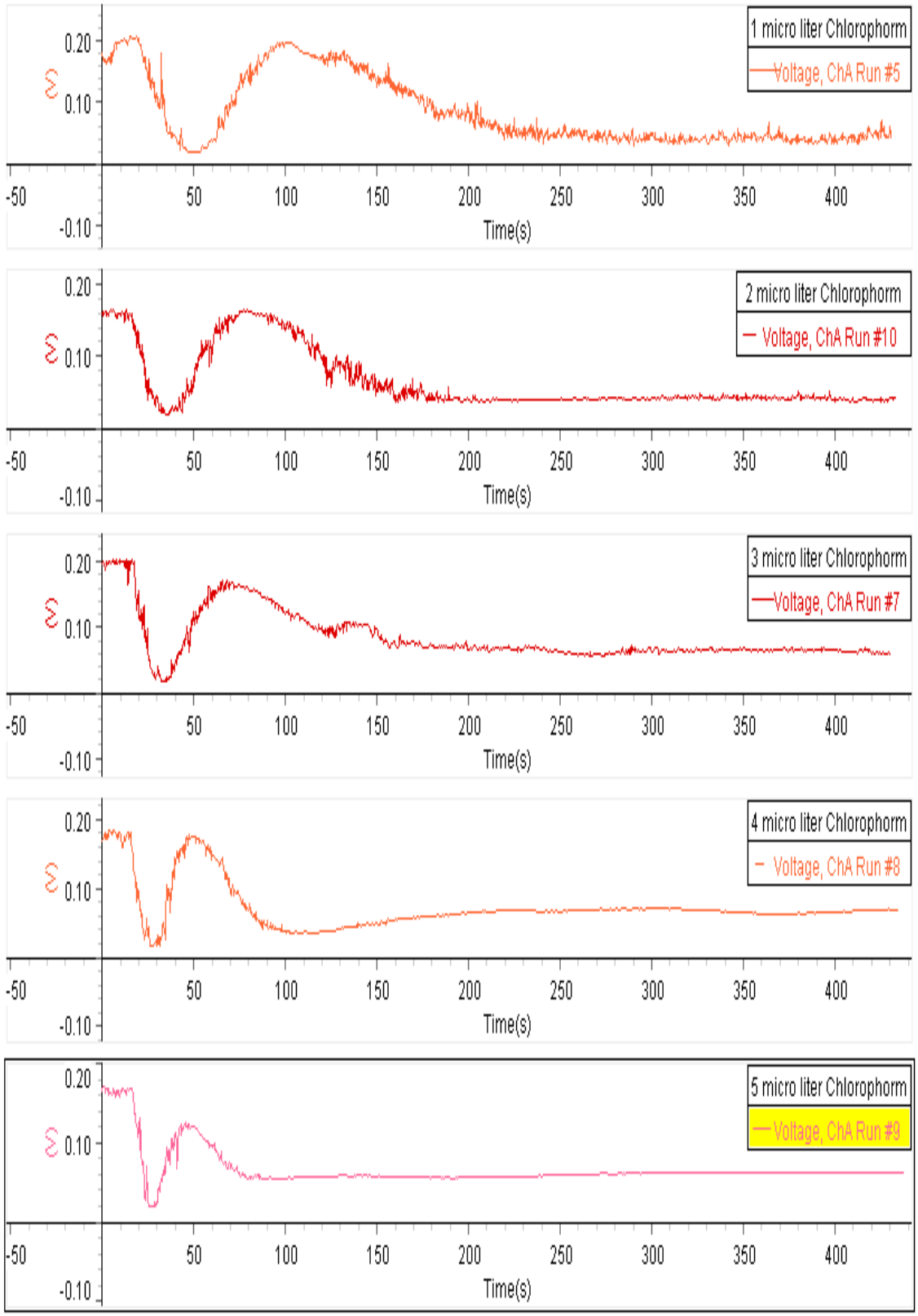

Fig 4.2 Effect of the Volume of chlorophorm sample on the Michelson fringe signal

The effect of changing the volume of the sample on the PA signal is shown in Fig 4.3 below.

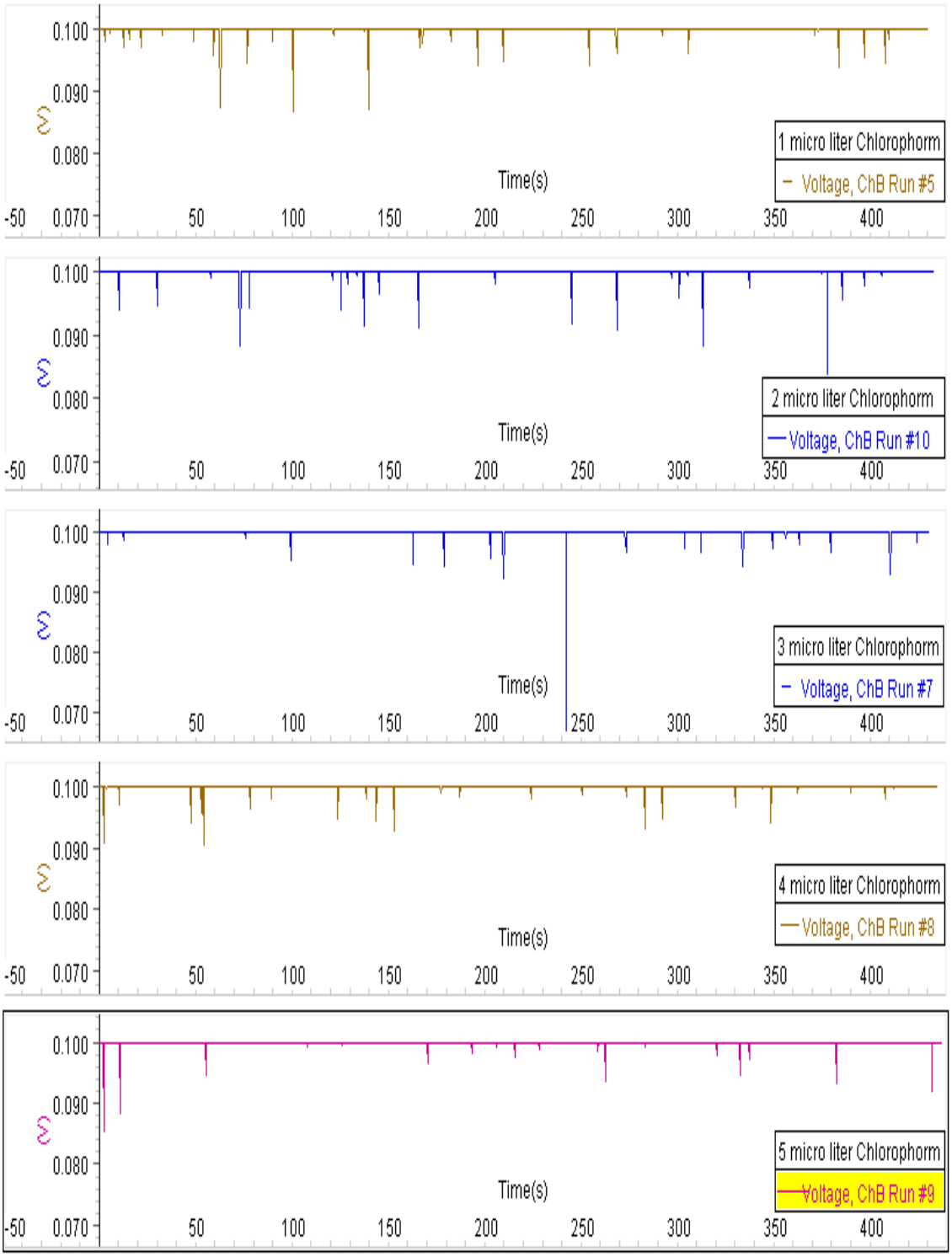

Fig 4.3 Effect of the Volume of the sample on the PA signal

4.4.2 Effect Of changing the frequency of modulation

The effect of changing the frequency of modulation on the combined Michelson-PA signal using the CMIPACT was investigated using Chlorophorm sample of 2 µl volume tested under different modulating frequencies at constant driving source current of 0.71 Amps. Modulating frequencies at which samples were tested were 12 Hz, 13 Hz**,** 14 Hz, 15 Hz, 16 Hz, 17 Hz, 18 Hz. The results were as shown in Fig 4.4 below:

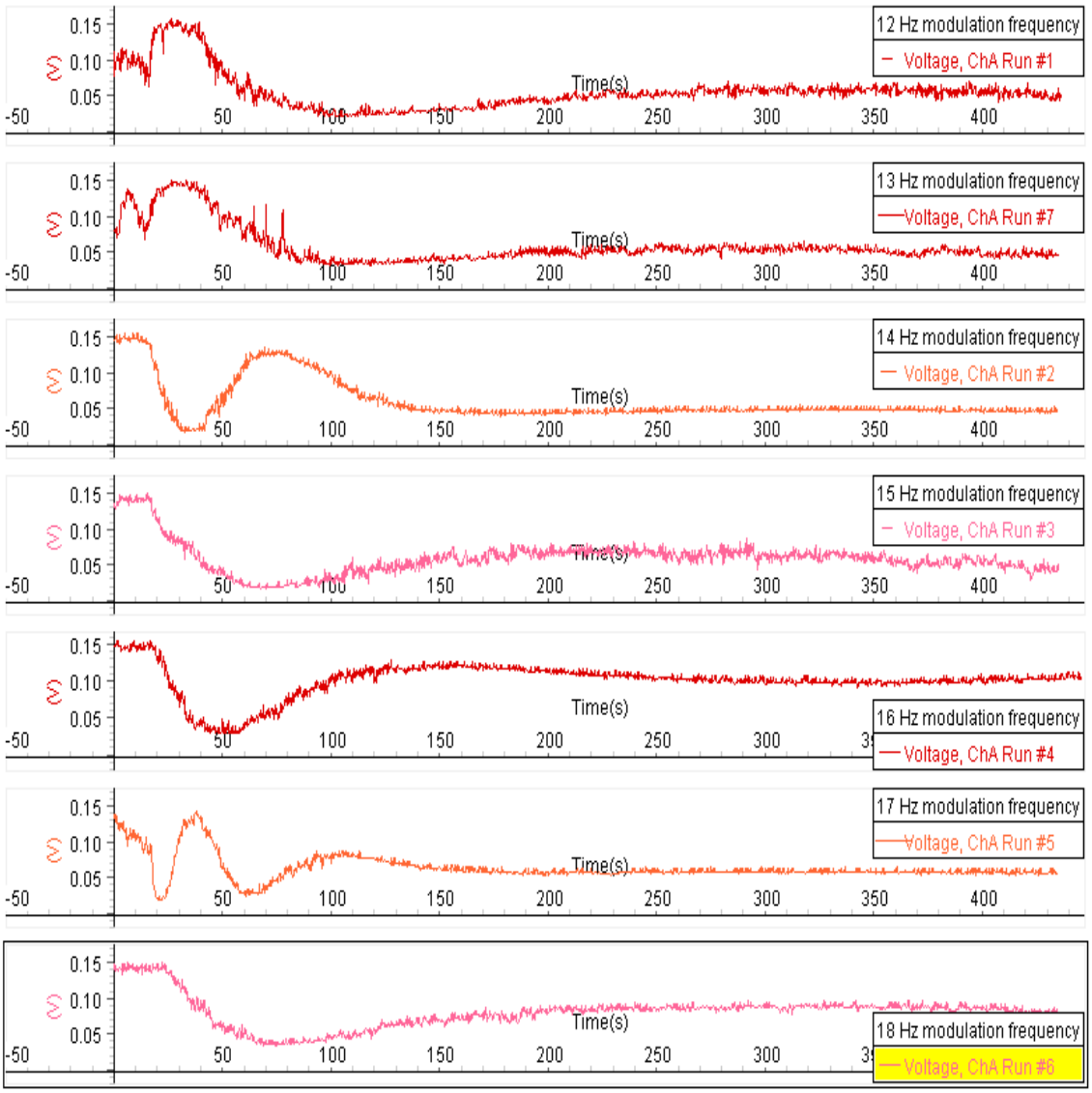

Fig 4.4 Effect of the modulating frequency on the Michelson fringe signal.

The effect of changing the modulating frequency of the IR source on the PA signal is shown in Fig 4.5 below.

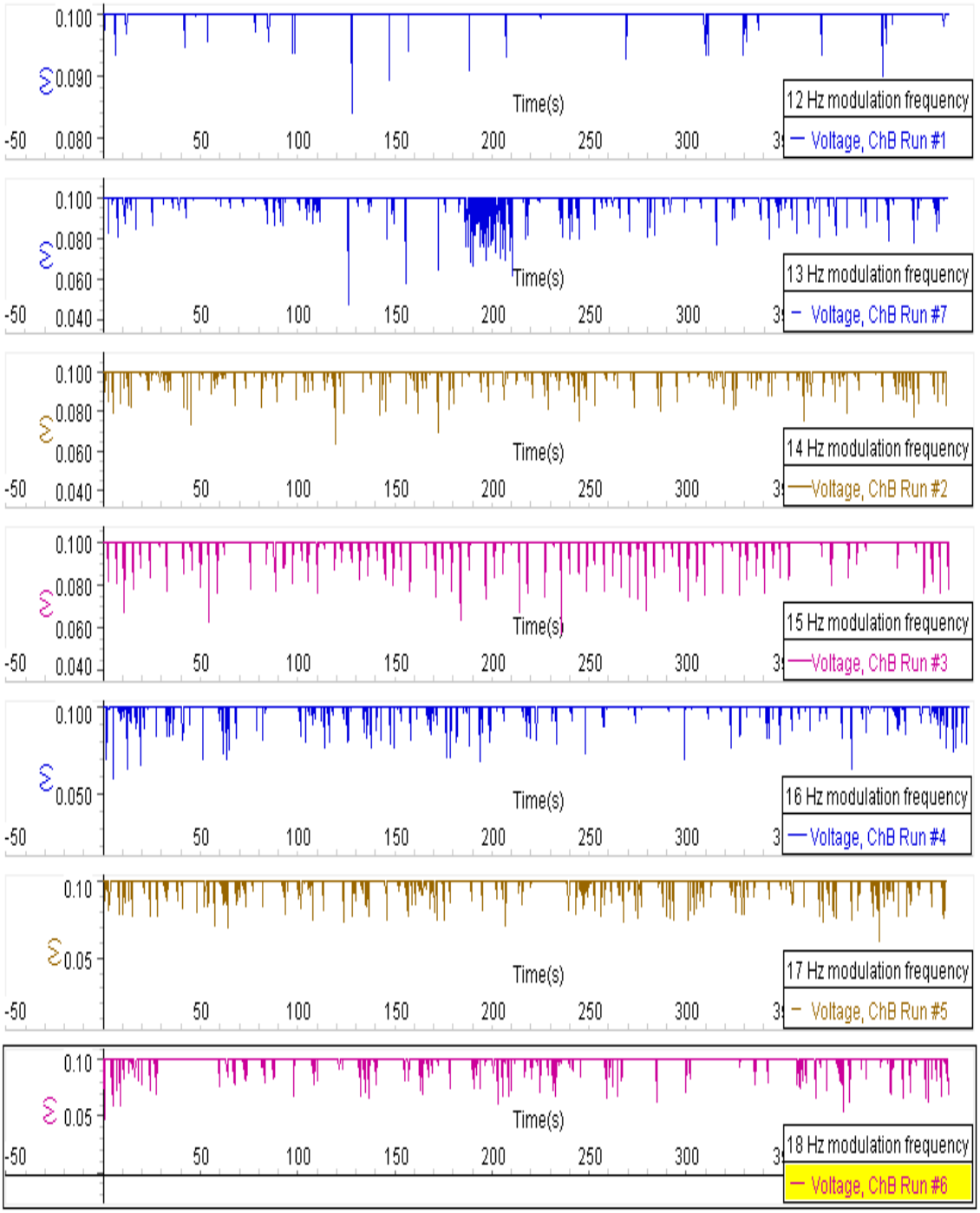

Fig 4.5 Effect of the modulating frequency on the PA signal

4.4.3 Effect Of changing the driving source current

The effect of changing the driving source current on the combined Michelson-PA signal using the CMIPACT was investigated using Chlorophorm samples of 2 µl volume tested under different driving source currents at constant modulating frequency of 14 Hz. The different driving source currents were 0.58 Amps, 0.61 Amps, 0.64 Amps, 0.67 Amps and 0.7 Amps. Results were as shown in Fig 4.6 below.

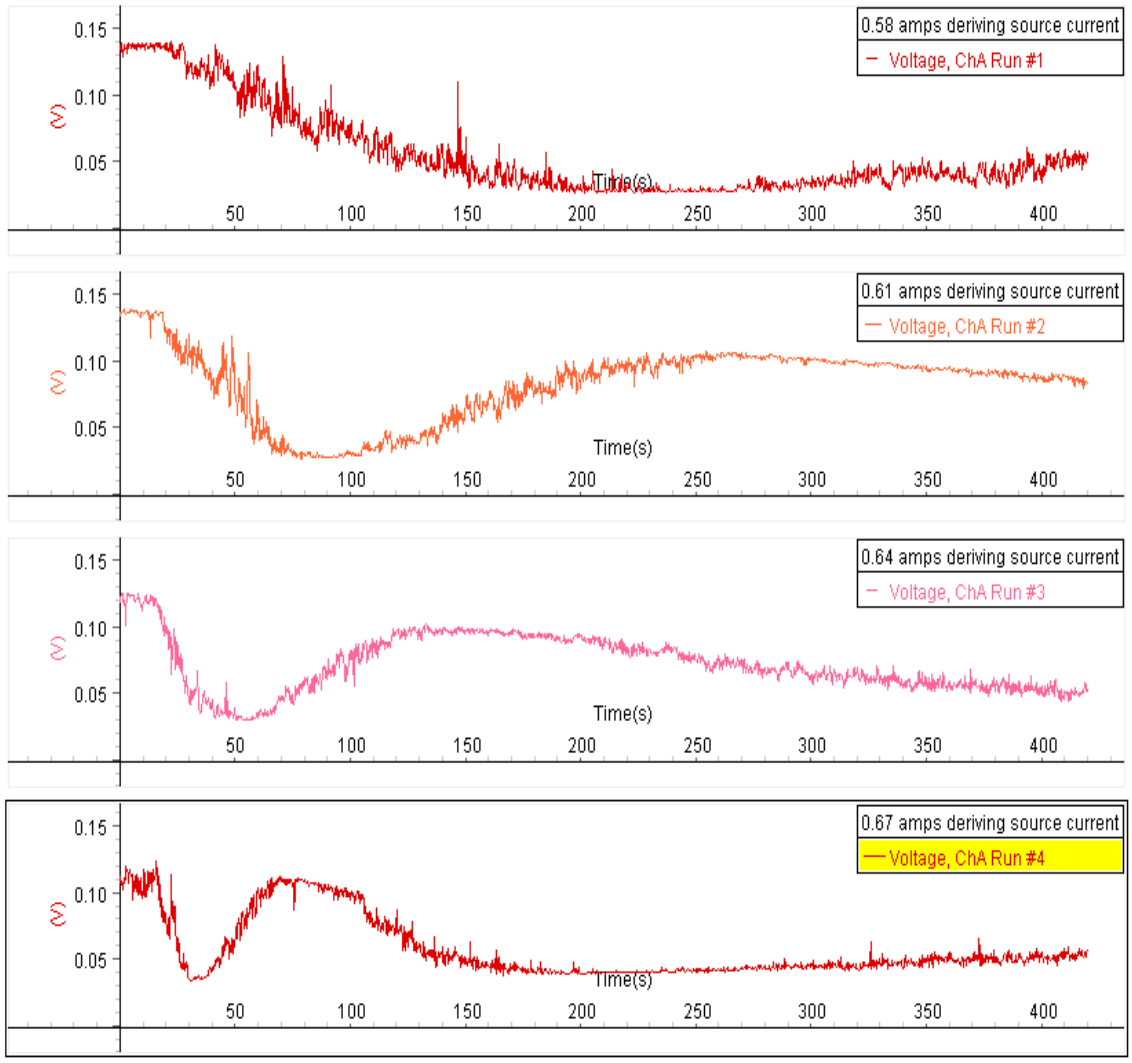

Fig 4.6 Effect of the driving source current on the Michelson fringe signal

The effect of changing the driving source current on the PA signal was as shown in Fig 4.7 below.

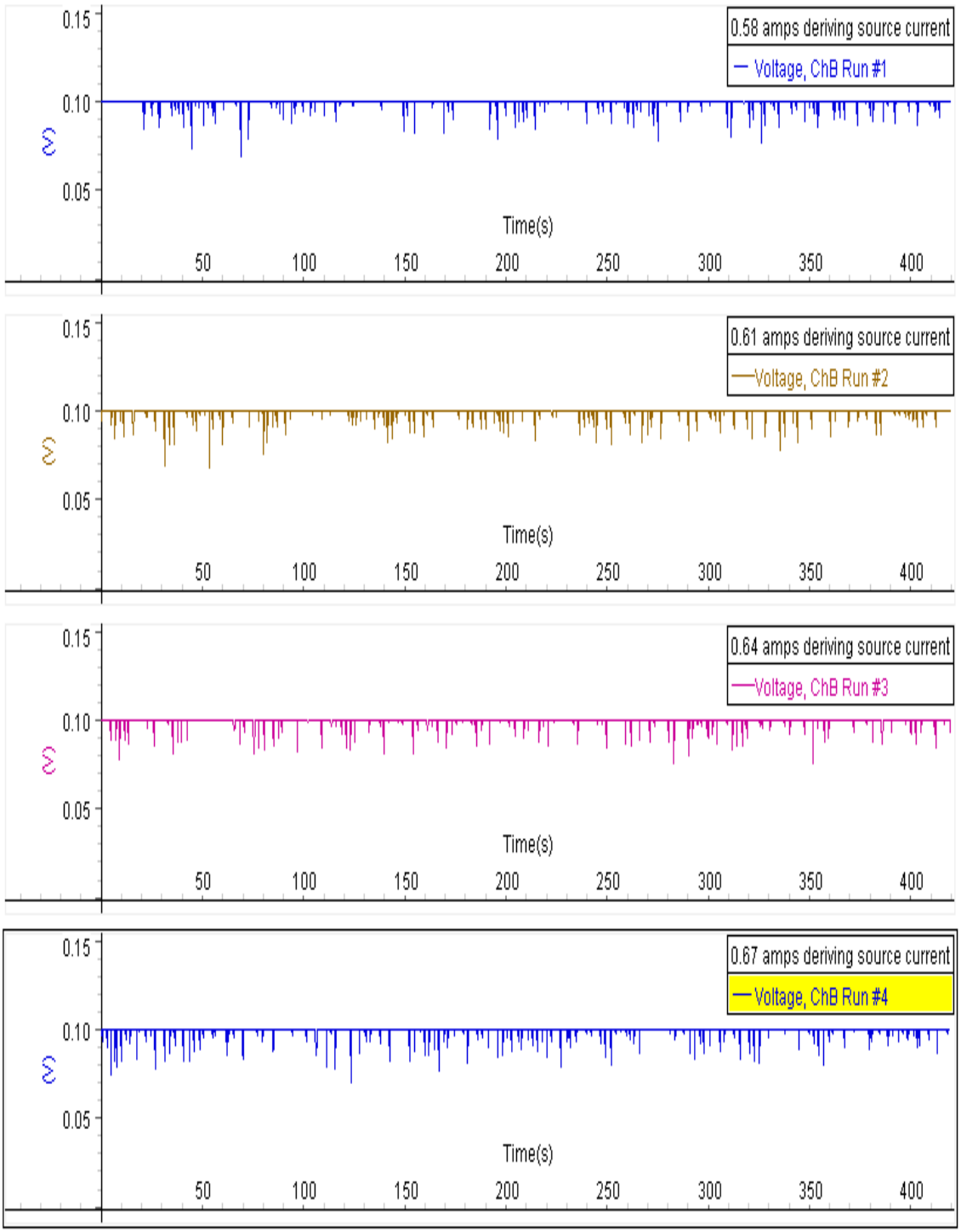

Fig 4.7 Effect of the driving source current on the PA signal

4.5 Results of Vapors driven from Essential Oils, Seeds and Plant Tissues

In general, once liquids are heated, they start changing their phases from liquid to gas. The evaporation rate depends on the volatility of the sample itself and of course on the heat absorbed. Once essential oils, seeds and plant tissues are heated up by means of a modulated IR beam of light, a trace gas – easily detectable by means of the PA technique – will be given.

In this part of the experiment, the combined Michelson-PA technique will be tested by investigating the vapors of some essential oils, seeds, plant tissues, tap water and Zamzam water. Results will be introduced in brief and sample by sample.

4.5.1 Results of Jasmine Oil and Flowers:

In this section, pure jasmine oil and jasmine flower petals were both investigated for trace gas detection by means of CMIPACT. Results will be introduced in brief in combination with their relative figures.

A 0.5 gm of jasmine flower petals and 4µl of jasmine pure oil were investigated using CMIPACT at 14 Hz modulating frequency and 0.7 Amps driving source current. Fig. 4.8 through 4.13 show Michelson's fringe signals versus evaporation time for jasmine oil and flower samples. For convenience, different experimental conditions are made clear in figure captions.

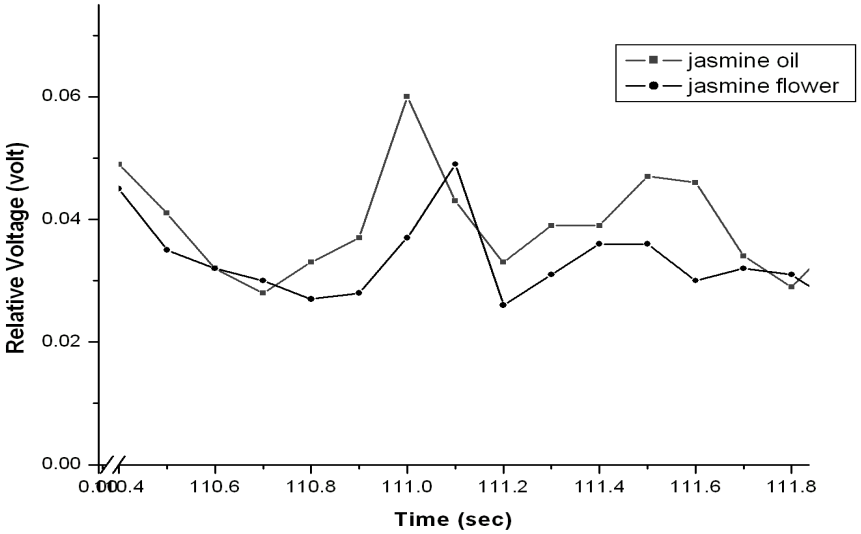

Fig 4.8 Michelson's fringe signal versus evaporation time for jasmine flower and oil samples over the time period 110.4 - 111.8

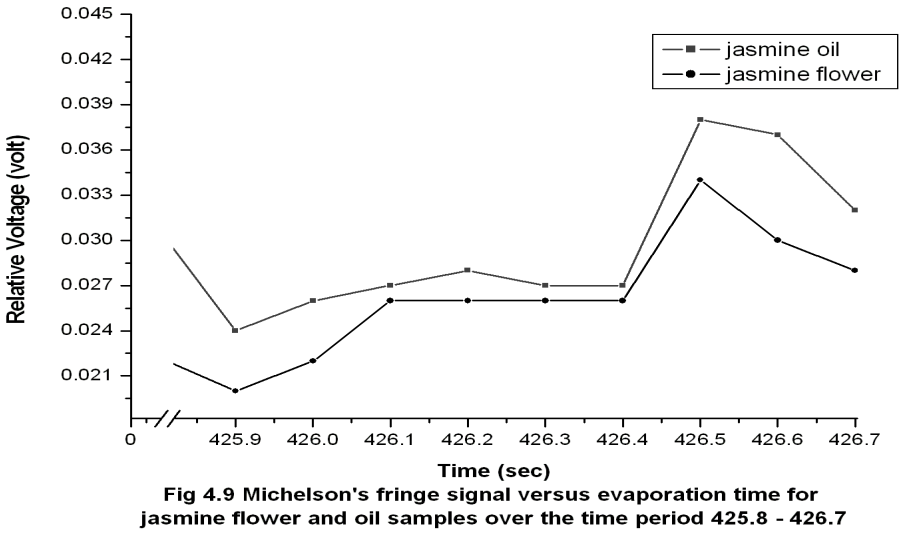

Fig 4.9 Michelson's fringe signal versus evaporation time for jasmine flower and oil samples over the time period 425.8 - 426.7

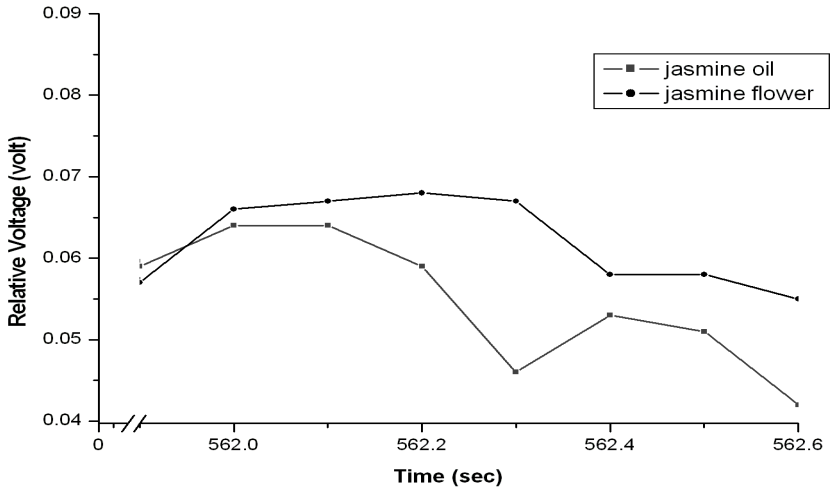

Fig 4.10 Michelson's fringe signal versus evaporation time for jasmine flower and oil samples over the time period 561.9 - 562.6

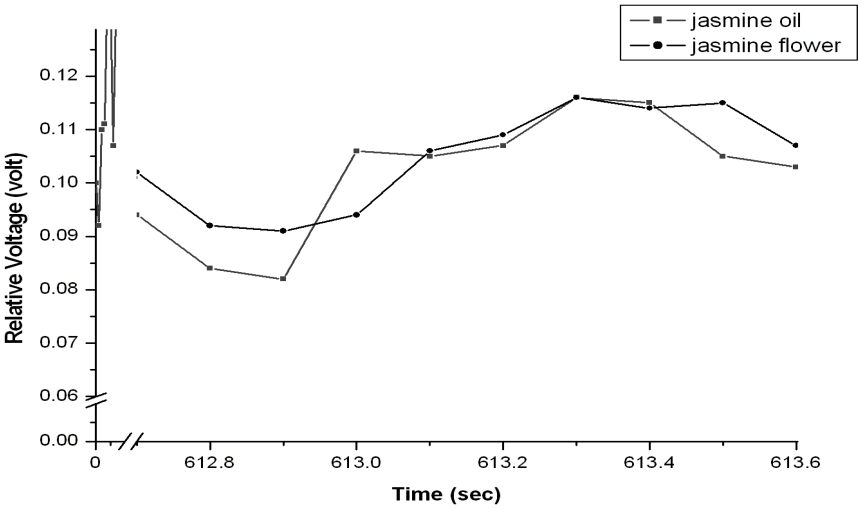

Fig 4.11 Michelson's fringe signal versus evaporation time for jasmine flower and oil samples over the time period 612.7 - 613.6

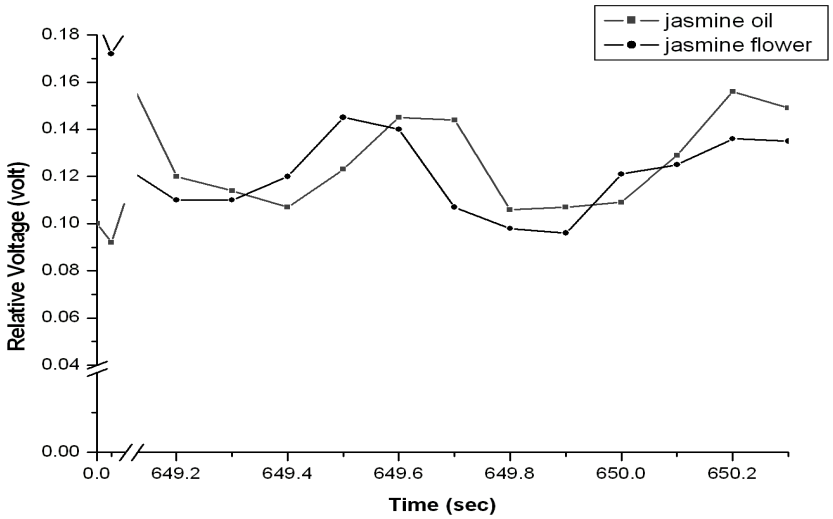

Fig 4.12 Michelson's fringe signal versus evaporation time for jasmine flower and oil samples over the time period 649.1 - 650.3

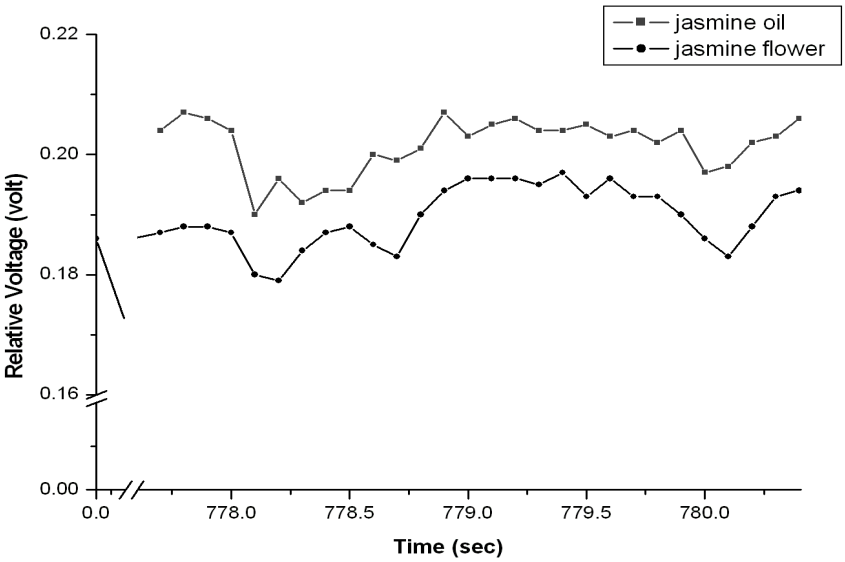

Fig 4.13 Michelson's fringe signal versus evaporation time for jasmine flower and oil samples over the time period 777.7 - 780.3

Figs 4.14 through 4.17 show the PA signal versus time for jasmine flower and oil samples.

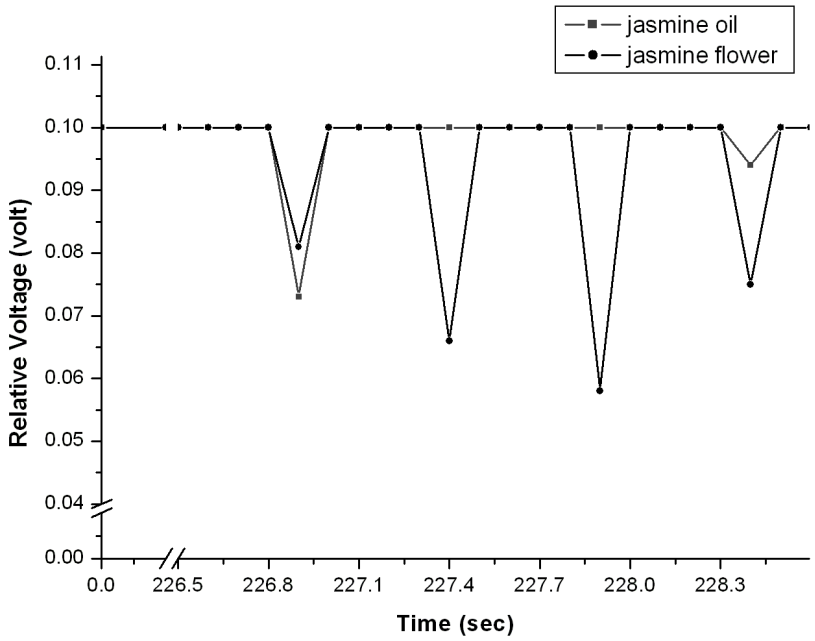

Fig 4.14 PA signal versus evaporation time for jasmine flower and oil samples over the time period 226.5-228.6

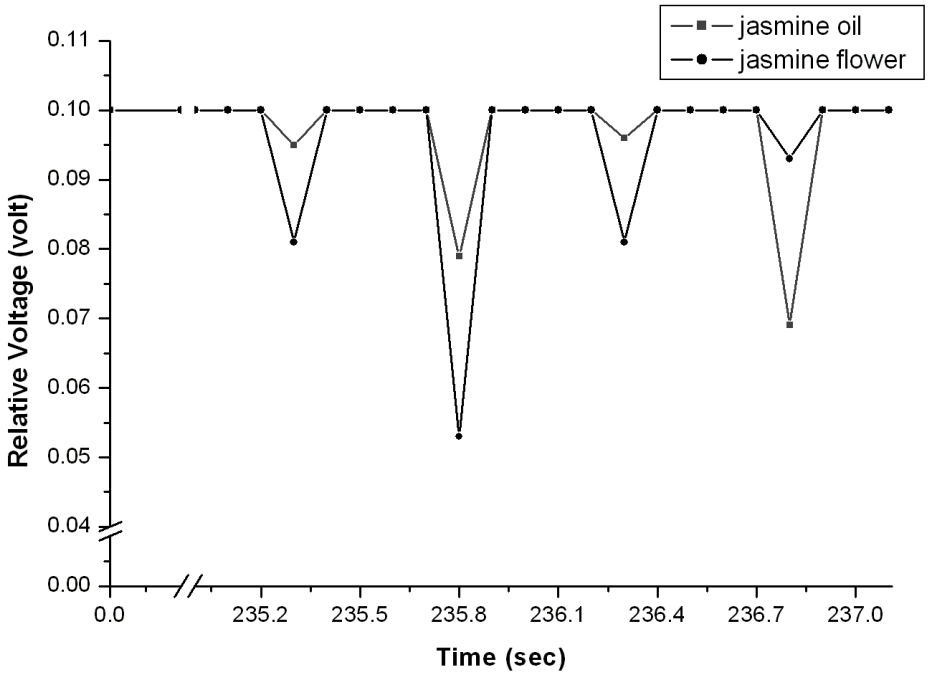

Fig 4.15 PA signal versus evaporation time for jasmine flower and oil samples over the time period 235.05 - 237.1

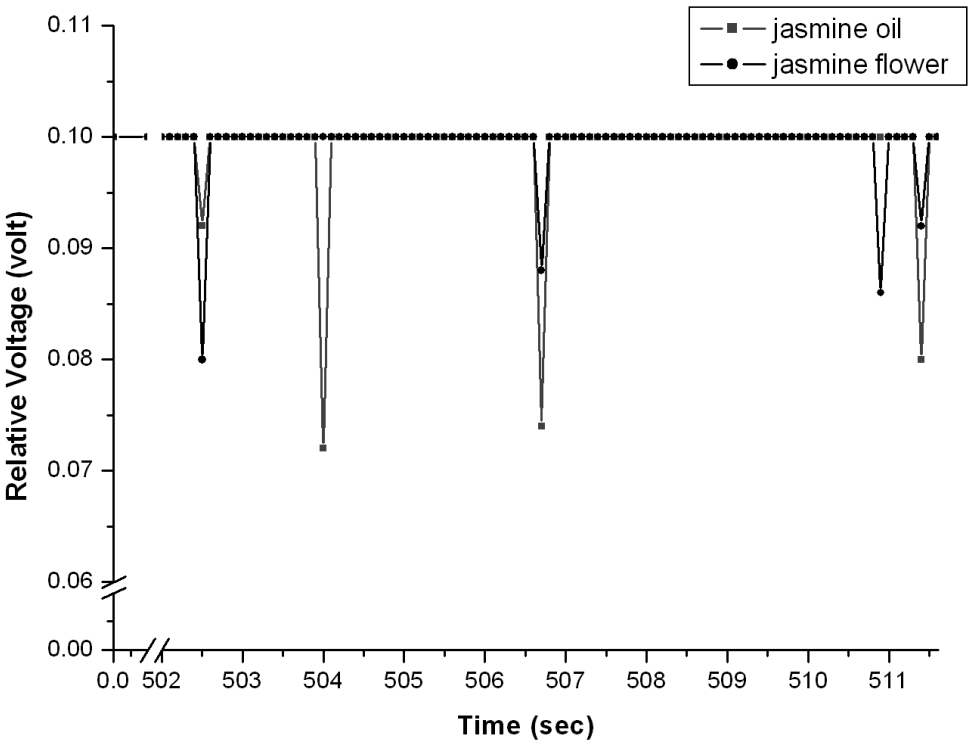

Fig 4.16 PA signal versus evaporation time for jasmine flower and oil samples over the time period 502 - 511.5

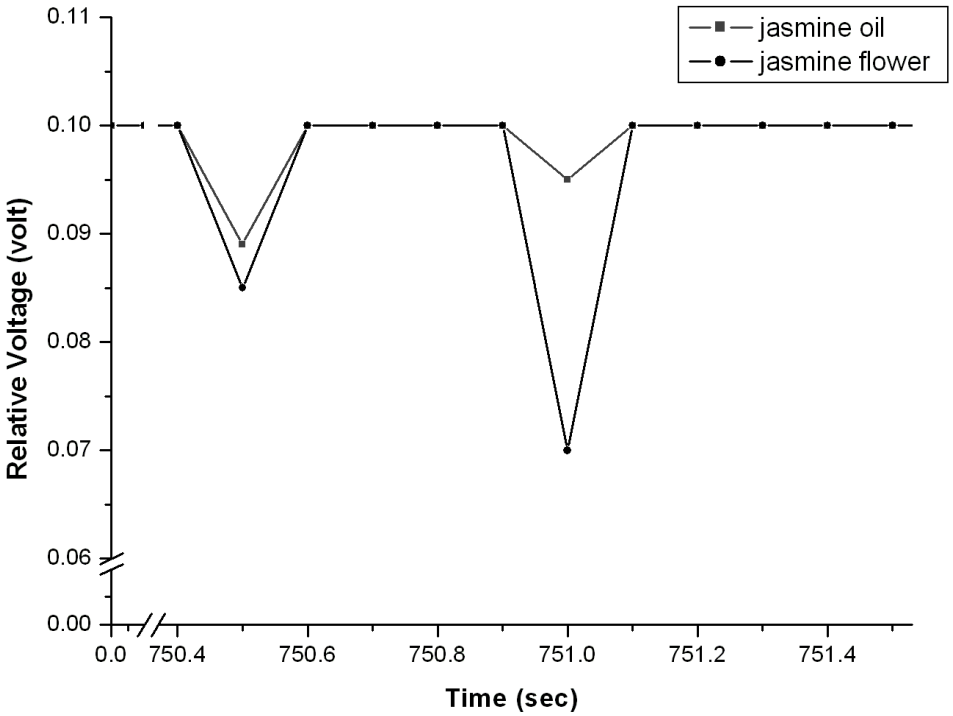

Fig 4.17 PA signal versus evaporation time for jasmine flower and oil samples over the time period 750.4 - 751.5

4.5.2 Results of Mint oil and leaves:

Samples of mint oil and leaves were tested via CMIPACT in order to investigate their gas traces. The samples of 0.1 gm mint leaves and 4 µl mint oil were heated using IR source at 14 Hz modulating frequency and 0.7 amps driving source current. For convenience, experimental conditions were made clear in figure captions. Results of Michelson fringe signal versus evaporation time of mint oil and leaves were as shown in Figs 4.18 through 4.23.

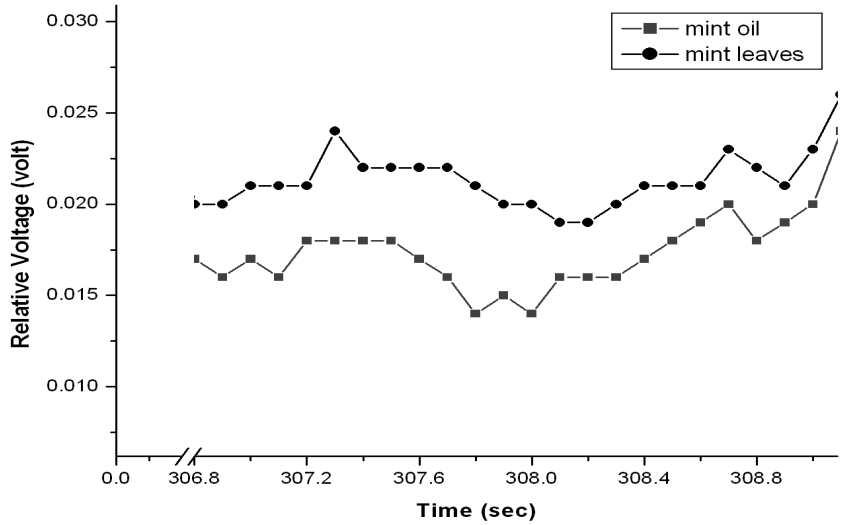

Fig 4.18 Michelson's signal versus evaporation time for mint oil and leaves samples over the time period 306.8 - 309

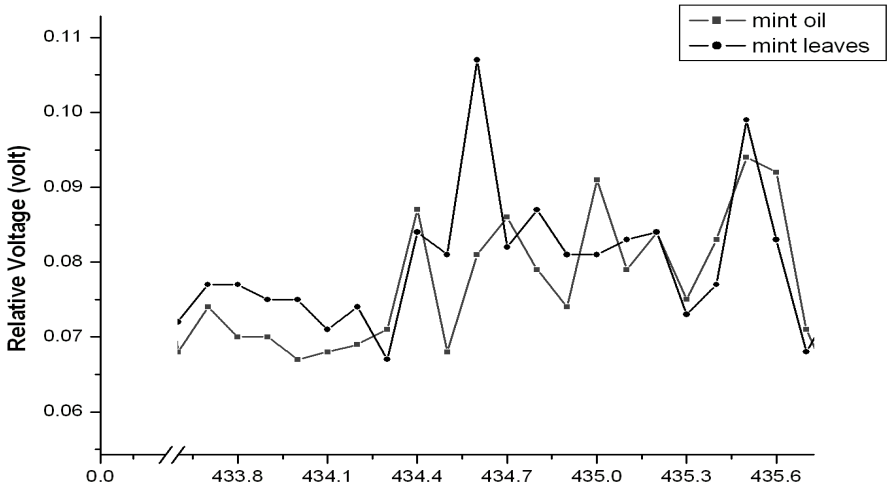

Fig 4.19 Michelson's signal versus evaporation time for mint oil and leaves samples over the time period 433.6 - 435.7

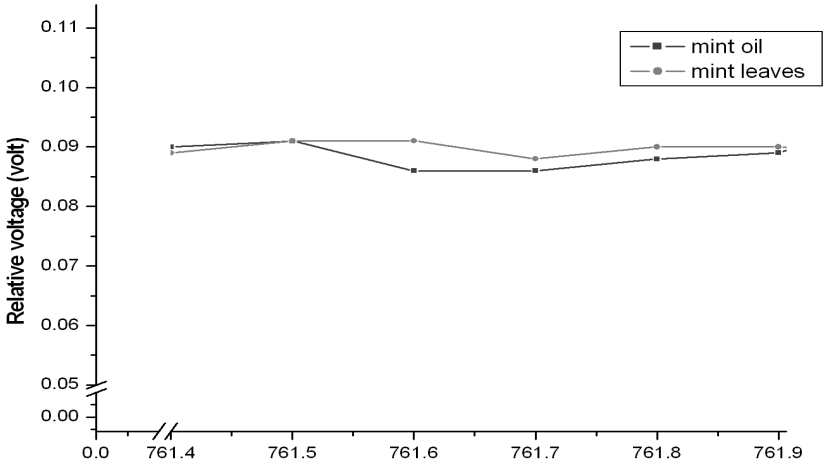

Fig 4.20 Michelson's signal versus evaporation time for mint oil and leaves samples over the time period 761.4 - 761.9

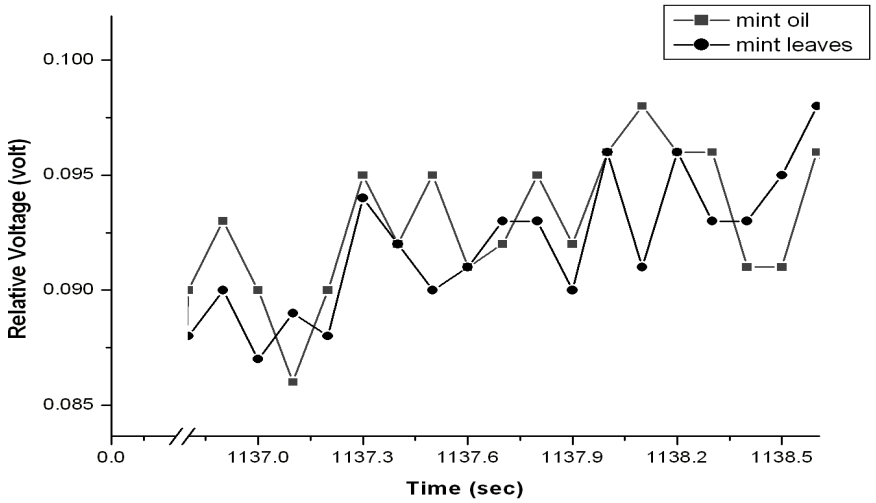

Fig 4.21 Michelson's signal versus evaporation time for mint oil and leaves samples over the time period 1136.8 - 1138.6

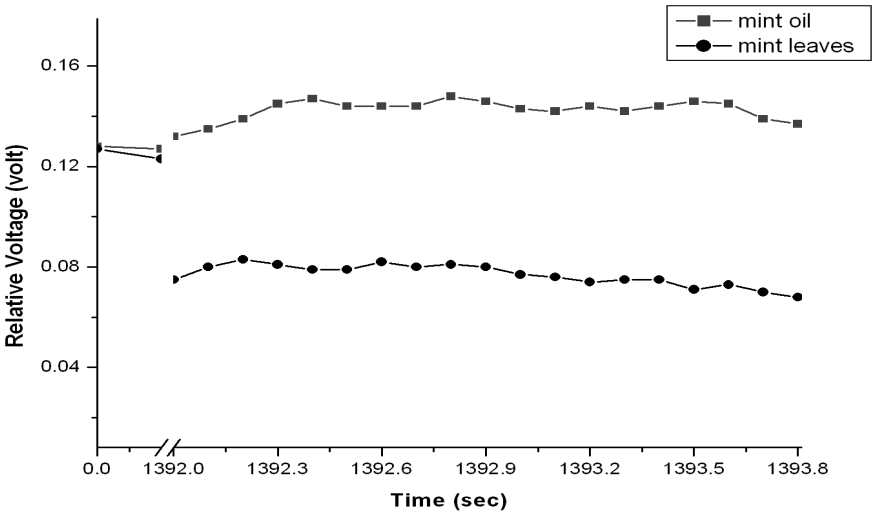

Fig 4.22 Michelson's signal versus evaporation time for mint oil and leaves samples over the time period 1392 - 1393.8

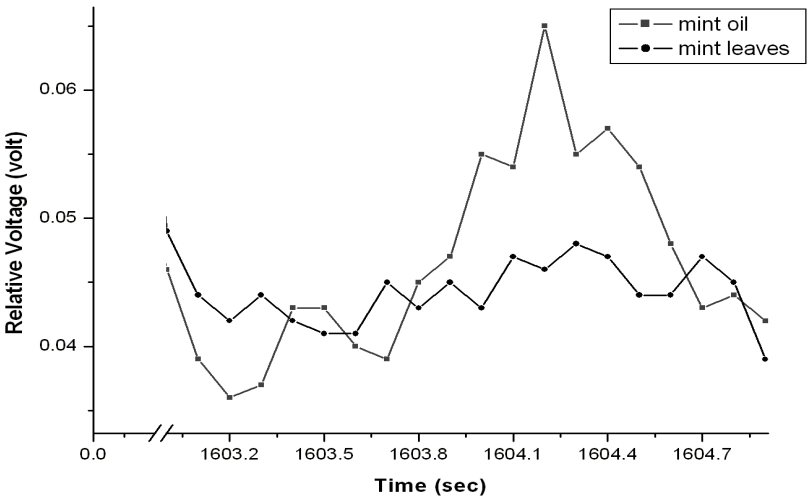

Fig 4.23 Michelson's signal versus evaporation time for mint oil and leaves samples over the time period 1603 - 1604.87

The PA signal versus time for mint oil and leaves are shown in Figs 4.24 through 4.29.

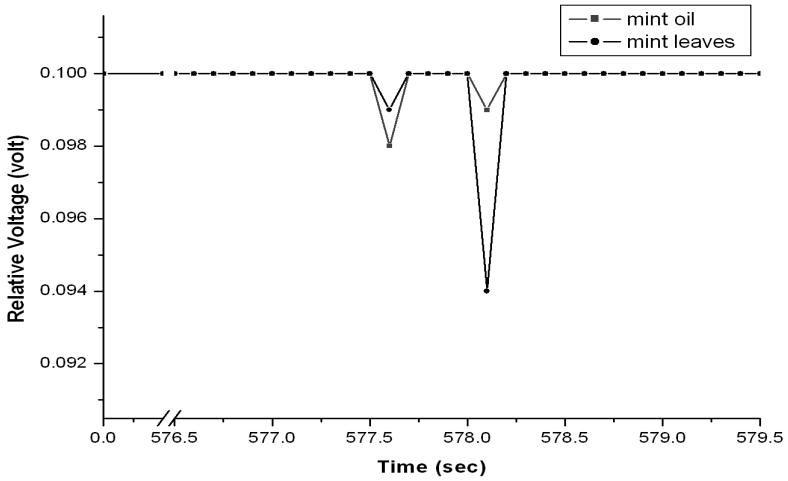

Fig 4.24 PA signal versus evaporation time for mint leaves and oil samples over the time period 576.5 - 579.5

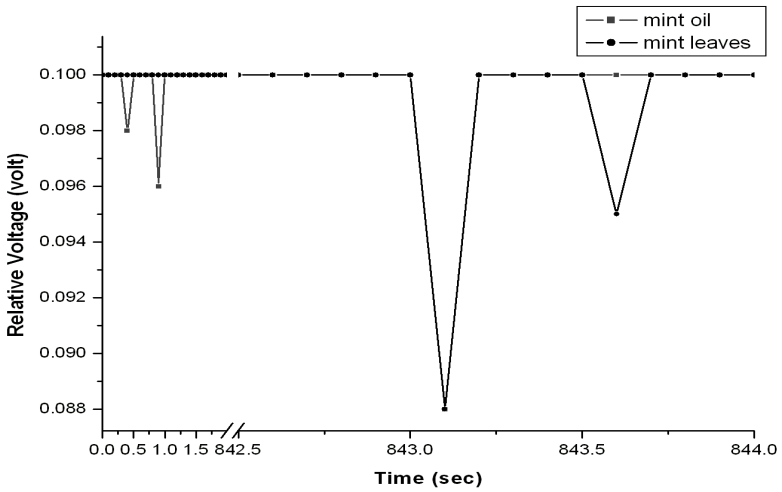

Fig 4.25 PA signal versus evaporation time for mint leaves and oil samples over the time period 842.5 - 844

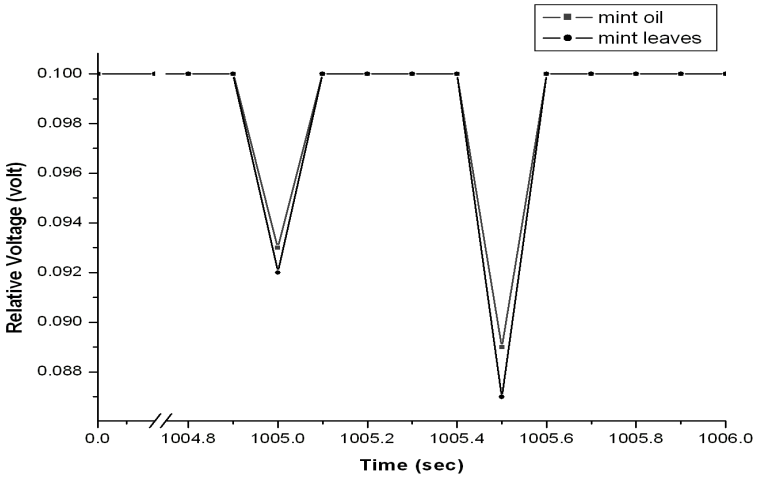

Fig 4.26 PA signal versus evaporation time for mint leaves and oil samples over the time period 1004.75 - 1006

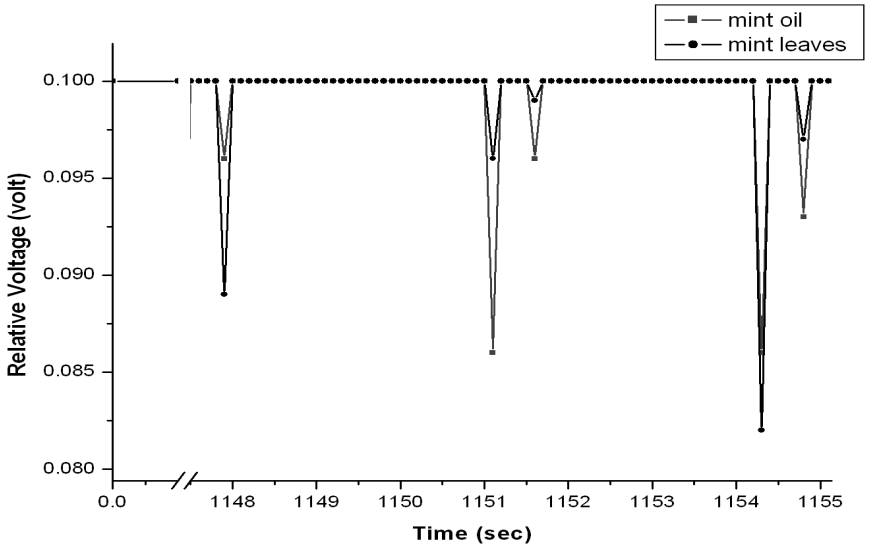

Fig 4.27 PA signal versus evaporation time for mint leaves and oil samples over the time period 1147.5 - 1155.5

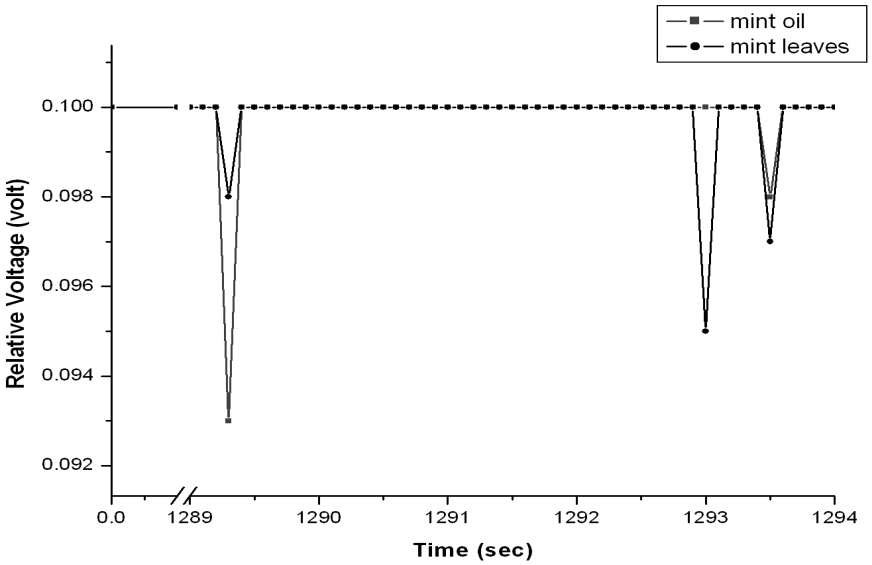

Fig 4.28 PA signal versus evaporation time for mint leaves and oil samples over the time period 1289 - 1294

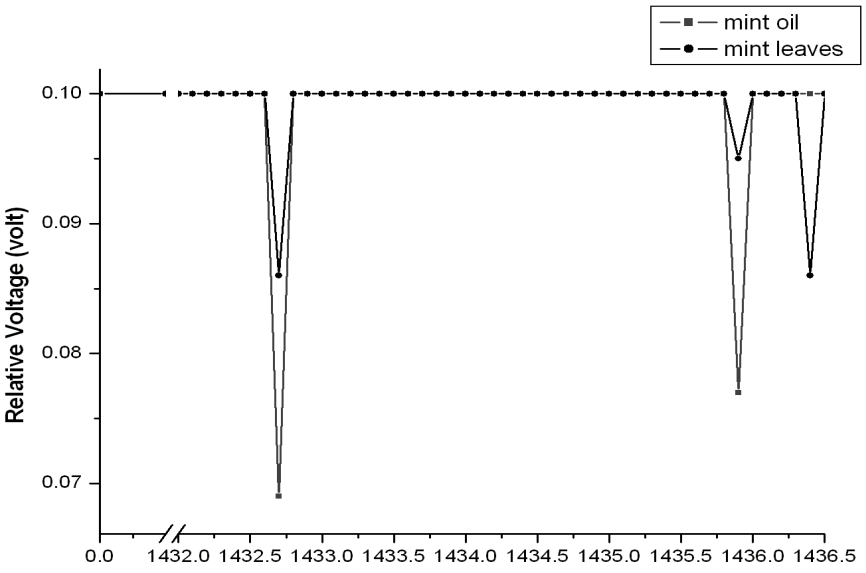

Fig 4.29 PA signal versus evaporation time for mint leaves and oil samples over the time period 1432 - 1436.5

4.5.3 Results of Nigella Sativa Oil and Seeds:

Samples of 1 gm of Nigella Sativa seeds and 4 µl of Nigella Sativa oil were tested for trace gas detection using the CMIPACT under 14 Hz modulating frequency and 0.7 amps driving IR source current. Figs 4.30 through 4.33 show Michelson's fringe signals for Nigella Sativa oil and seeds over different time periods.

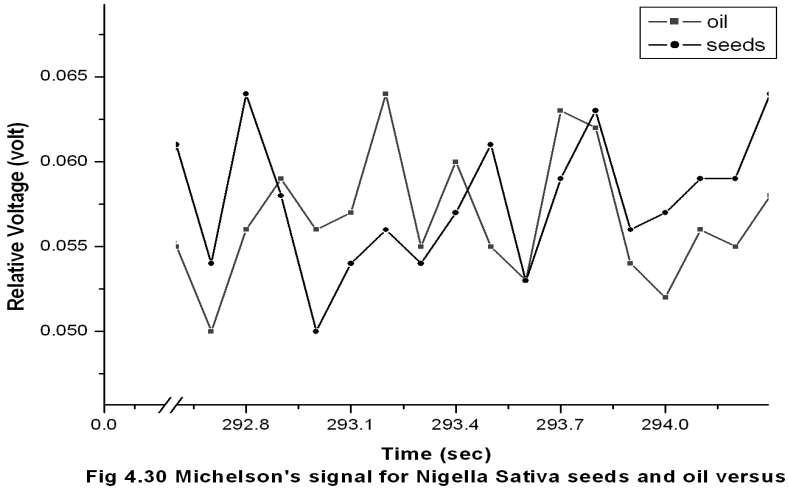

Fig 4.30 Michelson's signal for Nigella Sativa seeds and oil versus evaporation time over the time period 292.59 - 294.29 .

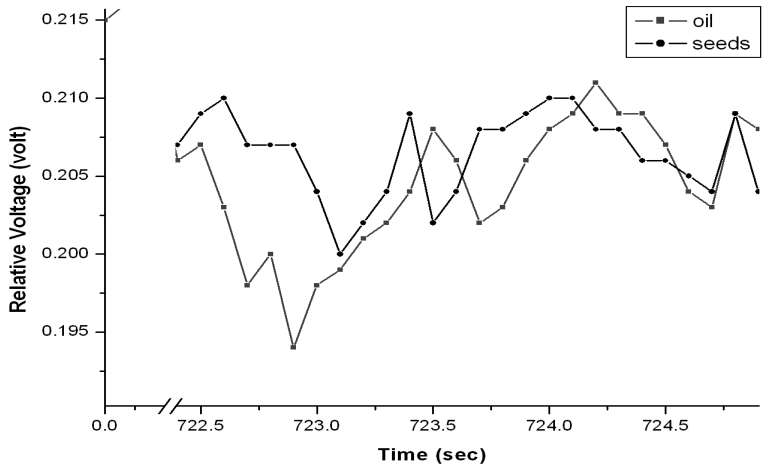

Fig 4.31 Michelson's signal for Nigella Sativa seeds and oil versus evaporation time over the time period 722.393 - 724.903

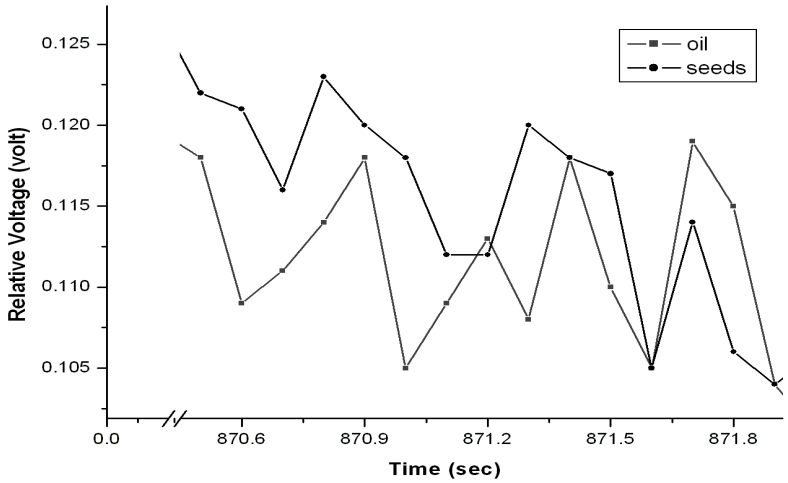

Fig 4.32 Michelson's signal for Nigella Sativa seeds and oil versus evaporation time over the time period 870.45 - 871.95

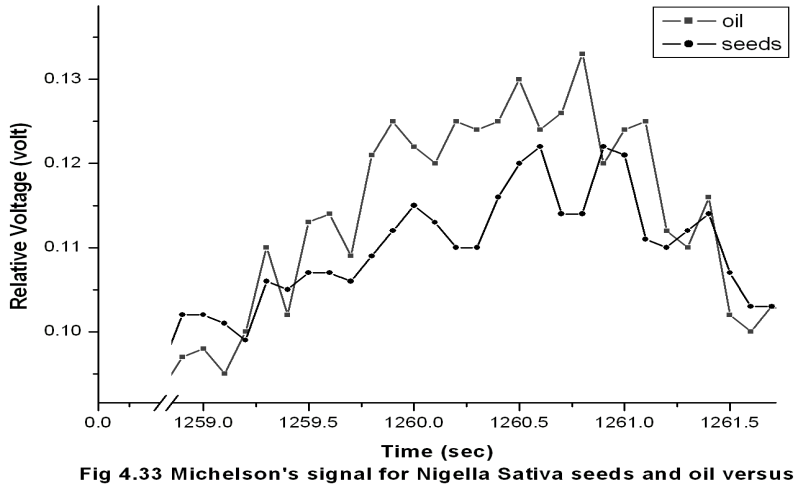

Fig 4.33 Michelson's signal for Nigella Sativa seeds and oil versus evaporation time over the time period 1258.85 - 1261.63

Figs 4.34 through 4.38 show the PA signal versus evaporation time for Nigella Sativa seeds and oil samples over different time periods.

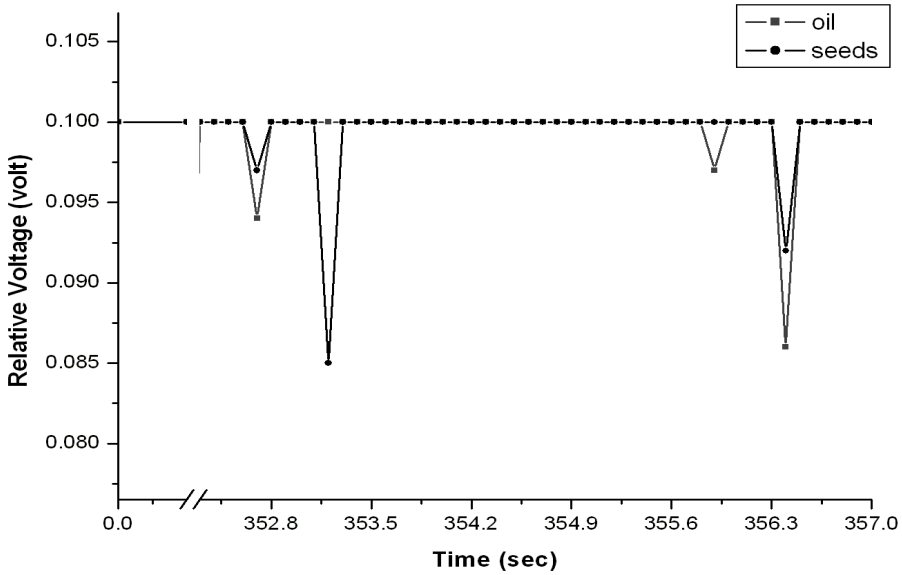

Fig 4.34 PA signal of Nigella Sativa seeds and oil versus evaporation time over the time period 352 - 357

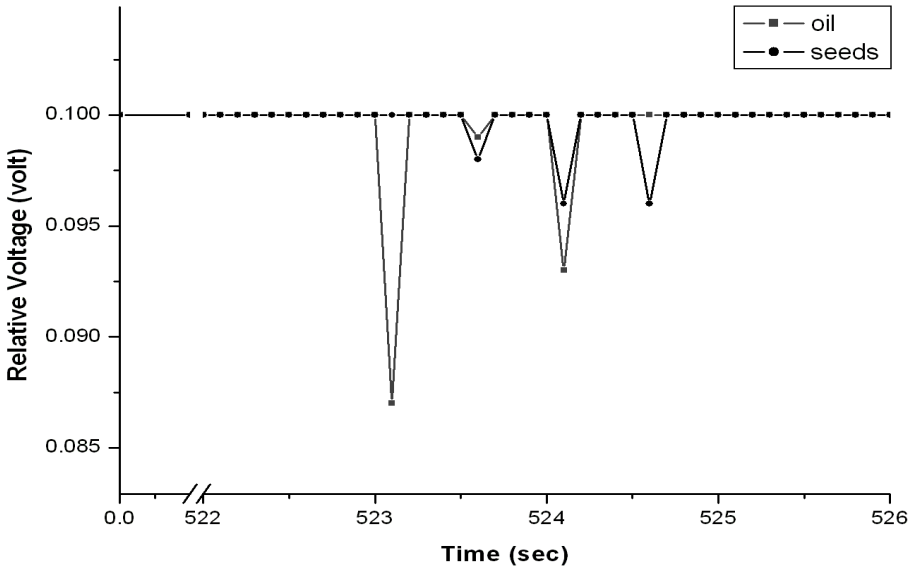

Fig 4.35 PA signal of Nigella Sativa seeds and oil versus evaporation time over the time period 522 - 526

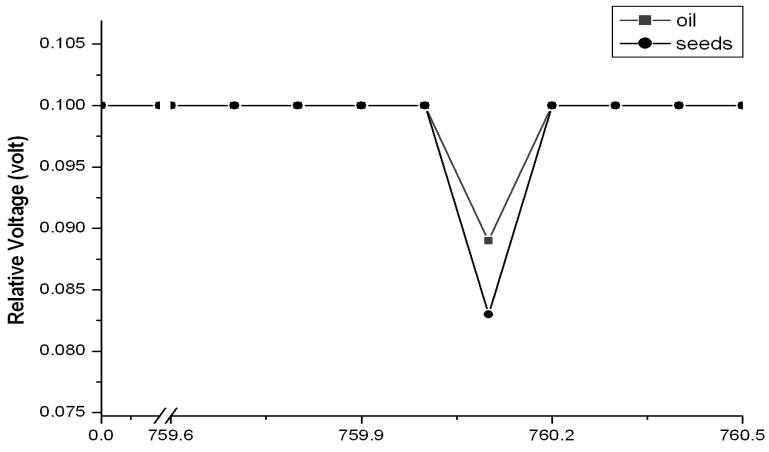

Fig 4.36 PA signal of Nigella Sativa seeds and oil versus evaporation time over the time period 352 - 357

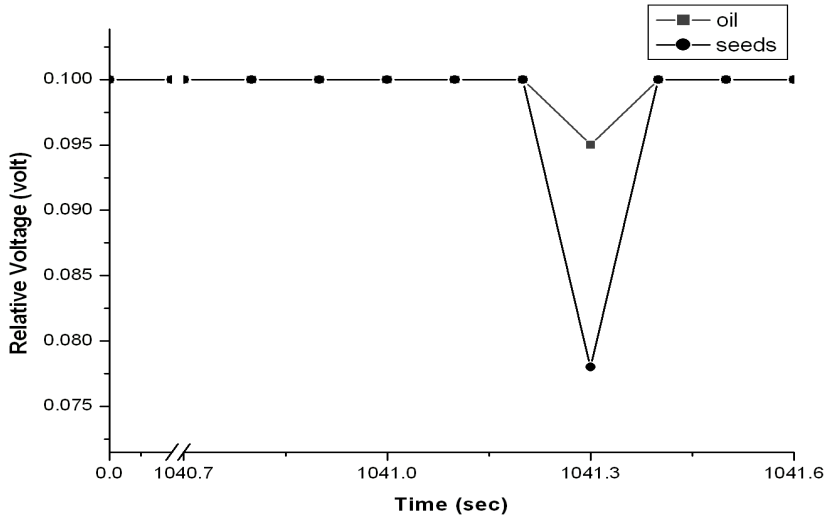

Fig 4.37 PA signal of Nigella Sativa seeds and oil versus evaporation time over the time period 1040.7 - 1041.6

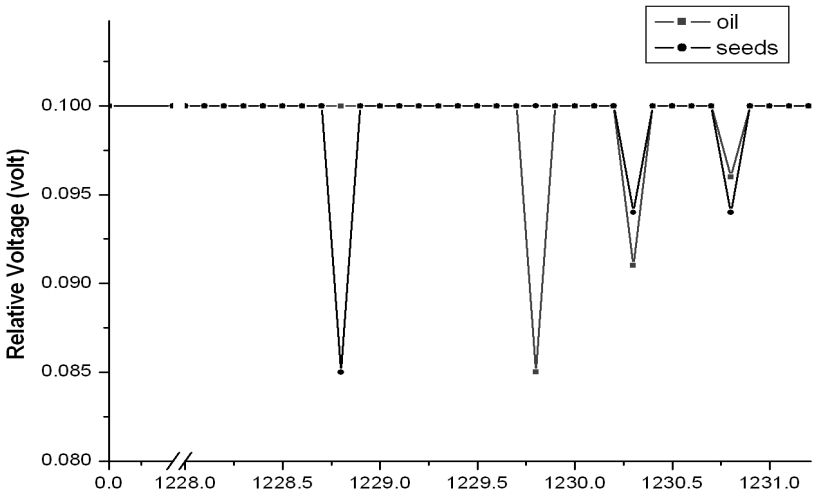

Fig 4.38 PA signal of Nigella Sativa seeds and oil versus evaporation time over the time period 1228 - 1231.5

4.5.4 Results of Anise Oil and Seeds:

Anise oil (*Pimpinella anisum*) or sweat cumin, containing about 1-4% volatile oil of which 72-90% is trans-anethole, has vast applications in food stuff, medicine and remedies.

Figs 4.39 through 4.42 show Michelson's fringe signal versus evaporation time for Anise seeds and oil samples over different time periods.

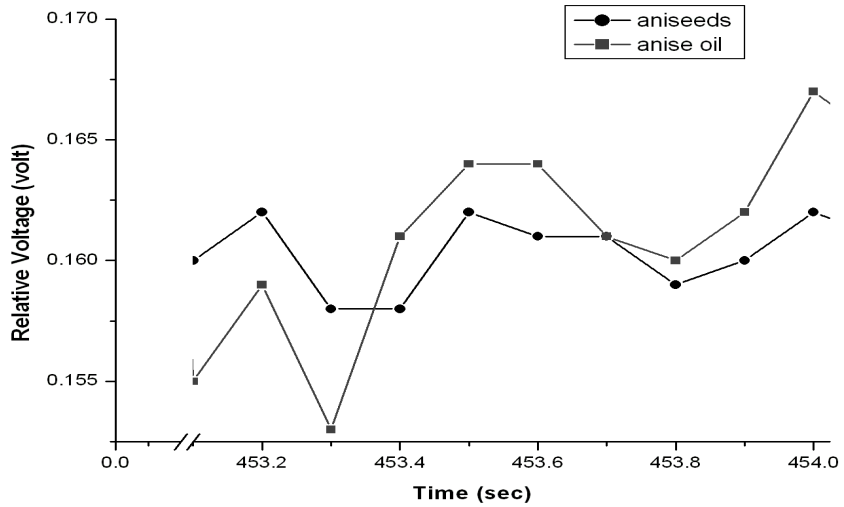

Fig 4.39 Michelson's signal versus evaporation time for anise seeds and oil over the time period 453.1 - 454

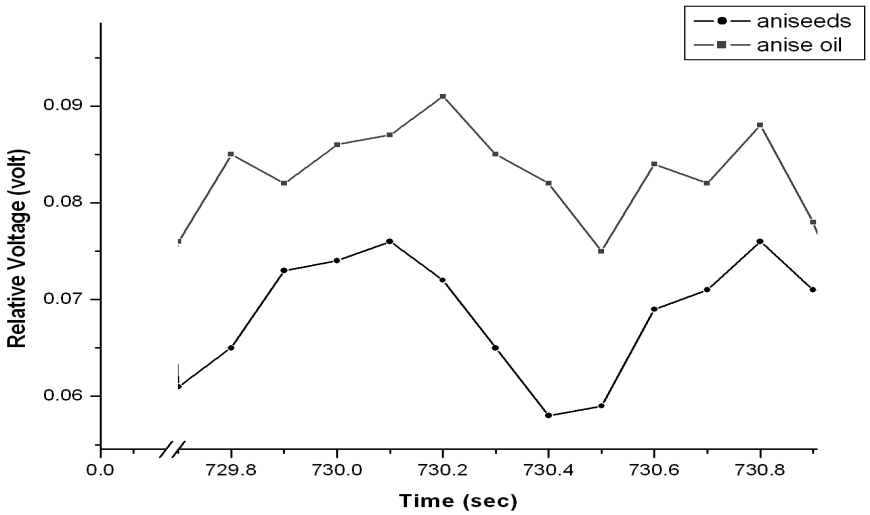

Fig 4.40 Michelson's signal versus evaporation time for anise seeds and oil over the time period 729.7 - 730.9

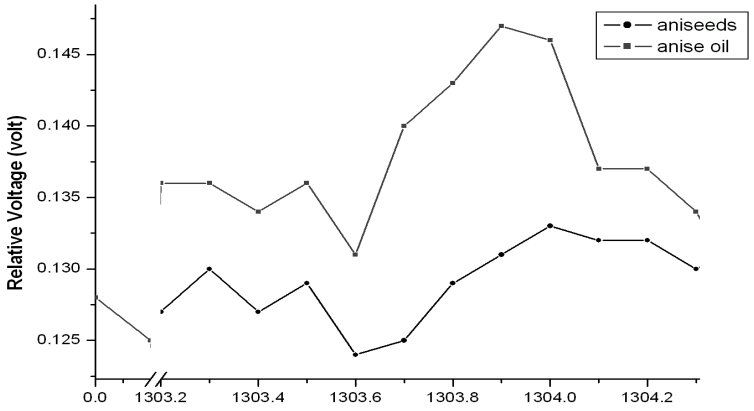

Fig 4.41 Michelson's signal versus evaporation time for anise seeds and oil over the time period 1303.2 - 1304.3

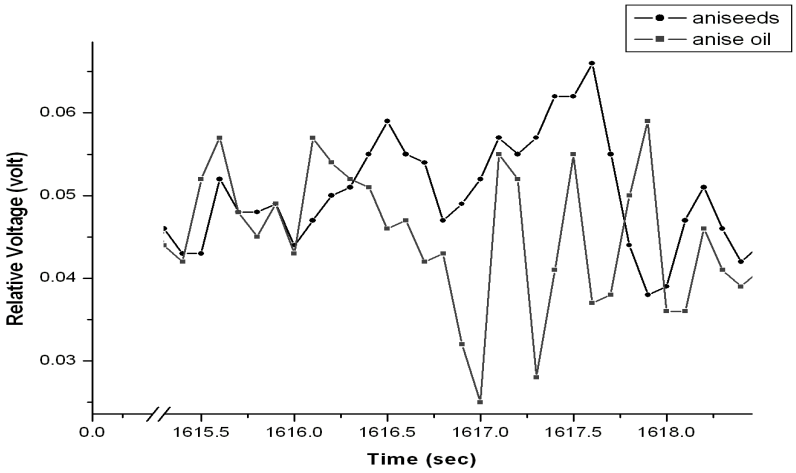

Fig 4.42 Michelson's signal versus evaporation time for anise seeds and oil over the time period 1615.3 - 1618.5

Figs 4.43 through 4.47 show the PA signal versus evaporation time for anise seeds and oil samples.

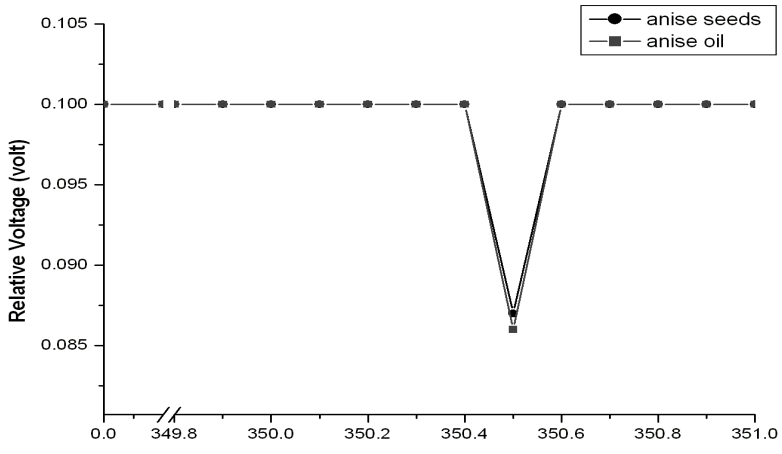

Fig 4.43 PA signal versus evaporation time for anise seeds and oil over the time period 349.8 - 351

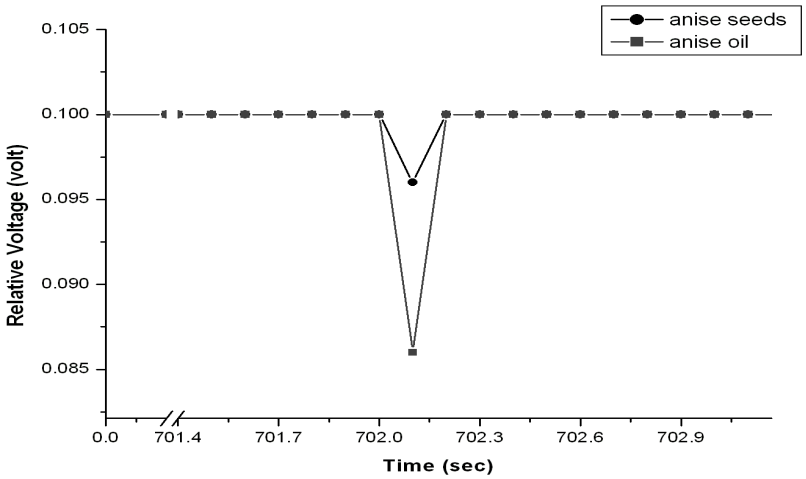

Fig 4.44 PA signal versus evaporation time for anise seeds and oil over the time period 701.4 - 702.6

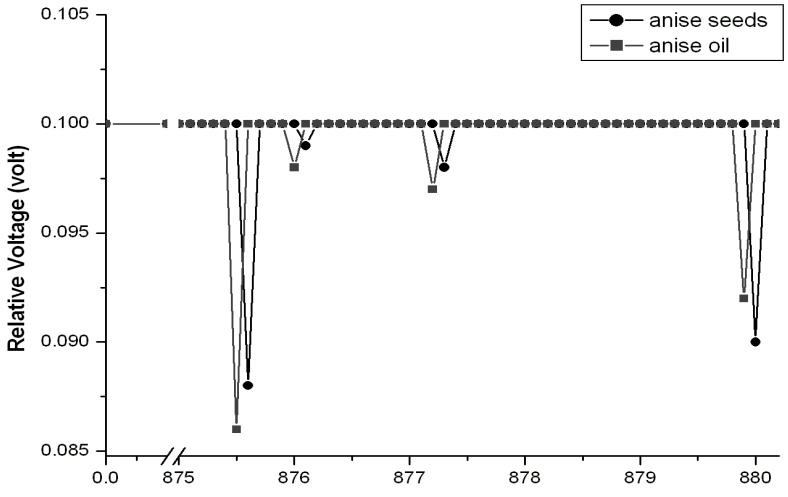

Fig 4.45 PA signal versus evaporation time for anise seeds and oil over the time period 875 - 880

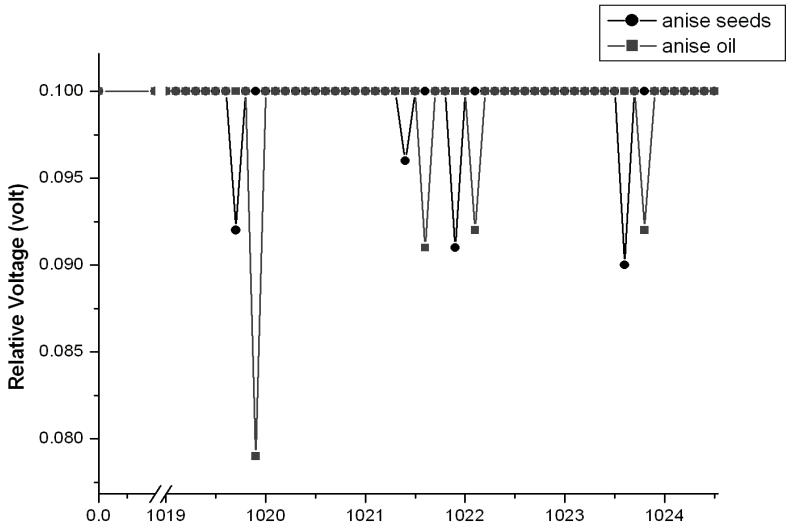

Fig 4.46 PA signal versus evaporation time for anise seeds and oil over the time period 1019 - 1024.5

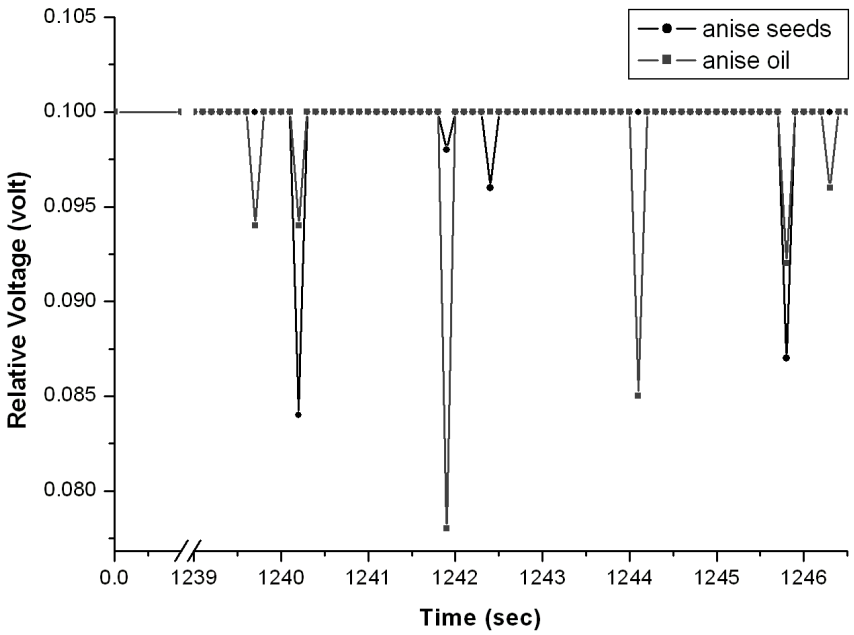

Fig 4.47 PA signal versus evaporation time for anise seeds and oil over the time period 1239 - 1246.5

4.6 Results of other liquid samples

In addition to previous investigated samples, the CMIPACT was used to investigate other liquid (non essential) samples regarding water. These samples were tap water and Zamzam water.

4.6.1 Results of tap Water:

Although this study is dealing with essential oil trace gas investigation, the researcher tested other trace gases in the vapors of non-essential materials like water.

The combined Michelson-PA signals versus evaporation time for a single drop of water (~ 4 µl) illuminated by IR source functioning at 12 Hz modulating frequency driven by 0.7 Amp's source current are shown in Fig 4.48 and 4.49 below.

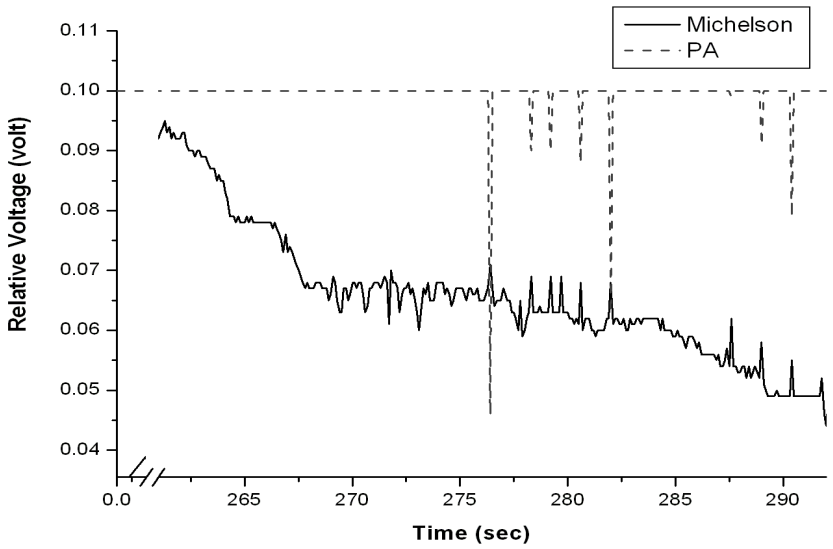

Fig 4.48 The combined Michelson-PA signal versus evaporation time for 4 micro liters of tap water over the time period 261 - 292

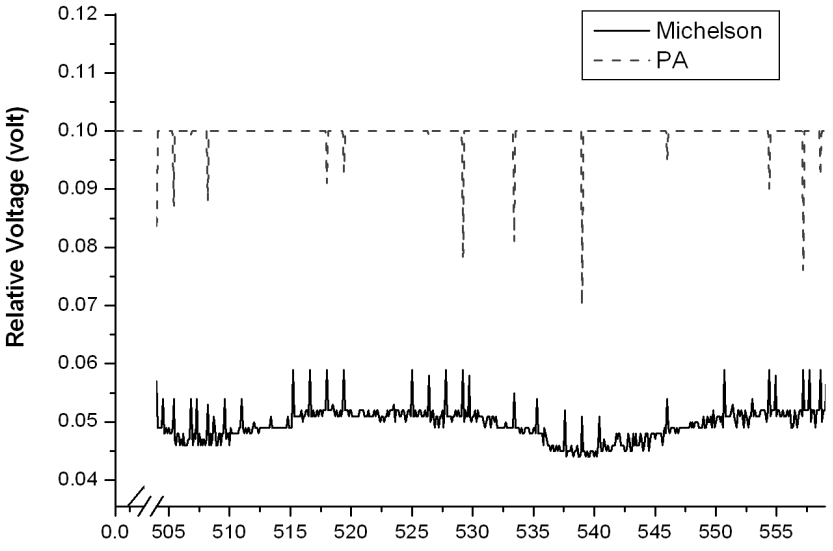

Fig 4.49 The combined Michelson-PA signal versus evaporation time for 4 micro liters of tap water over the time period 504 - 559

4.6.2 Results of Zamzam water:

Zamzam water is of a great religious value in Islam, it comes from the well-known Zamzam Well located near the holiest place in the earth (Alka'ba) in Saudi Arabia. Because of its healing capabilities – according to the words of our prophet Mohammad – the trace gas of Zamzam water was investigated in order to be compared with tap water.

The combined Michelson-PA signal versus evaporation time for a 4 µl sample of Zamzam water - being investigated under same conditions as tap water - were as shown in Fig 4.50 and 4.51 below.

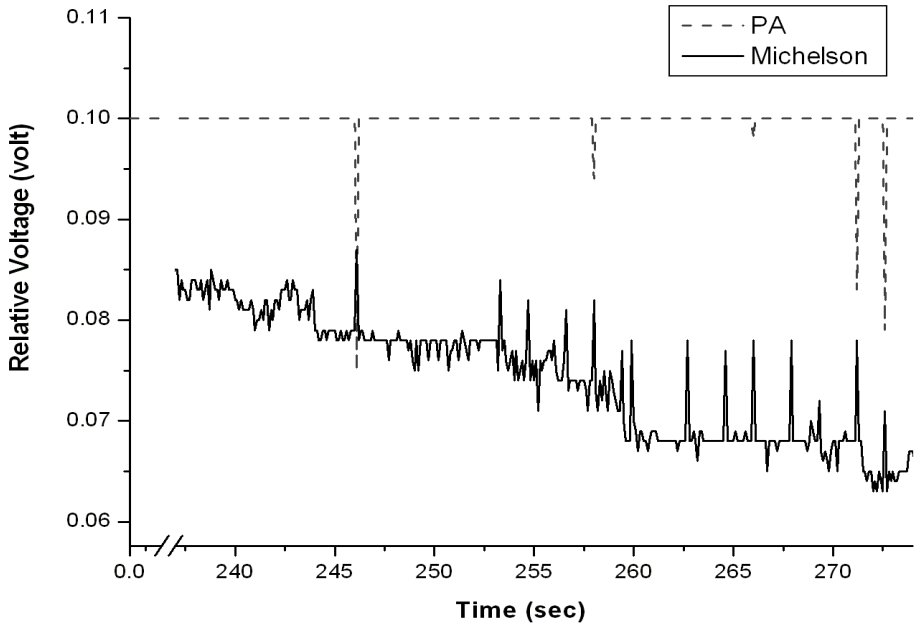

Fig 4.50 The combined Michelson-PA signal versus evaporation time for 4 micro liters of zamzam water over the time period 237 - 274

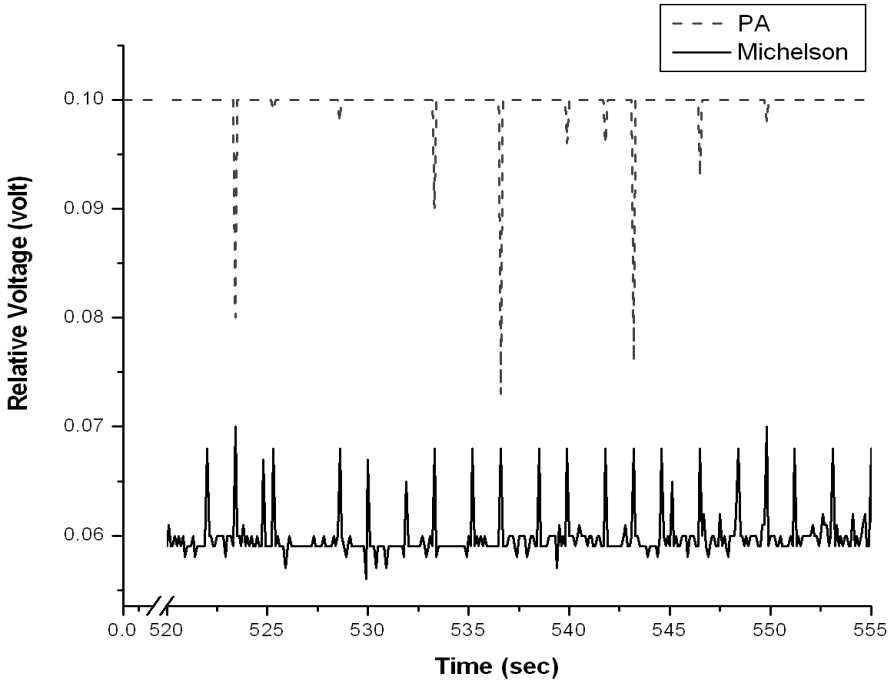

Fig 4.51 The combined Michelson-PA signal versus evaporation time for 4 micro liters of zamzam water over the time period 520 - 555

Figs 4.52 and 4.53 show a comparison between the traces of both, Zamzam and tap water.

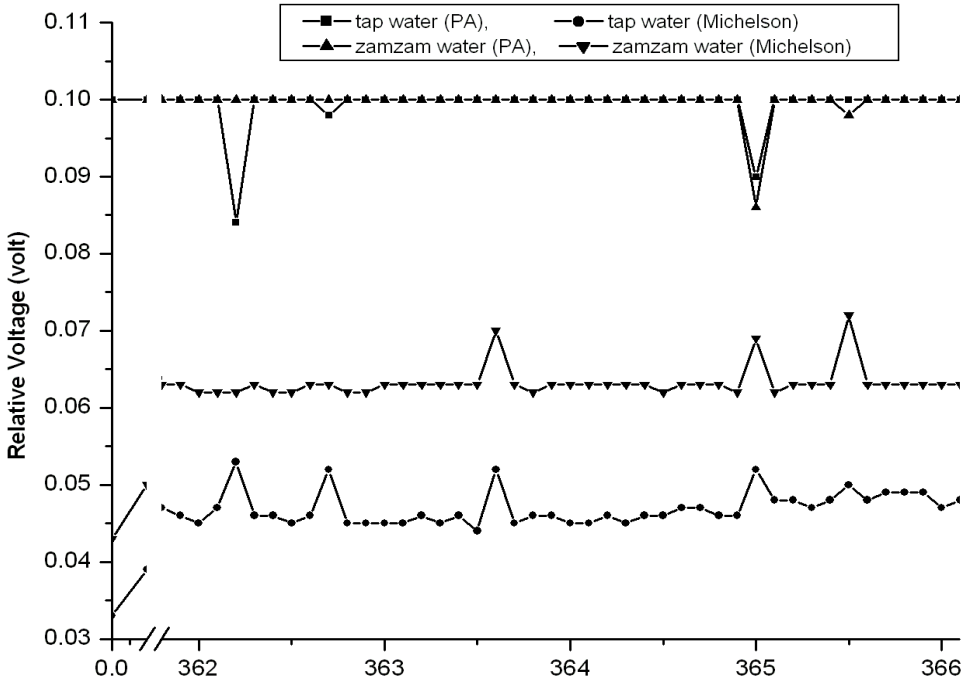

Fig. 4.52 A comparison between the combined Michelson-PA signals of zamzam water and tap water under same experimental conditions over the time period 361.8 - 366

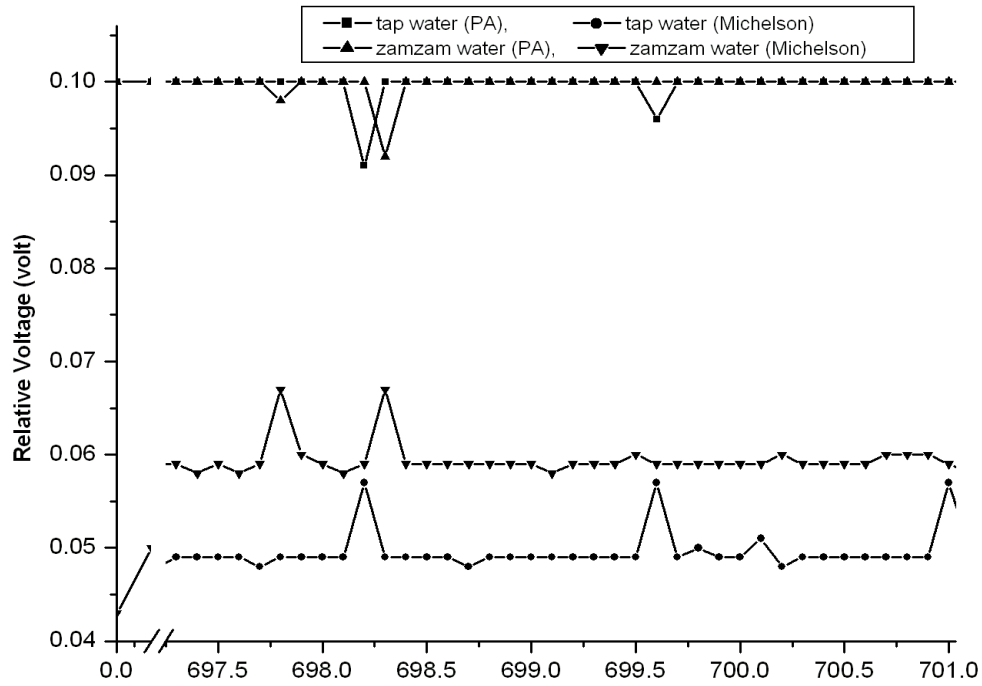

Fig. 4.53 A comparison between the combined Michelson-PA signals of zamzam water and tap water under same experimental conditions over the time period 697 -701

Chapter five

Discussion and Conclusions

Since data was collected to serve the main purpose of this study i.e., trace gas detection by means of PA method in conjunction with Michelson interferometry, they will be analyzed separately. A comparison between both signals will be done in order to judge the usefulness of using Michelson interferometry in trace gas monitoring. Although both signals were taken simultaneously, only for characterizing materials (materials used to investigate system's reliability and functioning) both signals will be compared. For the rest of the investigated samples, the spectrum of each essential oil will be compared with those of plant tissues from where they are usually extracted in both methods. Both signals has been detected simultaneously and monitored as a function of evaporation time. .

In dealing with IR absorption spectroscopy, normal modes are usually split into two main categories; skeletal vibrations and characteristic group vibrations. The former involves that all or nearly all atoms undergo the same displacement, while the later involves the different achieved displacements by some specific group of atoms rather than the others (Banwell, 1972). IR absorption by chemical molecules whether organic or inorganic compounds resulted in atomic vibration by stretching and contracting. These vibrations are influenced by atomic masses and the strength of the covalent bond between them. This situation is similar, to some extent, to that governed by Hook's law – with bonds replacing the spring and atoms assigning the masses – where the strength of the spring and the mass attached to determines the amount of energy needed to start the springiness. Thus, the amount of IR energy being absorbed is subject to the strength of the chemical bond between the atoms as

much as the mass of these atoms. Analogous to the mass-spring system, molecules are constrained to absorb the exact amount of IR energy subject to each vibration (http://www.oilanalysis.com/article_detail.asp?articleid=1109). The type of bonds (single – , double =, and or triple ≡) in a given molecule is subject to its chemical structure. Thus, a molecule containing more than one type of bonds is expected to result in at least two absorption bands when it is subjected to IR radiation i.e. characteristic IR absorption. According to Beer-Lambert law, the amount of IR energy being absorbed depends on both, concentration of the absorbing sample and thepath length through a direct proportionality (Robinson and Hons, 2000). In conjunction with electronic excitations, vibrational excitations might occur (vibronic transitions) giving rise to vibrational fine structure often observed in the gaseous phase (http://en.wikipedia.org/ wiki/molecular_vibration). The identity of the atoms being attached by some specific bond has a major effect on the IR frequency to be absorbed. The absorbed IR frequency is inversely related to the mass of these atoms i.e. the heavier the atoms, the lower the frequency at which absorption will occur. A good example of this is chlorophorm and deuterochlorophorm. A comparison between their spectra shows a shift of about 20 cm^{-1} relative to chlorophorm. Since deuterium is heavier than hydrogen, deuterochlorophorm will absorb at lower frequencies than chlorophorm (http://www.chem.ucla.edu/~webspectra/ irintro.html).

5.1 Combined Michelson-PA detection

The proposed detection technique involves simultaneous detection of both signals; fringe shift (based on Michelson interferometer) and PA. As mentioned in section 3.2, fringe shift was detected by means of a PASCO light intensity detector meanwhile; the PA signal was

detected by a KNOWLES microphone. Our – first time to be built – system's stability and reliability was checked using chlorophorm samples to set up its characteristics. Figs 4.1, 4.48 through 4.51 shows precisely the ability of the system to detect both signals at the same time. It is obvious that both signals are of the same origin. This can be illustrated as follows: IR absorption by gas molecules leads to thermal expansion through the nonradiative process which in turn results in the pressure fluctuations being detected by the microphone as the PA signal. During the thermal expansion process, heat deposition within the sample results in slight gradient changes in its refractive index forcing the fringes to a slight shift which is being detected as Michelson's fringe pattern signal. Through the above mentioned figures, spectra of different species shows different peaks i.e. different absorption frequencies which can be attributed to the double or triple bonds and or coupling of fundamental vibrations. Effects of samples volume, source driving current and modulating frequency were studied using chlorophorm samples.

5.2 Chlorophorm ($CHCl_3$)

Chlorophorm usually absorbs IR radiation in the range 3100 – 650 cm^{-1}. IR absorption by chlorophorm molecules is attributed to the type of motion atoms achieve through vibrational stretching or bending of the chemical bonds between them and so, individual bond is capable to absorb more than one IR frequency (http://www.chem.ucla.edu/ ~webspectra/irintro.html). The fundamental band frequencies at which chlorophorm absorbs in the gas phase are 3034, 1221, 769 and 681 cm^{-1}. These frequencies were attributed to C – H stretching, C – H bending, C – Cl stretching and C – Cl bending respectively (Kimoto and Yamada, 1968). The intensity of some signal (height) due to IR

absorption is usually referred to be weak, medium, strong, variable and or broad. Both C – H stretching and bending in chlorophorm achieves strong intensities, but the signal is sharp for bending and broadened for stretching. C – Cl stretching achieves higher intensity than both C – H stretching and bending meanwhile, C – Cl bending achieves very low intensity compared to the others (http://books.google.com/books?id=Ywzf4GyoUao C&pg= PA162&lpg).

Fig 4.1 show the combined Michelson-PA signals for chlorophorm. It is obvious that both signals have been generated at the same time, meaning that they are in phase and having the same origin. Different peaks in the PA signal denote different signal intensities achieved by different bond stretching or bending as discussed in the former paragraph. Increasing the volume of the sample increases the gas pressure within the cell leading to higher number of fringes to be translated. Fig 4.2 shows Michelson's fringe signal for different sample volumes. It is known that, the higher the volume of the sample, the higher the evaporation rate and so, the faster the change in the refractive index and pressure within the sample and the lower time needed to reach saturation, which is very compatible with Fig 4.2. The effect of changing the volume of the sample on the PA signal is shown in Fig 4.3, which shows that the signal increases as the concentration increases to some limit. Eqn. 2.18 predicts that heat production rate and so the amplitude of the PA signal increases as the molecular density increases.

According to Jenkins (1985), depth profiling decreases as the frequency of modulation increases. The higher the modulation frequency, the shallower the depths been probed, therefore, the lower the intensity of the PA signal. This is compatible with Fig 4.5, which shows the effect of modulating frequency on the PA signal. Fig 4.4 shows Michelson's fringe signal versus time at different modulating frequencies. It is obvious that the change in intensity is directly proportional to the frequency of modulation. This is explained in the

view of eqn. 2.7.20 as follows: increasing the modulation frequency will decrease the probed depth, thus decreasing the number of absorbing molecules, which results in lower heat production rate. This leads the refractive index to decrease slightly according to the inverse proportionality between the refractive index and temperature. In the view of eqn. 2.7.20, the change in the radius of the fringe is inversely proportional to the change in the refractive index i.e. the radius will slightly increase leading the intensity to be at some certain range. Decreasing the modulation frequency will increase the probed depth, thus leading to higher heat production rate and so, more decrease in the refractive index value. This leads the radius of the fringe to become larger which will result in lower amount of detected light, hence, lower intensity. Fig 4.6 shows the effect of changing the incident IR power by changing the source driving current on the fringe pattern. Increasing the incident power leads to refractive index change at a faster rate, this causes the fringes to achieve their shifts faster. For the PA signal, increasing the power of the incident radiation increases the probed depth and so, enhances much more molecules to vibrate giving rise to the number of the detected signals, this is, to some extent, compatible with Fig 4.7. Fig 4.1, 4.48 through 4.51 show good correlation between both signals except that, Michelson's fringe method has demonstrated higher ability in detecting weak signal, that microphone couldn't detect. Both spectra show different peaks with different intensities regarding the stretching and bending of the bond and the effect of evaporation rate on the heat production rate.

5.3 Essential Oils

Essential oils vary in their component constituents. This results in the presence of different absorption peaks within each essential oil spectrum. The number of peaks shown in some specific essential oil's spectrum is sensitive to the structure of that essential oil i.e. the presence of many double and triple bonds since most of their constituents are organic (Robinson and Hons, 2000). Studying the IR absorption of each component of the essential oil is a kind of tedious work since it needs analytical investigation, instead, essential oil studies usually undergoes band studies. In this work results from the oil samples are compared with those of the plant part where the oil is usually extracted from. Both signals were used to show how the oil and plant part spectrum's are related. In this section, results of essential oils are discussed separately.

5.3.1 Jasmine oil and flowers:

Fig 4.8 through 4.13 represent Michelson's fringe signals for both jasmine oil and flowers been compared to each other. All figures show the high correlation between both signals, which means that the oil is related to the part of plant from where it is usually been extracted, i.e. both release the same trace gas. Points of intersection through these figures denote that IR radiation being absorbed at the same rate in both samples oil and fresh flowers. The difference in intensity of both signals at some certain point is attributed to the concentration of the sample under investigation, in addition to the existence of water molecules in the flower sample but not to oil in samples. Strong absorption intensities in flower spectrum are related to the existence of water molecules since water is a good

absorber of infrared radiation especially at 3657, 3755, 1594 cm^{-1} in the gas phase (http://www.lsbu.ac.uk/water/index2.html, 2007). According to the above-mentioned figures, it is obvious that oil has sometimes achieved higher intensities and other times lower intensities than flower. Higher oil signal intensity attributes the presence of higher number of double and triple bonds regarding that, the amount of oil present in the trace of the flower is very small. Higher flower signal intensity is attributed to higher heat production rate regarding the fact that, eqn. 2.18 predicts that the higher the molecular density, the higher the heat production rate which results in higher change in the refractive index leading to greater fringe shifts. Fig 4.14 through 4.17 represents the PA signal of jasmine oil and flowers been compared with each other. All presented spectra show high correlation between relative signals. The variation in intensities of both signals attributes the fact that, IR absorption by some certain chemical bond can be expressed by vibrational motion as stretching and bending. The presence of some peaks in flower spectra that are not shown in that of the oil are attributed to many other molecules like water present in the trace of flowers but not in that of pure oil. Different peaks in the spectra of oil are the result of different absorbing components that oil contains. Since the composition of each essential oil is usually been dominated by one single compound, then signals corresponding to both traces are related to that dominant compound.

5.3.2 Mint oil and leaves:

Figs 4.18 through 4.23 show high similarity between the traces of mint oil and leaves been detected via Michelson interferometer. This similarity assures the usefulness of Michelson's interferometer in trace gas identification. Figs 4.18, 4.19 and 4.20 show that

leave trace has achieved higher intensity than oil, while Figs 4.21, 4.22 and 4.23 show opposite results. Both results are explained in the same manner as in jasmine. Analogous to jasmine flowers, peaks that are present in the trace of mint leaves but not in mint oil are the result of other constituents like water vapor present in leaves been evaporated, which is not the case for oil. Figs 4.18, 4.19 and 4.20 show that oil has achieved lower signal intensity than that of leaves. This can be also explained to be due to higher evaporation rate of leaves composite compounds rather than the small amounts of oil. Since leaves were emasculated, vapor being driven from them saturates first. After becoming in equilibrium with its vapor, IR absorption within the trace of the sample increases as the number of double and triple bonds increase. This also demonstrates the higher achieved signal intensity in the spectra of oil. Figures 4.24 to 4.29 show the PA signal for both mint oil and leaves been compared with each other. Spectra of both investigated samples show, in general, high similarity, indicating that both samples relate to each other. The rate of trace gas emission in mint leaves is higher than that of mint oil giving rise to higher absorption intensity for the signal of mint leaves in some spectra regarding predictions of eqn. 2.18. Peaks where the signal intensity achieved by both oil and leaves traces is the same denotes that the absorbing molecule has achieved the same vibrational stretching or bending motion due to IR frequency absorption. The variance in signal intensity of mint oil and leaves is attributed to the type of vibrational motion (stretching or bending) that the bond achieved because of IR absorption. Like jasmine, signals correlation corresponding to both traces denotes a single dominant compound in the essential oil.

5.3.3 Nigella Sativa oil and seeds:

Figs 4.30 through 4.33 show Michelson's fringe signal for both oil and seed traces been compared with each other. These figures show an overall high correlation between both trace, which denotes the relation between them i.e. being traces of two samples having almost common constituents. These spectra follow the same discussion procedure proposed for both jasmine and mint except one single important situation. In both jasmine and mint, the oil has reached sometimes higher intensity and other times lower intensity in (IR absorption) compared to those of flowers and leaves which was discussed in both mint and jasmine to be due two reasons, the first denotes the relation between heat production rate and molecular density which is affected by the evaporation rate giving rise to flowers and leaves to achieve higher intensities, while the second denotes the effect of having more double and triple bond contained in compounds giving rise to oil to reach higher absorption levels. In the case of Nigella sativa, seeds are the plant part from where oil is usually been extracted. The rate of trace released from seeds is expected to be lower than that of the oil. This leads to the prediction that the oil absorption signal will reach higher level earlier than that of the seeds due to both reasons. Figures 4.30 through 4.33 confirmed the right of these predictions.

Figs 4.34 through 4.38 show PA signals for both Nigella sativa oil and seeds. All figures show high similarity and correlation between both corresponding traces, indicating that they are both related to each other. Like jasmine and mint, signals correlation corresponding to both traces denotes the dominant compound in the essential oil. The difference in intensity achieved by both signals at some certain point is attributed to the type of vibrational motion accomplished within the bond; stretching or bending. Signals that are present in the trace of the seeds but not in the trace of the oil are explained to be

compounds present in the seeds but not in the oil, those might be related to volatiles that normally are not collected in the oil stream during seed squeezing.

5.3.4 Anise oil and seeds:

Figs 4.39 through 4.42 show Michelson's fringe signal for both anise oil and seeds. Since these figures show close fit between both traces and since anise oil has reached higher signal intensity than seeds did, then anise follow the same explanation proposed for Nigella sativa. Figs 4.43 through 4.47 show the PA signal for both anise oil and seeds been compared to each other. The close fit between curves of both signals asserts the relation between both investigated samples. Fig 4.45 and 4.46 shows a shift in the PA signal leading to partial and total incompatibility between both signals. This shift is explained to be the result of detection time lag. It might also be due to either one of the following reasons; the first denotes the probability of having two different molecules absorbing IR radiation at very close frequencies. This hypothesis can be explained using the C – H stretching in both Alkane and Alkene as an example, as follows: Alkanes achieve their highest C – H stretching characteristic absorption frequency at 3000 cm^{-1}, while Alkenes achieve their lowest =C – H stretching characteristic absorption frequency at 3010 cm^{-1} (http://www2. ups.edu/fuculty/hanson/spectroscopy/IR/IRfrequencies.html). The second reason denotes that the vibrating bonds in the absorbing compounds in one of the two traces is attached to one isotopic atom leading it to vibrate at a slower frequency compared to the same bond in the same compound in the trace of the other sample which has no isotopic atoms. An example of this is the shift occurred in the spectra of deuterated chlorophorm $CDCl_3$ relative to chlorophorm $CHCl_3$ (Kimoto and Yamada, 1968).

5.4 Other investigated samples

Figs 4.48 through 4.51 show both signals versus evaporation time for the following samples respectively: tap water (Figs 4.48, 4.49) and Zamzam water (Figs 4.50, 4.51). All these figures follow the same previous general discussion in showing the good correlation between Michelson fringe signal and that of the PA, in addition to the higher observed sensitivity of Michelson interferometer in trace gas detection over the PA method represented by the signals that appears in the spectrum of Michelson but not in that of the PA. Fig 4.52 and 4.53 show a comparison between the traces of Zamzam and tap water. The similarity and good correlation between both traces asserts that they have much in common and that they almost represent the same sample with slight differences. Higher sensitivity subject to IR absorption was observed in the Michelson fringe signals over those of PA. In addition to this, slight changes in both traces are explained to be the result of the slight difference in chemical composition and optical parameters of both water samples. Two separate studies – (http://iadr.confex.com/iadr/saudi06/preliminaryprogram /abstract_87084, 2009) and (El-Zaiat, 2007) – dealing with investigating the chemical composition and optical properties of zamzam water insures that zamzam and tap water have almost the same characteristics with some differences in mineral levels and optical parameters. Their results confirm the reliability and sensitivity of our new introduced investigation method.

5.5 Conclusions

In this thesis, a set of experiments were successfully carried out using the new simple, inexpensive and accurate combined Michelson-photoacoustic chamber technique being introduced and built for the first time by us. According to the results presented in chapter four and discussed in chapter five, a set of significant conclusions can be extracted. The most amazing and important one involves the high sensitivity and capability of the introduced system in trace gas detection. The new introduced technique was successfully applied to distinguish between different samples due to band absorption of IR radiation in the range of 2 – 9.5 μm. More precisely, the technique showed high ability to distinguish between similar samples having small differences relative to each other represented by the traces of tap and zamzam water samples.

Simultaneous detection of both signals using the new combined technique provides a set of conclusions among which the main goals of this study were shown to be achieved. These conclusions are:

- ✓ For the first time, photoacoustic signals have been successfully detected inside Michelson cavity.
- ✓ PA and Michelson fringe signals have shown good correlations compared with each other.
- ✓ The correspondence between the two detected signals insures that they have been generated at the same time in addition to having the same origin.
- ✓ The collected spectra (results) proved that Michelson interferometry has achieved higher sensitivity compared with conventional PAS for IR absorption in the region 2 – 9.5 μm.

- ✓ The new introduced technique in which the high expensive lasers are replaced by a wideband-pulsed IR source, have shown good capabilities in the field of trace gas detection.
- ✓ The new introduced technique demonstrates an edge over laser PAS for offering high possibilities of being portable.

In general, the combined technique has proved the usefulness of measuring the PA effect inside Michelson's cavity. The results are encouraging and show high possibilities of achieving sensitivities as low as ppb level in trace gas detection. The new introduced combined Michelson-PA chamber technique is expected to result in a deeper understanding of the investigated samples. The good correlation between PA and Michelson fringe signals offers a new scheme of correlation spectroscopy.

Chapter six

Further Work

In this study, the kind of work that was carried out using the new introduced combined technique and the good correlations between related spectra opens the door to different further applications. Some of these further applications are listed below.

- ☒ The introduced technique may be used to investigate similar experiments that depends on the emission of trace gases, for example, the biological activities of living creatures like insect respiration. It also might be used to monitor the meioses and mitosis processes in microscopic organisms to measure the rate at which they reproduce.
- ☒ Different enhancements could be done to increase the sensitivity of the system like replacing the amplitude-division interferometer by another time-division interferometer which is expected to result in higher resolution in the fringe pattern.
- ☒ The effect of the volume of the cell on the minimum detectable sensitivity could be investigated using different cells of different volumes.
- ☒ The good correlation and high compatibility between the traces of different oil samples and those of plant parts from where they are usually extracted opens the door for different agricultural researches regarding different traditionally used herbs in our country in their fresh or dried forms.

References:

1. Alvi M., Ahmad S. and Rehman K. (2001), **Preparation of menthol crystals from mint (Mentha arvensis)**. International journal of agriculture and biology, **4** : 527-528.
2. Aqel M. and Shaheen R. (1996), **Effects of the volatile oil of Nigella sativa seeds on the uterine smooth muscle of rat and guinea pig**. Journal of ethnopharmacology, **52** : 23-26.
3. Autrey T., Foster N., Hopkins D. and Price J. (2001), **Tunable ultraviolet visible photoacoustic detection Analysis of the sensitivity and selectivity provided by a Xenon flash lamp**. Analytica Chimica Acta, **434** : 217-222.
4. Banwell C. (1972), **Fundamentals of Molecular Spectroscopy**. Second edition, McGraw-Hill Book Company (UK) Ltd, p. xi, 27, 87, 88, 103-105.
5. Barr J. (1969), **Spectral emissivity by interferometric spectroscopy**. Infrared physics, **9** : 97-108.
6. Bartlett D., Hewitt R., Robinson L. and Tait G. (1977), **A study of far-infrared Michelson interferometer based of fast plasma scanning**. Infrared physics, **17** : 89-103.
7. Bartusiak M. (2000), **Einstein's unfinished symphony**. Joseph Henry Press, 27-28.
8. Basu D. (2001), **Dictionary of Pure and Applied Physics**. CRC Press, p. 238.
9. Benedetto G., Maringelli M. and Spagnolo R. (1987), **Method for the absolute calibration of photoacoustic cells**. Rev. Sci. Instrum. **58** (6) : 975-978..
10. Bernath P. (2000), **Infrared emission spectroscopy**. Annu. Rep. Prog. Chem., sect. C, **96** : 177-224.

11. Bernegger S. and Sigrist M. (1990), **CO-laser photoacoustic spectroscopy of gases and vapours for trace gas analysis**. Infrared phys. **30** (5) : 375-439.
12. Besson J., Schilt S. and Thevenaz L. (2008), **Molecular relaxation effects in hydrogen chloride photoacoustic detection**. Appl. Phys. B **90** : 191-196.
13. Bicanic D., Zuidberg B., Jalink H., Miklos A., Hartmans K. and Van Es A. (1990), **The assessment of laser photoacoustic spectroscopy as the analytical tool for studying the potato sprout suppressants carvone and pulegone**. Applied Spectroscopy, **44** (2) : 263-265.
14. Bin Hu, Da Chen and Qingde Su (2007), **Photoacoustic and luminescence spectra study on the effects of chlorine substituent on the energy transfer of Eu(III)-chlorobenzoic acid**. Spectrochimica Acta Part A, **66** : 273-277.
15. Burits M. and Bucar F. (2000), **Antioxidant activity of Nigella sativa essential oil**. Phytother. Res. **14** : 323-328.
16. Buyukozturk S., Gelincik A., Ozseker F., Genc S., Savran F., Kiran B., Yillar G., Erden S., Aydin F., Colakoglu B., Dal M., Ozer H. and Bilir A. (2005), **Nigella sativa (black seed) oil does not affect the T-helper 1 and T-helper 2 type cytokine production from splenic mononuclear cells in allergen sensitized**. J. of ethnopharmacology **100** : 295-298.
17. Cano R. and Mattioli M. (1967), **Far-infrared spectroscopy with a Michelson interferometer and an InSb detector**. Infrared physics, **7** : 25-35.
18. Carmichael R. (2008), **the Theory of Relativity**. BiblioBazaar, LLC, 10-13.
19. Chanaud R. (1997), **Effects of geometry on the resonance frequency of Helmholtz resonators, part II**. Journal of sound and vibration, **204** (5) : 829-834.

20. Ciftci M., Guler T., Dalkilic B. and Ertas O. (2005), **The effect of anise oil (Pimpinella anisum L.) on broiler performance**. International J. of poultry science **4** (11): 851-855.
21. Crippa P. and Viappiani C. (1990), **Photoacoustic studies of non-radiative relaxation of excited states in melanin**. Eur. Biophys J. **17** : 299-305.
22. Cristina E. (2004), **Understanding true aromatherapy: understanding essential oils**. Home health care management & practice, **16** (6) : 474-479.
23. Dakin J., Edwards H. and Weigl B. (1995), **Progress with optical gas sensors using correlation spectroscopy**. Sensors and actuators B **29** : 87-93.
24. Dawa B. and Gowland A. (1978), **Infrared studies of carboxylic acids and pyridine in chloroform and methanol**. Can. J. Chem. **56** : 2567-2571.
25. Dewey Jr C., Kamm R. and Hackett C. (1973), **Acoustic amplifier for detection of atmospheric pollutants**. Appl. Phys. Lett., **23** (11) : 633-635.
26. Donini J. and Michaelian K. (1984), **Effect of cell resonance on depth profiling in photoacoustic FTIR spectra**. Infrared Phys. **24** (2/3) : 157-163.
27. Ebru U., Burak U., Yusuf S., Reyhan B., Arif K., Faruk T., Emin M., Aydin K., Atilla I., Semsettin S. and Kemal E. (2008), **Cardioprotective effects of Nigella sativa oil on Cyclosporine A-induced Cardiotoxicity in rats**. Nordic pharmacological society, **103** : 574-580.
28. El-Kahlout A., Al-Jourani M., Abu-Taha M. and Laine D. (1998), **Laser photoacoustic detection of the essential oil vapours of thyme, mint and anise**. SPIE, **3405** : 578-583.
29. Fowles G. (1989), **Introduction to Modern Optics**. Second edition, Courier Dover Publications, 63-65.
30. French A. (1968), **Special Relativity**. First edition, CRC Press, 50-53.

31. Gamow G. (1961), **One, two, three-- infinity**. Courier Dover Publications, 92-94.
32. Gebbie H. and Stone N. (1964), **A Michelson interferometer for far infrared spectroscopy of gases**. Infrared physics, **4** : 85-92.
33. Genzel L. and Kuhl J. (1978), **A new version of a Michelson interferometer for fourier transform infrared spectroscopy**. Infrared physics, **18** : 113-120.
34. George N., Paul T., Radhakrishnan P., Nampoori V., Vallabhan C. and Sebastian M. (2000), **Photacoustic investigation of the effect of excess lead oxide on thermal diffusivity of PLZT ceramic**. Journal of materials science letters **19** : 499-501.
35. George N., Vallabhan C., Nampoori V., George A. and Radhakrishnan P. (2000), **Use of photoacoustic effect for the detection of phase transitions in liquid crystal mixtures**. J. Phys. D: Appl. Phys. **33** : 3228-3232.
36. Haisch C. and Niessner R. (2002), **Light and sound - photoacoustic spectroscopy**. Spectroscopy Europe **14** (5) : 11-15.
37. Hallam H. (1968), **Recent advances and applications of infrared spectroscopy**. Proc. Soc. Analyt. Chem. **1** : 25-26.
38. Halliday D. and Resnick R. (1988), **Fundamentals of Physics**. Third edition, John Wiley & Sons Inc., p. 420, 913.
39. Hariharan P. (2003), **Optical interferometry**. second edition, Academic Press: 2-3.
40. Hariharan P. (2006), **Basics of interferometry**. second edition, Academic Press: 15-18.
41. Hazelett R. and Turner D. (1979), **The Einstein myth and the Ives papers**. Hope Publishing House: 177-180.
42. Hecht E. and Zajac A. (1979), **Optics**. First edition, Addison-Wesley Publishing Company Inc.: 7-10, 320-322.

43. Herbert S., Biel K. and Vogelmann T. (2006), **A photoacoustic method for rapid assessment of temperature effects on photosynthesis**. Photosynthesis research, **87**: 287-294.

44. Hollas J. (1996), **Modern Spectroscopy**. Third edition, John Wiley & Sons Ltd, 35-47

45. Jenkins T. (1985), **Photoacoustic characterization of semiconductors**. Prog. Crystal Growth and charact. **11** : 41-55.

46. Jongbloets H., Van De Steeg M., Van Der Werf E., Stoelinga J. and Wyder P. (1980), **Spectrum distortion in far-infrared Fourier spectroscopy by multiple reflections between sample and Michelson inetrefrometer**. Infrared physics, **20** : 185-192.

47. Kastle R. and Sigrist M. (1996), **Temperature-dependent photoacoustic spectroscopy with Helmholtz resonator**. Appl. Phys. B **63** : 389-397.

48. Khan M. and Diebold G. (1996), **The photoacoustic effect generated by laser irradiation of an isotropic solid cylinder**. Ultrasonics, **34** : 19-24.

49. Kimoto A. and Yamada H. (1968), **Infrared spectra of crystalline $CHCl_3$ and $CDCl_3$.** Bulletin of the chemical society of Japan, **41** : 1096-1104.

50. Kirkbright G. and Miller R., **Thermal wave imaging of optically thin films utilizing the photoacoustic effect**. Analyst, **107**: 798-802.

51. Kobayashi T. and Misawa K. (1997), **Novel interferometers for femtosecond phase spectroscopy**. Journal of nuclear materials **248** : 386-391.

52. Kouznetsov V., Bohorquez A. and Stashenko E. (2007), **Three-component imino Diels-Alder reaction with essential oil and seeds of anise: generation of new tetrahydroquinolines**. Tetrahedron Letters **48** : 8855-8860.

53. Lachish U., Rotter S., Adler E. and El-Hanany U. (1987), **Tunable diode laser based spectroscopic system for ammonia detection in human respiration**. Rev. Sci. Instrum. **58** (6) : 923-927.

54. Lai E., Voigtman E. and Winefordner J. (1982), **Photoacoustic probe for spectroscopic measurements in condensed metter: Convenient and corrosion-resistant**. Applied Optics, **21** (17) : 3126-3128.

55. Laine D., Al-Jourani M., Carpenter S. and Sedgbeer M. (1997), **Pulsed wideband IR source**. IEE Proc.-Optoelectron, **144** (5): 315-322.

56. Matan N. and Matan N. (2008), **Antifungal activities of anise oil, lime oil, and tangerine oil against molds of rubberwood (Hevea brasiliensis)**. International biodeterioratin & biodegradation **62** : 75-78.

57. Mayorga-Cruz D., Marquez-Aguilar P., Sarmiento-Martinez O. and Uruchurtu-Chavarin J. (2007), **Evaluation of corrosion in electrochemical systems using Michelson interferometry**. Optics and lasers in engineering **45** : 140-144.

58. McLennan J. (2003), **A0 and A1 studies on the violin using CO_2, He, and air/helium mixtures**. *Acustica*, **89** : 176-180.

59. Meyer P. and Sigrist M. (1990), **Atmospheric pollution monitoring using CO_2-laser photoacoustic spectroscopy and other techniques**. Rev. Sci. Instrum. **61** (7) : 1779-1807.

60. Miklos A. and Feher M. (1996), **Optoacoustic detection with near-infrared diode lasers: trace gases and short-lived molecules**. Infrared physics and technology **37** : 21-27.

61. Montgomery P., D. Montaner D., Manzardo O., Flury M. and Herzig H. (2004), **The metrology of a miniature FT spectrometer MOEMS device using white light scanning interference microscopy**. Thin Solid Films **450** : 79-83.

62. Mukoyama T. (2004), **Theory of X-ray absorption and emission spectra**. Spectrochimica Acta part B **59** : 1107-1115.

63. Muratikov K. and Glazov A. (2003), **Theoretical and experimental investigation of the photoacoustic effect in solids with residual stresses**. CEJP **3** : 485-515.

64. Philip K A., Joseph L., Irimpan L., Krishnan B., Radhakrishnan P., Nampoori V. and Natarajan R. (2007), **Thermal characterization of ceramic tapes using photoacoustic effect**. Phys. Stat. sol., **204** (3) : 737-744.

65. Pinchasov Y., Berner T. and Dubinsky Z. (2006), **The effect of lead on photosynthesis, as determined by photoacoustics in synechococcus leopoliensis (cyanobacteria)**. Water, air and solid pollution, **175**: 117-125.

66. Qin W., Lin J. and Qibiao W. (2007), **Effect of three extraction methods on the volatile component of Illicium verum hook. f. analyzed by GC-MS**. Wuhan university journal of natural sciences, **12** (2) : 529-534.

67. Ramadan M. (2007), **Nutritional value, functional properties and nutraceutical applications of black cumin (Nigella sativa L.): an overview**. International journal of food science and technology, **42** : 1208-1218.

68. Reverchon E., Porta G. and Gorgoglione D. (1995), **Supercritical CO_2 fractionation of Jasmine Concrete**. Journal of supercritical fluids, **8** : 60-65.

69. Robins J. (1999), **The science and art of aromatherapy**. Journal of Holistic Nursing, **17** (1) : 5-17.

70. Robinson N. and Hons B. (2000), **Monitoring oil degradation with infrared spectroscopy**. Wearcheck division of Set Point Technology, **5** : 1-8.

71. Rosencwaig A. and Pines E. (1977), **A photoacoustic study of newborn rat stratum corneum**. Biochimica andet Biophysica Acta, **493** : 10-23.

72. Sathiyamoorthy K. and Vijayan C. (2007), **Photoacoustic investigations on self-organization effects in metallopophyrins on glass substrates**. Materials Letters **61**: 4156-4159.

73. Schmidt K. and Beckmann D. (1998), **Biomass monitoring using the photoacoustic effect**. Sensors and actuators B **51** : 261-267.

74. Sears F. and Salinger G. (1975), **Thermodynamics, Kinetic theory, and Statistical Thermodynamics**. Third edition, Addison-Wesley Publishing Company, Inc., p. 108.

75. Selamet A., Dickey N. and Novak J. (1995), **Theoretical, computational and experimental investigation of Helmholtz resonators with fixed volume: lumped versus distributed analysis**. Journal of sound and vibration, **187** (2) : 358-367.

76. Simeoni D., Singer C. and Chalon G. (1997), **Infrared atmospheric sounding interferometer**. Acta astronautica, **40** (2-8) : 113-118.

77. Simpson J. (2008), **The obstetric memories and contributions of James Y. Simpson**. Adam and Charles Black, 778-790.

78. Steel W. (1983), **Interferometry**. second edition, CUP Archive, 7-10.

79. Szurkowski J. (2001), **Application of photoacoustic spectroscopy in studies of environmental contamination effect on needles of Scots Pine (Pinus silvestris L.)**. Pull. Environ. Contam. Toxicol. **66**: 683-690.

80. Tang S. (2005), **On Helmholtz resonators with tapered necks**. Journal of sound and vibration **279** : 1085-1096.

81. Tolman R. (1987), **Relativity, Thermodynamics and Cosmology**. Courier Dover Publication, 13-15.

82. Toyoda T., Arae D. and Shen Q. (2002), **Effect of size confinement on CdSe nanocrystals in a GeO_2 glass matrix characterized by photoacoustic spectroscopy**. Physica B **316-317** : 476-478.

83. Valentin A. (1996), **Tunable diode laser wavelength control by a Michelson interferometer**. Spectrochimica Acta part A, **52** : 823-833.
84. Villegas-Lelovsky L., Gonzalez de la Cruz G. and Gurevich Y. (2003), **Electron and phonon thermal waves in semiconductors: the effect of carrier diffusion and recombination on the photoacoustic signal**. Thin solid films **433** : 371-374.
85. Wajs A., Bonikowski R. and, Kalemba D. (2008), **Composition of essential oil from seeds of Nigella sativa L. cultivated in Poland**. Flavour Fragr. J. **23**: 126-132.
86. Workman J. and Springsteen A. (1998), **Applied Spectroscopy**. Academic Press, 15-17.
87. Yang Y. and Zhang S. (2003), **Photoacoustic spectroscopy study on the co-florescence effect of Eu^{3+} - La^{3+}** - Hba solid complexes. Journal of Physics and Chemistry of solids, **64** : 1333-1337.

Internet sites

88. http://dhs.wisconsin.gov/eh/chemFS/pdf/chloro.pdf,2000
89. http://en.wikipedia.org/wiki/Absorption_ spectroscopy,2009
90. http://en.wikipedia.org/wiki/essential_oil,2009
91. http://en.wikipedia.org/wiki/Helmholtz_resonator,2009
92. http://en.wikipedia.org/wiki/infrared_spectroscopy,2009
93. http://en.wikipedia.org/wiki/microphone,2009
94. http://en.wikipedia.org/wiki/molecular_vibration,2009
95. http://iadr.confex.com/iadr/saudi06/preliminaryprogram/abstract_87084, 2009
96. http://galileoandeinstein.virginia.edu/lectures/michelson.html,1996
97. http://orgchem.colorado.edu/hndbksupport/IRtutor/tutorial.html,2002

98. http://physics.usask.ca/~angie/ep421/lab3/theory.html,2009

99. http://scienceworld.wolfram.com/physics/Helmholtzresonator.html,2009

100. http://skiper.physics.sunysb.edu/~ralf/phy300/lab6.pdf,2006

101. http://teaching.shu.ac.uk/hwb/chemistry/tutorials/molspec/irspec1.html, 2009

102. http://www.answers.com/topic/spearmint,2009

103. http://www.atsdr.cdc.gov/tfacts6.pdf,1997

104. http://www.aurumindia.com/ereports/menthaoil.pdf,2006

105. http://www.chem.ucla.edu/~webspectra/irintro.html,2009

106. http://www.colorado.edu/physics/phys5430/Michelsoninterferometer.pdf,2001

107. http://www.knowles.com,2009

108. http://www.le.ac.uk/chemistry/pdf/teachersworkshops.pdf,2009

109. http://www.mediacollege.com/audio/microphones/condenser.html,2009

110. http://www.movar.pate.hu/~mathphys/pas.html,2009

111. http://www.oilanalysis.com/article_detail.asp?articleid=1109,2007

112. http://www.physics.uiowa.edu/~rvogel/int_lab_2007_1/docs/B1_Michelson _V4.doc,2007

113. http://www.prenhall.com/settle/chapters/ch15.pdf,2009

114. http://www.umsl.edu/~orglab/documents/IR/IR2.html,1997

115. http://www2.ups.edu/faculty/hanson/spectroscopy/IR/IRfrequencies.html,2009

دراسة الغازات باستخدام الأثر الصوت ضوئي بالتزامن مع مقياس تداخل مايكلسون

إعداد: أحمد "سيف الدين" أمين جبر

إشراف: البروفيسور محمد إبراهيم أبو طه

ملخص:

في هذه الأطروحة، و لأول مرة في تاريخ المطيافية، تم رصد و قياس الأثر الصوت ضوئي الذي اكتشفه العالم أجراهام بيل في العام 1880 م داخل خلية مقياس تداخل مايكلسون، نسبة للعالم الأمريكي ألبرت مايكلسون الذي اخترع هذا الجهاز في العام 1880 م، بنجاح. هذا و قد تم بناء الجهاز المستخدم في رصد الإشارات و قياسها، و الذي يتكون من مزيج من مقياس تداخل مايكلسون و خلية هيلمهولتز ينتهي أحد طرفيها بمايكروفون حساس، بواسطة الباحث داخل مختبر البحث العلمي الكائن في الطابق الثالث في كلية العلوم و التكنولوجيا في جامعة القدس. و قد تم تشغيل الجهاز لأول مرة في نهاية شهر أيلول من العام 2008 في حين تم دراسة العينات و فحصها و تجميع المعلومات في الفترة الواقعة ما بين شهر تشرين الثاني من العام 2008 و شهر كانون الثاني من العام 2009.

بالنظر الى عنوان الرسالة فإنه يبدو جلياً انها تتمحور حول دراسة الغازات و استكشافها باستخدام الاثر الصوت ضوئي بالتزامن مع مقياس تداخل مايكلسون في محاولة لإيجاد رابط او علاقة بين كل من الإشارتين؛ اشارة الأثر الصوت ضوئي و اشارة مقياس مايكلسون. هذا و قد استخدمت عينات من مادة الكلوروفورم لفحص نجاعة و ثبات النظام الذي تم بناؤه، في حين استخدمت عينات من الزيوت الطيّارة و بعض الأنسجة النباتية، التي يتم استخلاص تلك الزيوت منها مثل أوراق النعناع الطازجة و بعض أزهار الياسمين و بذور كل من حبة البركة و اليانسون، في محاولة لاستنتاج علاقة بين الإشارتين سالفتين الذكر. كما تم أيضاً فحص عينات من ماء الصنبور و ماء زمزم في محاولة لتقصّي مدى حساسية النظام (الجهاز) للفروقات البسيطة بين العينات، إضافةً الى التمييز بين الإشارتين سالفتين الذكر من حيث القدرة على رصد التغيرات البسيطة الحادثة داخل العينة اثناء امتصاصها للأشعة تحت الحمراء في المدى 2 – 9.5 مايكروميتر.

اما فيما يتعلق بمنهجية البحث المتبعة في هذه الأطروحة، فقد تم اتباع منهجية البحث العلمي القائم على التجربة و المقارنة و التحليل و استخلاص النتائج و تتبع مدى توافقها مع النظريات العلمية السائدة. هذا و قد تم استخدام النظام (الجهاز) الذي تم بناؤه في دراسة و مقارنة أبخرة مواد مختلفة مثل ابخرة الزيوت الطيارة و الأبخرة المنبعثة من بعض الأنسجة النباتية إضافة الى ماء الصنبور و ماء زمزم. و قد تبين بعد الاطلاع على النتائج و مقارنة

الرسومات البيانية و تحليلها مدى التوافق و التطابق بين العينات ذات الصلة مثل عينات زيت النعناع و عينات أوراق النعناع اضافة الى عينات ماء الصنبور و ماء زمزم.

لقد كان من أهم نتائج هذا البحث المتواضع ان تم رصد و قياس إشارات الأثر الصوت ضوئي داخل خلية مقياس تداخل مايكلسون – و لأول مرة – بنجاح. كما ان الرسومات البيانية قد بينت مدى التوافق و التزامن بين اشارات الأثر الصوت ضوئي و اشارات مقياس تداخل مايكلسون الأمر الذي يوضح ان كلا الإشارتين نتجتا عن أصل واحد و هو امتصاص جزيئات بخار العينة للأشعة تحت الحمراء على الرغم من اختلاف طريقة تولد و رصد كلا الإشارتين. و فضلاً عما سبق ذكره، فقد تبين من خلال مقارنة النتائج ان مقياس تداخل مايكلسون قد أظهر دقة أعلى من الأثر الصوت ضوئي في رصد التغيرات الحادثة على العينة نتيجة لأمتصاصها للأشعة تحت الحمراء.

لقد كانت نتائج هذا البحث المتواضع مشجعة الى حدٍ ما، كما انها فتحت الباب على مصراعيه لاستخدام هذا النظام في جميع الأبحاث التي تتمحور حول الأبخرة المنبعثة من المواد المختلفة خصوصاً الأبحاث الزراعية و الصحية القائمة على طب الأعشاب أو الطب البديل.